SPACE SHUTTLE

Solid Rocket Motors
Thiokol Corporation
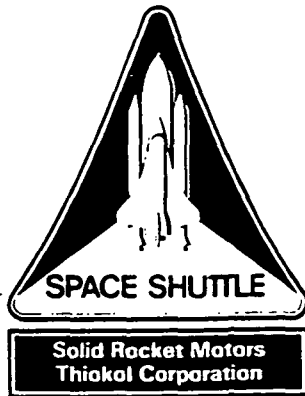
Technical Evaluation Motor No. 7 (TEM-7) Final Test Report

April 1991

Prepared for:

National Aeronautics and Space Administration
George C. Marshall Space Flight Center
Marshall Space Flight Center, Alabama 35812

Thiokol CORPORATION

SPACE OPERATIONS

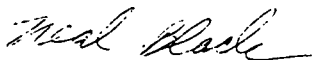*Thiokol* CORPORATION
SPACE OPERATIONS

Technical Evaluation Motor No. 7 (TEM-7)
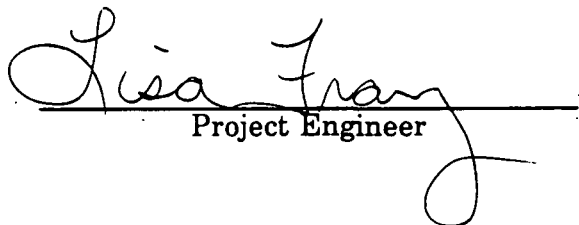Final Test Report

Prepared by:

_____
Certification/Planning
Systems Engineer
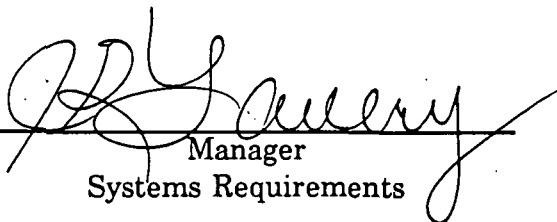
Approved by:
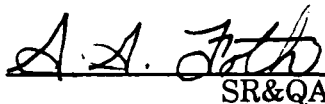
_____
Supervisor
Certification Planning

_____
Project Engineer

_____
Manager
Systems Requirements

_____
SR&QA

_____
Program Manager

_____
Data Management/
Release

Major contributors to this report were:

Project engineer:	L. Frary
Instrumentation:	D. South
Case/leak check/seals:	T. Swauger, R. Ash, G. Abawi
Insulation:	J. Passman, S. Manz
Nozzle:	R. George, R. Lange, F. Weiler
Joint protection systems:	C. Prokop, K. Rees
Ballistics/mass properties:	A. Drendel
Aero/thermal:	R. Buttars, E. Mathias, D. Ruddell
Structural analysis:	M. Fairbourn, D. Bright
Postfire hardware evaluation:	J. Curry
Photo instrumentation:	C. Larsen

ABSTRACT

The Technical Evaluation Motor No. 7 (TEM-7) test was a full-scale, full-duration static test firing of a high performance motor-configuration solid rocket motor with nozzle vectoring. The test took place on 11 Dec 1990 at Thiokol Corporation Static Test Bay T-97.

This final test report documents the procedures, performance, and results of the static test firing of TEM-7. All observations, discussions, conclusions, and recommendations included in this report are complete and final except for the TEM-7 fixed housing unbond investigation, which is reported in TWR-61585.

Included are a presentation and discussion of TEM-7 performance, anomalies, and test result concurrence with the objectives outlined in CTP-0107, Rev A, Space Shuttle Technical Evaluation Motor No. 7 (TEM-7) Static Fire Test Plan.

Thiokol CORPORATION
SPACE OPERATIONS

CONTENTS

Thiokol CORPORATION
SPACE OPERATIONS

CONTENTS (cont)

Thiokol CORPORATION
SPACE OPERATIONS

APPENDIXES

(Appendixes are in a separate volume)

FIGURES

FIGURES (cont)

Thiokol CORPORATION
SPACE OPERATIONS

FIGURES (cont)

Thiokol CORPORATION
SPACE OPERATIONS

TABLES

ACRONYMS AND ABBREVIATIONS

ac	alternating current
APU	auxiliary power unit
ASRM	Advanced Solid Rocket Motor
ATVC	ascent thrust vector control
CCP	carbon-cloth phenolic
CEI	Contract End Item
CF/EPDM	carbon-fiber-filled ethylene-propylene-diene monomer
CO_2	carbon dioxide
CP	circular perforated
CTPB	carboxyl-terminated polybutadiene
dc	direct current
DM	development motor
ET	external tank
ETM	engineering test motor
FSM	flight support motor
GCP	glass-cloth phenolic
HPM	high performance motor
HPU	hydraulic power unit
Hz	hertz
ID	inside diameter
ips	inches per second
lb	pound
lbm	pound mass
in.	inch
LDI	low-density indication
MAEHS	modified aft end heating system
MAP	manual/automatic panel
MEOP	maximum expected operating pressure
min	minute
ms	millisecond
NA	not available
NARC	North American Rayon Corporation
NBR	nitrile butadiene rubber

NCPT	Nozzle Component Program Team
OD	outside diameter
OPT	operational pressure transducer
PBAN	polybutadiene acrylic acid acrylonitrile terpolymer
PFAR	postfire anomaly record
PFOR	postfire observation record
pps	pictures per second
psig	pounds per square inch gage
PVM	production verification motor
QM	qualification motor
RPRB	Redesign Program Review Board
RSRM	redesigned solid rocket motor
RTV	room-temperature vulcanizing rubber
S & A	safe and arm
SAPMD	stand-alone pressure measuring device
SBRE	surface burn rate error
sccs	standard cubic centimeters per second
sec	second
SII	SRM ignition initiator
SINDA	Systems Improved Numerical Differencing Analyzer
SRB	solid rocket booster
SRM	solid rocket motor
STS	space transportation system
TEM	technical evaluation motor
TVA	thrust vector actuation

ACRONYMS AND ABBREVIATIONS (cont)

TVC	thrust vector control
V	volt
1-D	one dimensional
1-L	first longitudinal
2-D	two dimensional
2-L	second longitudinal
3-D	three dimensional

1

INTRODUCTION

Technical Evaluation Motor No. 7 (TEM-7) was successfully static test fired at 1300 hours on 11 Dec 1990 at Thiokol Corporation Static Test Bay T-97. The ambient temperature at the time of the test was 44°F and the propellant mean bulk temperature was 65°F. Ballistics performance values were within the specified requirements.

The TEM-7 test was a full-scale, full-duration static test fire of a high-performance motor (HPM)-configuration solid rocket motor (SRM). TEM-7 was the first full-scale test motor on which all segments were more than five years old and was the first TEM static test motor with nozzle vectoring. The TEM-7 test arrangement included the modified aft end heating system (MAEHS) normally used for static tests with vectored nozzles plus a nozzle-to-case joint heater normally used for TEM static tests.

The primary purpose of TEM static tests is to recover SRM case and nozzle hardware for use in the redesigned solid rocket motor (RSRM) flight program; however, TEM static tests also provide windows of opportunity to evaluate or certify various design, process, and supplier issues for the RSRM flight program. Accordingly, TEM-7 was the first full-scale static test for qualification of North American Rayon Corporation (NARC) rayon in all nozzle carbon-cloth phenolic (CCP) liners. Two additional full-scale nozzles will be static tested for qualification of the NARC rayon as outlined in the second source rayon program plan, TWR-18965. Low-cost nozzle improvements, previously incorporated into the TEM-6 static test, to be qualified on TEM-7 included a change in the CCP liner ply angle of the cowl, improved inner and outer boot ring phenolic cure cycles, and an extended belly band flexible bearing protector design.

Instrumentation measurements consisted of forward and aft end chamber pressure; igniter chamber pressure; stiffener stub strains; nozzle components temperatures and strains; temperature for deluge control; nozzle deflections; nozzle boot cavity temperature and pressure; plume radiation measurements; test stand water deluge pressure; and timing.

2

TEST OBJECTIVES

The TEM-7 test objectives of CTP-0107, Rev A, were derived from the objectives of System Test Summary Sheet TGX-21.6 to satisfy specific requirements of Contract End Item (CEI) Specification CPW1-3600A, dated 3 Aug 1987.

Qualification objectives of this test were as follows:

A. Certify NARC rayon for use in nozzle CCP liners (CPW1-3600A, Para 3.2.1.4.13, 3.3.6.1.2.7, and 3.3.6.1.2.8).

B. Certify nozzle inner boot ring cure cycle improvement (CPW1-3600A, Para 3.3.6.1.2.8).

C. Certify nozzle outer boot ring cure cycle improvement (CPW1-3600A, Para 3.3.6.1.2.8).

D. Certify the nozzle cowl ring with an ablative liner ply angle change (from 0 to -50 deg) (CPW1-3600A, Para 3.2.1.4.13 and 3.3.6.1.2.8).

E. Certify the improved nozzle bearing protector (CPW1-3600A, Para 3.3.6.1.2.8).

Other test objectives included:

F. Recover case and nozzle hardware for RSRM flight and static test programs.

G. Obtain data on the effect of five-year storage of loaded SRM case segments upon motor ignition and performance.

H. Demonstrate the performance of an improved nose assembly-to-cowl assembly process for the nozzle (CPW1-3600A, Para 3.2.3, 3.2.3.1, and 3.3.1.1).

I. Demonstrate the performance of increased cowl vent hole size (0.375 in. nominal diameter) for reducing boot cavity delta pressure (CPW1-3600A, Para 3.3.6.1.2.8).

J.   Obtain additional data on the low-frequency chamber pressure oscillations in the motor forward end and correlate with chamber pressure oscillation measurements in the motor aft end.

K.   Obtain additional data on chamber pressure drop down the bore by the use of aft end pressure transducers.

L.   Obtain additional data on cowl boot cavity/aft end (fixed housing) pressurization and temperature.

M.   Obtain additional data on the performance of the aft stiffener segment with known outer ligament cracks in the stiffener stubs.

N.   Obtain thermal radiation data from the nozzle plume for the Advanced Solid Rocket Motor (ASRM) program.

3

EXECUTIVE SUMMARY

3.1 SUMMARY

Inspection and instrumentation data indicate that the TEM-7 static test firing was successful overall. Data were gathered at instrumented locations during pretest, test, and post-test operations. The information assembled from the test procedures has supplied valuable knowledge and understanding about the performance of the HPM- and RSRM-design components utilized in TEM-7.

Overall, the postburn condition of the NARC rayon nozzle liners was very good (TWR-61490). The performance margins of safety of all NARC rayon nozzle liners were positive. The erosion of the throat and throat inlet rings was smooth, with the typical rippled erosion pattern occurring on the aft 6 in. of the throat ring (0.1 in. deep maximum). The postburn mean throat diameter was 56.07 inches. This is within the historical database of RSRM/HPM throat diameters. The throat erosion rate was 9.20 mils/sec.

Performance margins of safety for the -50-degree cowl ring were positive and met or exceeded flight baseline experience. The cowl ring erosion was smooth and did not exhibit the typical wash areas seen on RSRM (0-deg ply wrap) cowls.

The nozzle inner and outer boot rings (improved cure cycles) performed nominally. The performance margins of safety for the outer boot ring were positive.

Performance of the improved cowl assembly process (joint No. 2) was excellent. EA 913NA did not mix with the RTV. The RTV extended well below the char line, full circumference. No blow paths were present.

TEM-7 was configured with a bearing protector in which the belly band was lengthened and thickened. The belly band was extended to place the region of maximum erosion in the thickened portion of the bearing protector. On TEM-7 the

belly band was additionally thickened to accommodate potential for increased erosion due to enlarged cowl vent holes. After removal of the TEM-7 fixed housing from the bearing, the bearing protector was found to be deeply eroded in the areas where gas impinged from the cowl vent holes. Maximum erosion was centered in this lengthened and thickened belly band region of the bearing protector. Damage to the improved nozzle bearing protector and flex bearing resulted in failure to demonstrate acceptable performance of increased cowl vent hole size (0.375-in. nominal diameter).

After nozzle disassembly, the fixed housing phenolic insulation was found to be almost 100 percent adhesively unbonded from the metal. This adhesive bondline failure was attributed to contamination of the fixed housing bonding surface coupled with the stress concentration induced on the housing by gas pressure through the four pressure ports. The fixed housing strain gage and the aft end pressure transducer responses indicated that an anomalous event occurred at approximately 2 sec. Details of the TEM-7 fixed housing unbond investigation study are contained in TWR-61585.

The TEM-7 ballistic performance was within expected limits and compared well with previous TEM performance and HPM historical data. The five-year storage of loaded case segments did not appear to affect motor performance.

Strain gage data for evaluation of stiffener stubs with outer ligament cracks were obtained. Thermal radiation data from the nozzle plume were successfully obtained. Only limited aft end and nozzle boot cavity pressure data were recorded during the TEM-7 test. All pretest requirements for TEM-7 were met.

3.2 CONCLUSIONS

The following conclusions are listed as each specifically relates to the test objectives and applicable CEI specification (CPW1-3600A) paragraphs. Additional information about each conclusion can be found in the referenced sections of this report.

	Objective	CEI Paragraph	Conclusions
A.	Certify NARC rayon for use in nozzle CCP liners	3.2.1.4.13, Nozzle Liner Design 3.3.6.1.2.7, Nozzle Design Safety Factors 3.3.6.1.2.8, Nozzle Performance Margin of Safety	*Certification requirements for this test were met. First of three full-scale static tests.* Performance margins of safety were positive and were equal to or better than baseline. Post-test condition of the nozzle liners was nominal. (Sections 6.6.2, 6.6.3, 6.6.4, 6.6.4.1, 6.6.4.5).
B.	Certify nozzle inner boot ring cure cycle improvement.	None. Nozzle performance margin of safety does not apply to this component.	*Certification requirements for this test were met. Second of three full-scale static tests.* Pre-test X-rays verified no LDIs. The inner boot ring performed nominally. (Sections 6.6.2, 6.6.3, 6.6.4.1).
C.	Certify nozzle outer boot ring cure cycle improvement.	3.3.6.1.2.8, Nozzle Performance Margin of Safety	*Certification requirements for this test were met. Second of three full-scale static tests.* Performance margins of safety were positive and equal to or better than baseline. Pre-test X-rays verified no LDIs. Post-test condition of the outer boot ring was nominal. (Sections 6.6.2, 6.6.3, 6.6.4, 6.6.4.1, 6.6.4.5).
D.	Certify the nozzle cowl ring with an ablative liner ply angle change (from 0 to -50 deg).	3.2.1.4.13, Nozzle Liner Design 3.3.6.1.2.8, Nozzle Performance Margin of Safety	*Certification requirements for this test were met. Second of three full-scale static tests.* Performance margins of safety met or exceeded flight baseline. The cowl ring surface eroded smoothly and contained none of the wash areas typically seen on present RSRM cowl rings with the 0-deg CCP ply wrap. (Sections 6.6.2, 6.6.3, 6.6.4, 6.6.4.1, 6.6.4.5).

<u>Objective</u>	<u>CEI Paragraph</u>	<u>Conclusions</u>
E. Certify the improved nozzle bearing protector.	None. Nozzle performance margin of safety does not apply to this component.	*Invalid test due to possible effects of other configuration changes.* Gas impingement was located within the thickened, extended portion of the bearing protector. Configuration changes to cowl vent holes (see Objective I) may have contributed to more severe erosion than anticipated. (Sections 6.6.2, 6.6.4.1).
F. Recover case and nozzle hardware for RSRM flight and static test programs.	None.	Case and nozzle hardware is available for refurbishment. (Sections 6.3.2, 6.6.2).
G. Obtain data on the effect of five-year storage of loaded SRM case segments upon motor ignition and performance.	None.	*Data obtained.* Motor performance was nominal. Five-year storage did not appear to affect motor ignition and performance. (Sections 6.9.2, 6.9.3, 6.9.4).
H. Demonstrate the performance of an improved nose assembly-to-cowl assembly process for the nozzle.	3.2.3, Reliability; 3.2.3.1, Primary Structure, Thermal Protection, Pressure Vessels; 3.3.1.1, Selection of Materials, Parts, and Processes	*Demonstrated.* EA-913NA adhesive did not squeeze out and mix with the room-temperature vulcanizing rubber (RTV) in joint No. 2 as is typically seen. The RTV was below the char line, full circumference. No blowpaths were observed. (Sections 6.6.2, 6.6.4.1, 6.6.4.2).

Objective	CEI Paragraph	Conclusions
I. Demonstrate the performance of increased cowl vent hole size (0.375-in. nominal diameter) for reducing boot cavity delta pressure.	None. Nozzle Performance Margin of Safety does not apply to this configuration change.	*Not demonstrated.* Boot cavity pressure (Objective L) was not obtained to verify performance, although 18 of 36 holes remained open compared to the postflight average of five open vent holes. However, the increased cowl vent hole size contributed to the severe erosion of the bearing protector (Objective E). (Sections 6.6.2, 6.6.4.1).
J. Obtain additional data on the low-frequency chamber pressure oscillations in the motor forward end and correlate with chamber pressure oscillation measurements in the motor aft end.	None.	*Data partially obtained.* No useable aft end pressure due to the aft end phenolic insulation unbond. Headend dynamic pressure was obtained. (Sections 4.2, 4.4.1, 6.9.4).
K. Obtain additional data on chamber pressure drop down the bore by the use of aft end pressure transducers.	None.	*Data partially obtained.* Aft end pressure data were obtained from T - 0 to T + 2 sec only, due to the aft end phenolic insulation unbond. (Sections 4.2, 4.4.1, 6.9.4).
L. Obtain additional data on cowl boot cavity/aft end (fixed housing) pressurization and temperature.	None.	*Data partially obtained.* Boot cavity pressure data were obtained by one Teledyne Taber pressure transducer from T - 0 to T + 20 sec. No data were obtained from three other (two SAPMD and one Teledyne Taber) transducers. The thermocouple data were erratic throughout the firing. (Sections 4.2, 4.4.1)

Objective	CEI Paragraph	Conclusions
M. Obtain additional data on the performance of the aft stiffener segment with known outer ligament cracks in the stiffener stubs.	None.	*Data obtained.* The instrumented stiffener stub hole strain gages all recorded data except for the lone referee strain gage mounted inside a stiffener stub hole. (Sections 4.2, 4.4.3, 6.3.2, 6.3.4.1).
N. Obtain thermal radiation data from the nozzle plume for the ASRM program.	None.	*Data obtained.* Twenty-one of 22 radiometers provided good data for plume radiation studies. (Sections 4.2, 4.4.5).

3.3 RECOMMENDATIONS

Based on the results of this test, it is recommended that demonstration and qualification activities for the following changes continue:

1. NARC rayon for nozzle CCP liners.

2. Inner boot ring cure cycle improvement.

3. Outer boot ring cure cycle improvement.

4. Minus 50-deg cowl ply angle.

5. Improved nose-to-cowl assembly process (joint No. 2).

6. Extended bearing protector belly band.

Thiokol *CORPORATION*
SPACE OPERATIONS

4

INSTRUMENTATION

4.1 INTRODUCTION

TEM-7 instrumentation measurements consisted of forward and aft end chamber pressure; igniter chamber pressure; stiffener stub strains; nozzle component temperatures and strains; temperature for deluge control; nozzle deflections; nozzle boot cavity temperature and pressure; plume radiation measurements; test stand water deluge pressure; and timing.

TEM-7 was instrumented with four aft end chamber pressure transducers installed through special instrumentation holes drilled through the fixed housing and phenolic insulation. TEM-6 also contained this arrangement. The objective of this instrumentation was to obtain aft end chamber pressures for ballistics modelling and pressure oscillations.

Boot cavity temperature and pressure and aft end chamber pressure measurements were made for a second time on the TEM program. New, improved stand-alone units with thermocouples were used for the first time in the cowl boot cavity. TEM-7 was instrumented to gather data on cracked stiffener stub holes as a followup on data gathered on Flight Support Motor No. 1 (FSM-1). The metal component parts on the nozzle using NARC material were instrumented with temperature sensors and strain gages. Plume radiation measurements were taken again to enhance data gathered on FSM-1.

4.2 OBJECTIVES/CONCLUSIONS

The objectives and corresponding conclusions from Section 2 regarding instrumentation performance were:

Objective	Conclusion
J. Obtain additional data on the low-frequency chamber pressure oscillations in the motor forward end and correlate with chamber pressure oscillation measurements in the motor aft end.	There were no useable aft end pressure oscillation data due to the aft end phenolic insulation unbond. However, headend dynamic pressure was obtained.
K. Obtain additional data on chamber pressure drop down the bore by the use of aft end pressure transducers.	Aft end pressure data were obtained from only T - 0 to T + 2 sec, probably due to the aft end phenolic insulation unbond. However, those two seconds of aft end pressure data provided good insight to the pressure drop down the bore.
L. Obtain additional data on cowl boot cavity/aft end (fixed housing) pressurization and temperature.	One of two Teledyne Taber pressure transducers recorded data until T + 20 sec then the data became erratic. Software anomaly is believed to have caused both SAPMDs to be inoperable prior to test. The thermocouple data were erratic throughout the firing, but did demonstrate the increased temperature into the boot cavity resulting from increased vent hole diameters. Boot cavity pressure data were obtained by one pressure transducer from T - 0 to T + 20 sec. No data were obtained from three other (two SAPMD and one Teledyne Taber) transducers.
M. Obtain additional data on the performance of the aft stiffener segment with known outer ligament cracks in the stiffener stubs.	The instrumented stiffener stub hole strain gages all recorded data except for the lone referee strain gage mounted inside a stiffener stub hole. There was a large variation between measured and predicted strains at holes with outer ligament cracks. Measured strains at holes with intact outer ligaments correlated well to predicted strains.
N. Obtain thermal radiation data from the nozzle plume for the ASRM program.	One of the 22 radiometers failed prior to the firing, but all other sensors provided very good data for plume radiation studies.

4.3 RECOMMENDATIONS

TEM-7-configured instrumentation for aft end chamber pressures is not planned for future full-scale static test motors. Detailed analyses must be performed to better understand hardware impact prior to any future implementation.

4.4 RESULTS/DISCUSSION

4.4.1 Pressure

Forward pressure measurements were nominal, but aft end chamber pressure measurements dropped off unexpectedly at T + 2 sec. The aft end chamber pressure transducers were heat affected as a gas path developed in the fixed housing insulation liner. The data from pressure gages and strain gages gave a time history of the unbonding sequence.

No anomalous conditions were found on the three headend chamber pressure transducers or their O-rings. No damage to the transducer threads or sealing surfaces was found. Each secondary O-ring had typical puncture marks caused by the removal tool.

The igniter pressure transducer secondary O-ring had a typical puncture mark caused by the removal tool. No damage was found on the primary O-ring. No damage to the plug threads or sealing surfaces was observed.

The four aft end pressure transducers on the fixed housing were heat affected. The findings from the heat-affected pressure transducers that were presented to the Redesign Program Review Board on 9 Jan 1991 were confirmed in the M-53 metallography lab. Two of the four primary seals were heat affected, which was caused by heating of the transducers and *not* by direct gas impingement. The other two primary seals were not heat affected. The worst-case heat-affected pressure transducer burned through from inside to outside at the primary O-ring groove. It was also plugged with aluminum slag. No heat effects were found on any secondary O-ring. The secondary O-ring on the aft end operational pressure transducer

(OPT)-type pressure transducer was damaged during assembly due to a grease overfill condition. Details of the lab work are included in this final report.

The installed pressure transducers in the boot cavity and thermocouple were erratic. One pressure transducer recorded data until T + 20 sec and the other failed. The thermocouple data were erratic throughout the firing but did demonstrate the increased temperature into the boot cavity resulting from increased vent hole diameters.

Two postflight anomaly reports were written; one was on the OPT secondary O-ring overfill condition, and the other was on the heat-affected primary O-rings on two transducers.

4.4.2 Temperature

Temperature data were nominal. The ambient temperature was 44°F and the propellant mean bulk temperature was 65°F at T - 0 (ignition). Joint and case temperature sensors all performed nominally.

Temperature sensors on the nozzle components performed and recorded no anomalies associated with the unbond anomaly.

4.4.3 Strain

Strain gages near the aft end chamber pressure transducers confirmed the unbond which occurred to the fixed housing insulation. All other strain gages on the nozzle components performed and recorded no anomalies associated with the unbond anomaly.

The instrumented stiffener stub holes strain gages all recorded data except for the lone referee strain gage mounted inside a stiffener stub hole.

4.4.4 Position

Aft skirt and nozzle positioning measurements all performed as expected.

4.4.5 Radiometers

One of the 22 radiometers failed prior to the firing, but all other sensors provided very good data for plume radiation studies.

5

PHOTOGRAPHY

Photographic coverage was required to document the test, test configuration, instrumentation, and any anomalous conditions which may have occurred. The TEM-7 photographs and video tapes are available from the Thiokol Corporation's Photographic Services.

5.1 STILL PHOTOGRAPHY

Still color photographs of the test configuration were taken before, during, and after the test. Photographs were taken of joints each 45 deg minimum and at anomalous conditions.

5.2 MOTION PICTURES

Color motion pictures of the test were taken with nine high-speed cameras, two real-time documentary cameras, and four video cameras. Documentary motion pictures are recorded on Roll 8330, high-speed motion pictures on Roll 8331, and videotape on T0118 through T-0121. Cameras are listed in Table 5-1. The camera setup is shown in Figure 5-1.

Table 5-1. Photography and Video Coverage

Camera	Station	Location	Type	Coverage
1	7	Thrust block	High speed	Igniter port
2	1	North forward barricade	High speed	Center forward and center joints
3	1	North forward barricade	Video	Overall motor and plume
4	2	North aft barricade	High speed	Center aft and nozzle-to-case joints
5	2	North aft barricade	Documentary	Aft case, nozzle and plume
6	2	North aft barricade	High speed	Nozzle, 200 ft of plume
7	3	South aft barricade	Documentary	Overall motor and plume
8	3	South aft barricade	Video	Aft case, nozzle, plume, deluge
9	4	South center barricade	Video	Aft joint, nozzle, plume
10	4	South center barricade	High speed	Nozzle, 200 ft of plume
11	4	South center barricade	High speed	Center aft and nozzle-to-case joints
12	5	South forward barricade	High speed	Center forward and center joints
13	7	Thrust block	High speed	Igniter port
14	7	Thrust block	Video	Top of case, nozzle, and plume
15	7	Thrust block	High speed	Top of case, nozzle, and plume

Note: Nine high speed cameras (300 pps); two documentary cameras (24 pps); four video cameras (real time)

(Doc)

(Vid)

7

8

South Aft Bar
(Sta 3)

(HS)

6

(Doc)

5

(HS)

4

North Aft Bar
(Sta 2)

9 (Vid)

10 (HS)

11 (HS)

South Center Bar
(Sta 4)

(Vid)

3

(HS)

2

North Forward Bar
(Sta 1)

(HS)

1

14 15

(Vid) (HS)
T-Block

(Sta 7)   A020563aR1

13 (HS)

12 (HS)

South Forward Bar
(Sta 5)

Code
Doc – Documentary
HS – High Speed
Vid – Video
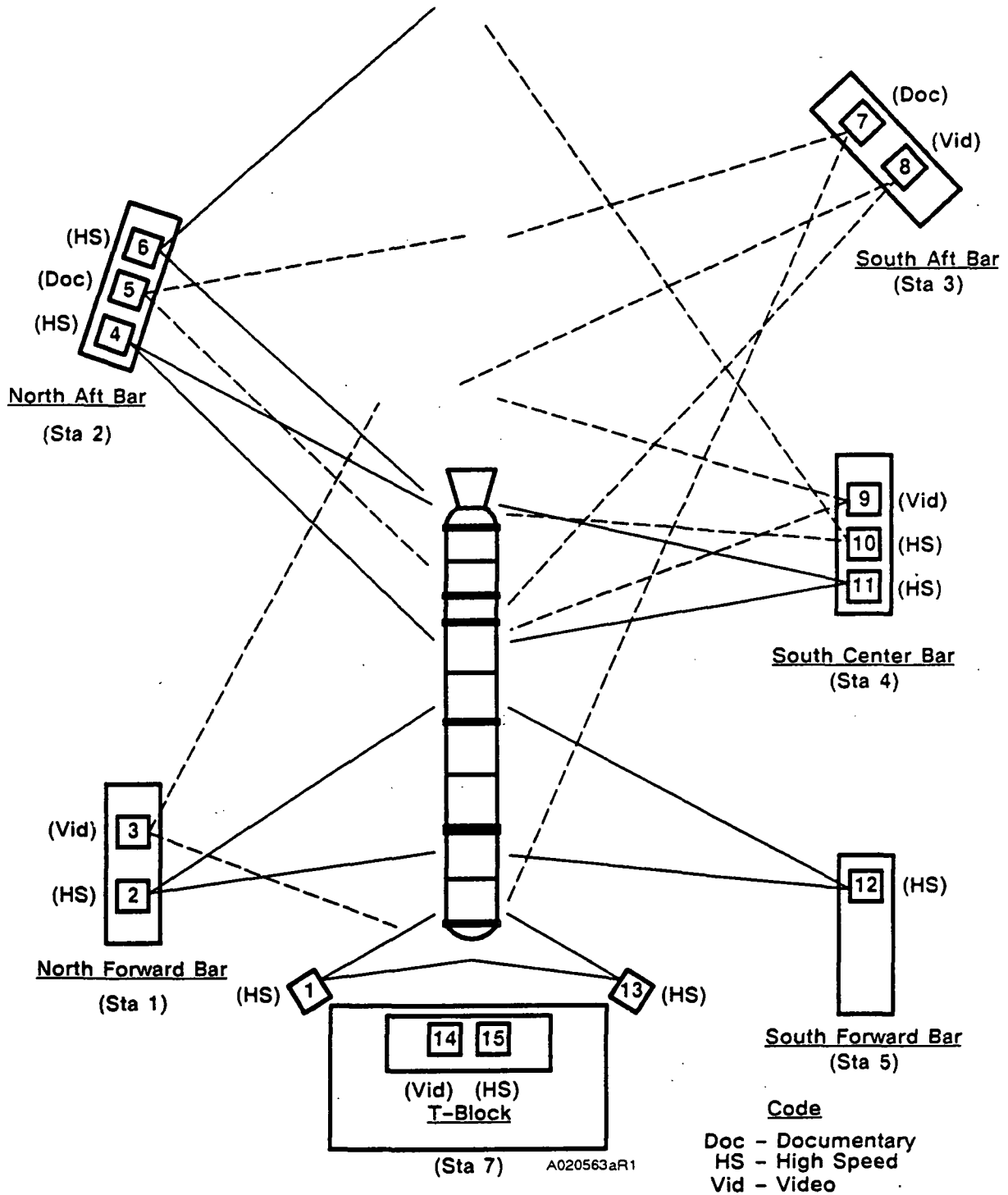
Figure 5-1.   T-97 Photography Coverage—TEM-7

Thiokol CORPORATION
SPACE OPERATIONS

6

TEST DESCRIPTION AND RESULTS

6.1 TEST ARTICLE DESCRIPTION

The TEM-7 test article was assembled in accordance with Drawing 7U76879. The motor was instrumented to provide data to satisfy the test objectives. An overall view of the test article is shown in Figure 6-1. A TEM-7 drawing tree is included in Appendix A.

TEM-7 consisted of HPM-configuration motor segments that had been fabricated and loaded with propellant more than five years before the static test firing on 11 Dec 1990. A listing of each segment, segment flight identification, cast date, and storage and transportation history is shown in Table 6-1.

Table 6-1. TEM-7 Segment History

TEM-7 Segment	Forward	Forward Center	Aft Center	Aft
Flight Identification	SRM-28B	SRM-28B	SRM-28B	SRM-26A
Casting Date	24 Sep 1985	21 Oct 1985	14 Oct 1985	17 Jul 1985
Shipped to KSC	31 Jan 1986	10 Jan 1986	7 Jan 1986	26 Dec 1985
Shipped to Thiokol	27 Mar 1987	18 Jan 1989	25 Jul 1989	24 Mar 1988
Arrived at Thiokol	10 Apr 1987	25 Jan 1989	31 Jul 1989	10 Apr 1988
Shipped to KSC	10 Jun 1987	--	--	--
Shipped to Thiokol	22 Feb 1989	--	--	--
	29 Feb 1989	--	--	--

The high-performance SRM static test motor consisted of a lined, insulated, segmented rocket motor case loaded with solid propellant; an ignition system complete with electro-mechanical safety and arming device, initiators, and loaded igniter; and
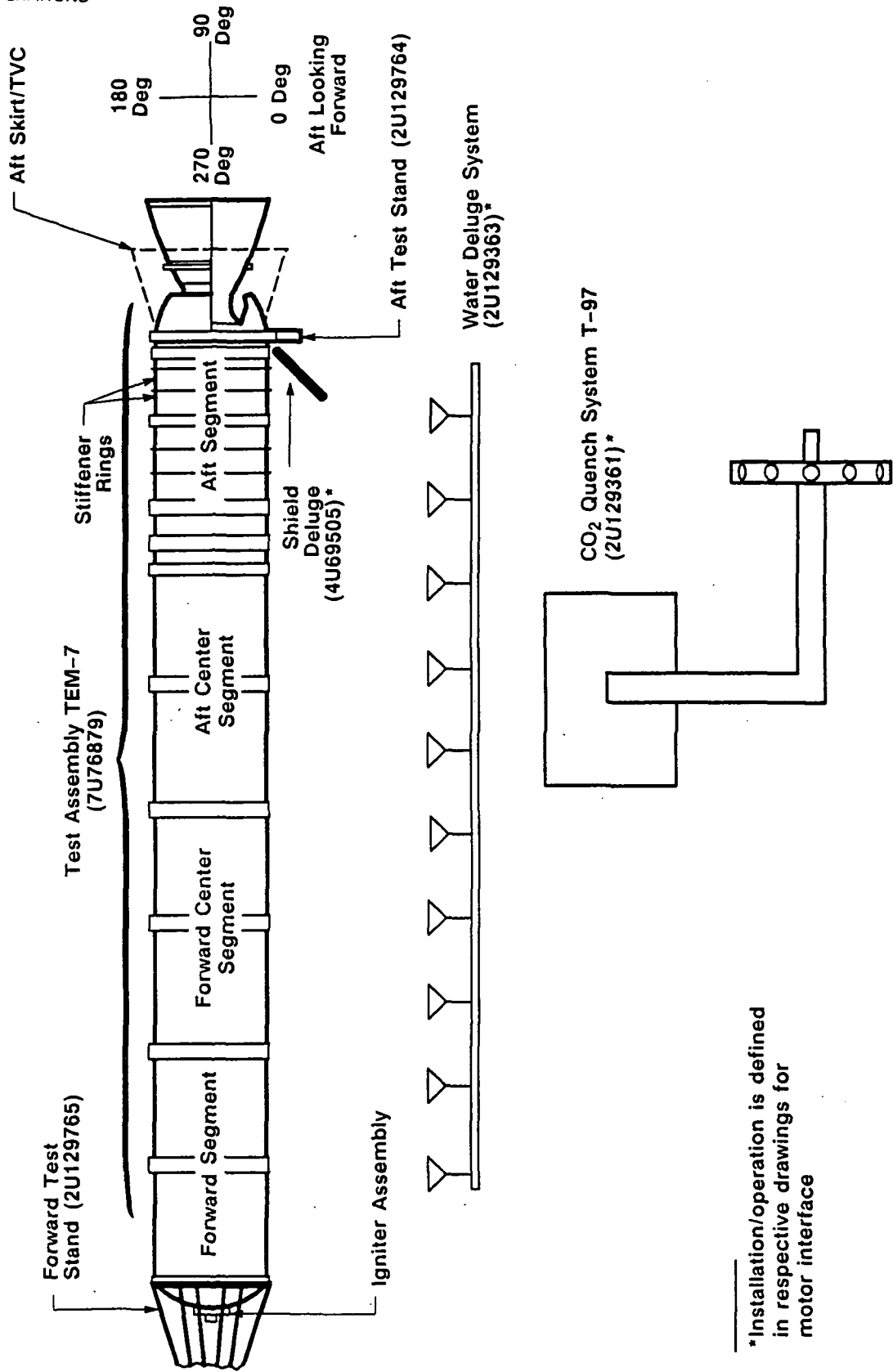
A026864aR1

Figure 6-1. TEM-7 Static Test Arrangement

Aft Skirt/TVC

180 Deg
270 Deg
90 Deg
0 Deg
Aft Looking Forward

Aft Test Stand (2U129764)

Water Deluge System (2U129363)*

Stiffener Rings

Aft Segment

Shield Deluge (4U69505)*

Test Assembly TEM-7 (7U76879)

Aft Center Segment

CO_2 Quench System T-97 (2U129361)*

Forward Center Segment

Forward Segment

Forward Test Stand (2U129765)

Igniter Assembly

*Installation/operation is defined in respective drawings for motor interface

a movable nozzle with flexible bearing and exit cone. For this test, the nozzle was vectored.

The assembled static test motor was approximately 116 ft in length and 12 ft in diameter. The test item configuration was controlled by released engineering drawings (refer to TEM-7 drawing tree) and the test plan, CTP-0107, Rev A. Deviations to this configuration were processed through the normal configuration control system and approved by the integration engineer, program manager and NASA, and are included in this final test report.

Postfire hardware evaluation of TEM-7 was accomplished in accordance with TWR-60273 and TWR-61209. Observations were recorded on the postfire observation records (PFOR) included in Appendix E. Any anomalous condition or limits violation which was a first-time occurrence was documented on a PFAR. A list of PFARs is included in Appendix E.

6.2 TEST ARRANGEMENT AND FACILITIES

The TEM-7 static test arrangement was assembled in accordance with Drawing 2U129760. T-97 was equipped with a water deluge system and a CO_2 quench. The test motor included a government-furnished equipment and United Space Boosters, Inc.-supplied solid rocket booster (SRB) aft skirt assembly, which contains the thrust vector control (TVC) subsystem and the heat shield installation. The thrust vector actuation (TVA) system comprises two SRB actuators and two hydraulic power units (HPU) located in the aft skirt. The HPU ground test controller, HPU manual/automatic panel (MAP), and the ascent thrust vector control units (ATVC) serve as the control units for the TVC subsystem.

6.3 CASE AND CASE SEALS PERFORMANCE

6.3.1 Introduction

The case consisted of 11 individual weld-free segments: the forward dome, six cylinder segments, the external tank (ET) attach segment, two stiffener segments, and

the aft dome. The 11 segments were preassembled into four subassemblies to facilitate propellant casting.

The four loaded assemblies were the forward segment assembly (Drawing 7U76899), the forward center segment assembly (Drawing 1U52566), the aft center segment assembly (Drawing 1U52566), and the aft segment assembly (Drawing 7U76882). These segments were joined by means of tang and clevis field joints, which, in turn, were held in place by pins.

Both flanges of the aft stiffener cylinder (1U50185-06, S/N 027) have outer ligament cracks:

1. At 240 deg on aft stub
2. At 276 deg on aft stub (saw cut through)
3. At 278 deg on aft stub
4. At 280 deg on aft stub
5. At 282 deg on aft stub
6. At 232 deg on forward stub
7. At 288 deg on forward stub (not instrumented)

The motor was equipped with a stiffener T-ring assembly on the flanges which had the severed outer ligaments. The T-ring is known to help reduce flange stresses, thus reducing concerns generated by the severed outer ligaments. This is also representative of the flight configuration (Figure 6-2).

Instrumented outer ligament cracks and instrumented referee holes are illustrated in Figures 6-3, 6-4, and 6-5.

Systems tunnels were removed from the aft center segment and partially removed from the aft segment for this test.

The nozzle-to-case joint was formed by bolting the HPM nozzle fixed housing into the aft dome with 100 axial bolts. The field joints had a standard HPM

T-ring

Stub Flange

A032010a

Forward
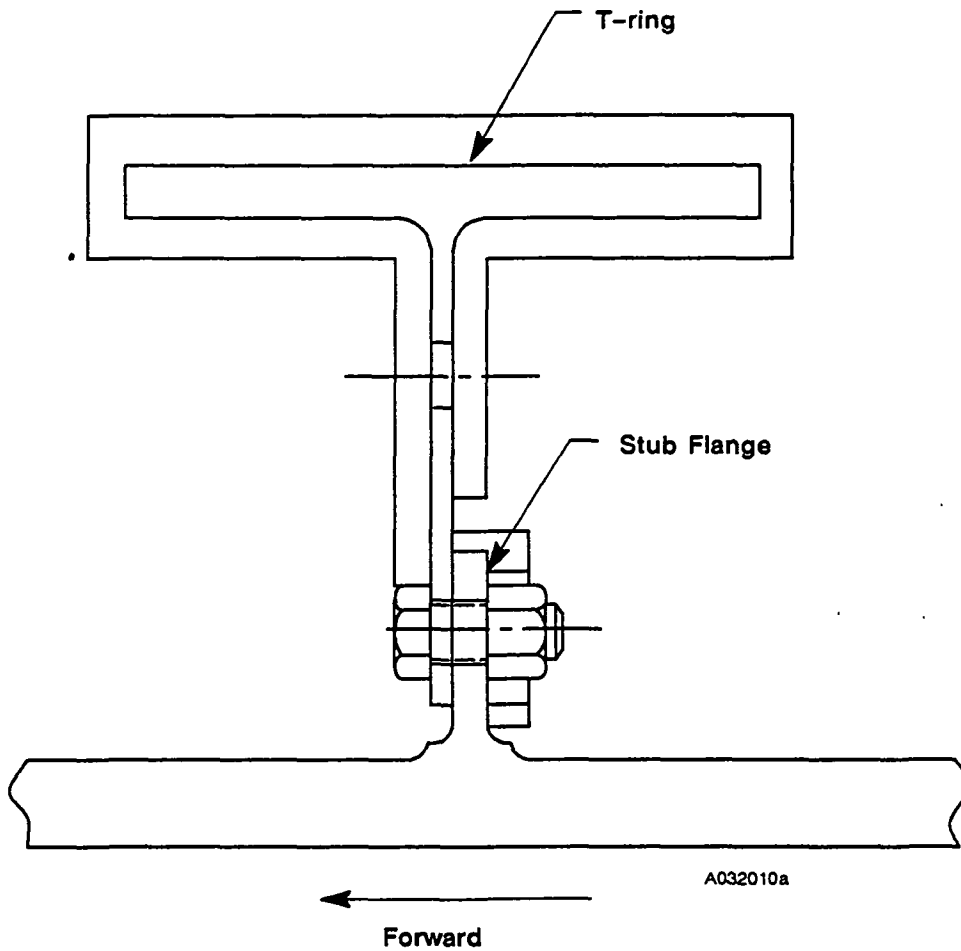
Figure 6-2. TEM-7 T-ring Configuration

Outer Ligament Crack

Strip Gage

Cracked Hole

Aft Stub: 276 Deg
Aft Stub: 280 Deg
Forward Stub: 232 Deg

Shims

Strip Gages

Referee Hole

Aft Stub: 148 Deg
Aft Stub: 152 Deg

Shims

Stiffener Flange   A029978a

Forward

Note: All gages oriented to measure hoop strains
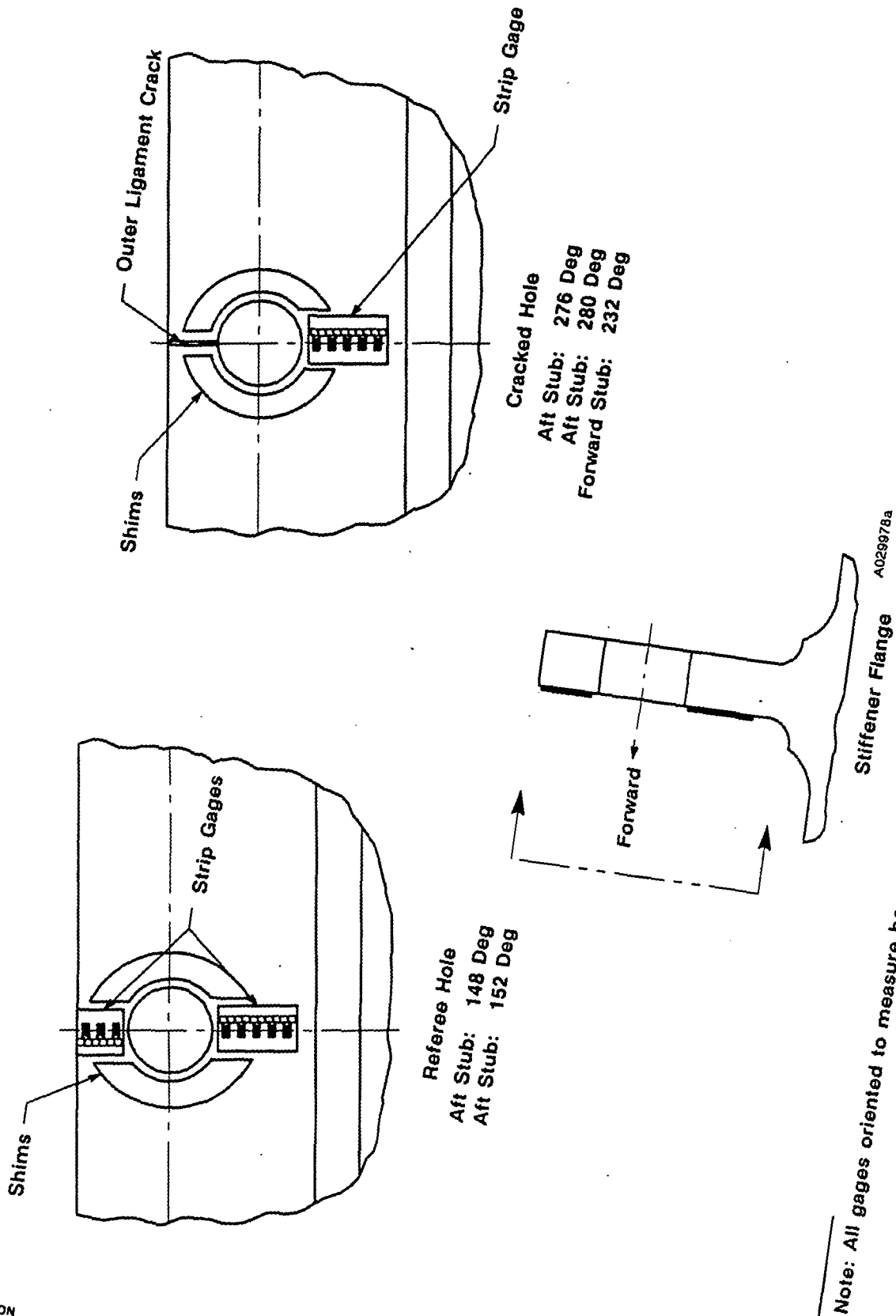
Figure 6-3. Stiffener Stub Outer Ligament Cracks and Instrumentation

Outer Ligament Crack

Single High–Strain–
Capacity Gages

Shim

Cracked Hole

Aft Stub: 240 Deg
Aft Stub: 278 Deg
Aft Stub: 282 Deg

Single High–Strain–
Capacity Gages

Shim

Referee Hole

Aft Stub: 146 Deg
Aft Stub: 150 Deg

Shim

Forward

Stiffener Flange

A029978a

Note: All gages oriented to measure hoop strains
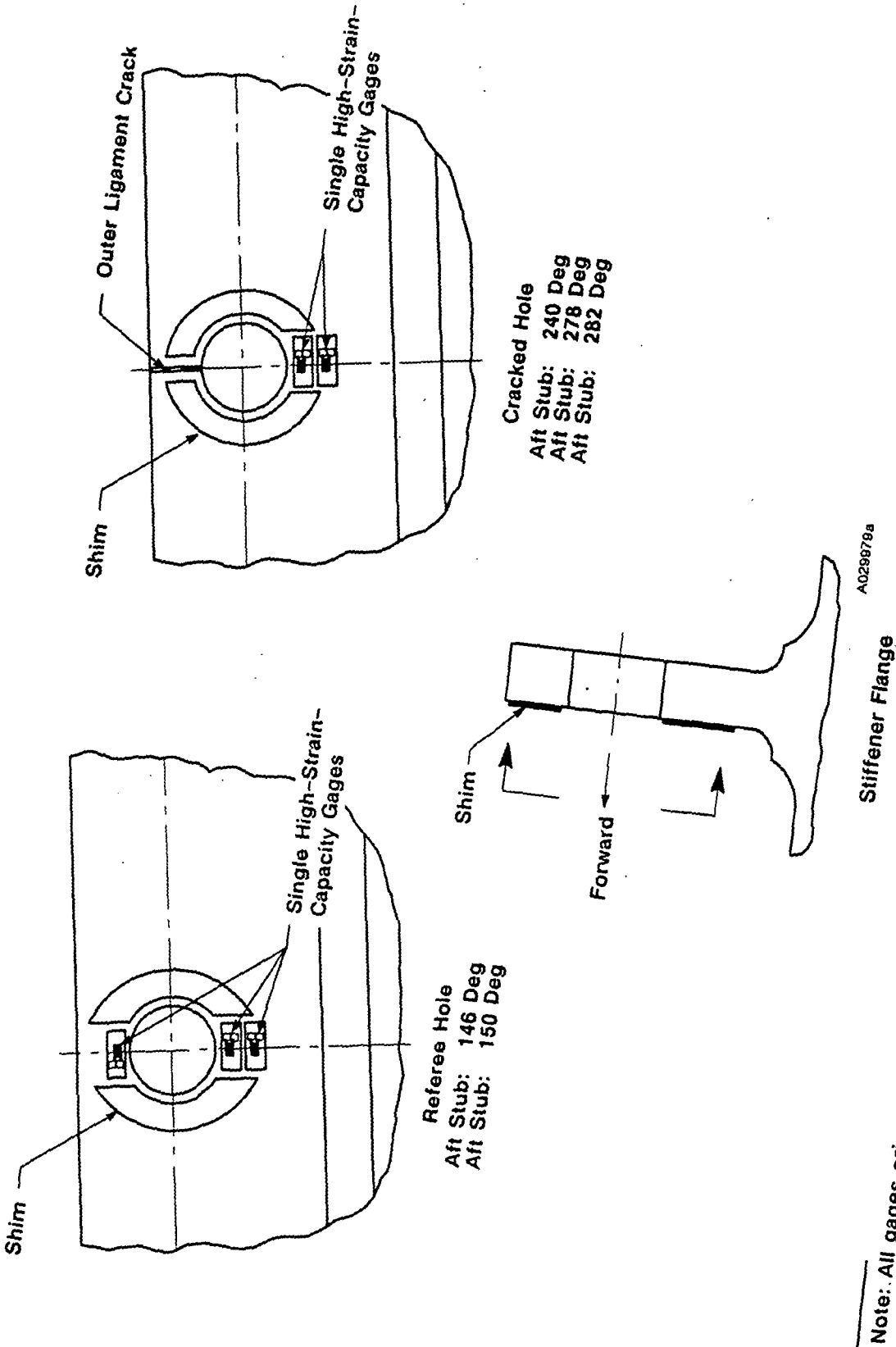
Figure 6–4. Stiffener Stub Outer Ligament Cracks and Instrumentation

Single High-Strain-
Capacity Gage

B – B
Aft Stub: 330 Deg

A029980a

Stiffener Flange

Forward

Referee Hole
A – A
Aft Stub: 330 Deg

Note: All gages oriented to measure hoop strain
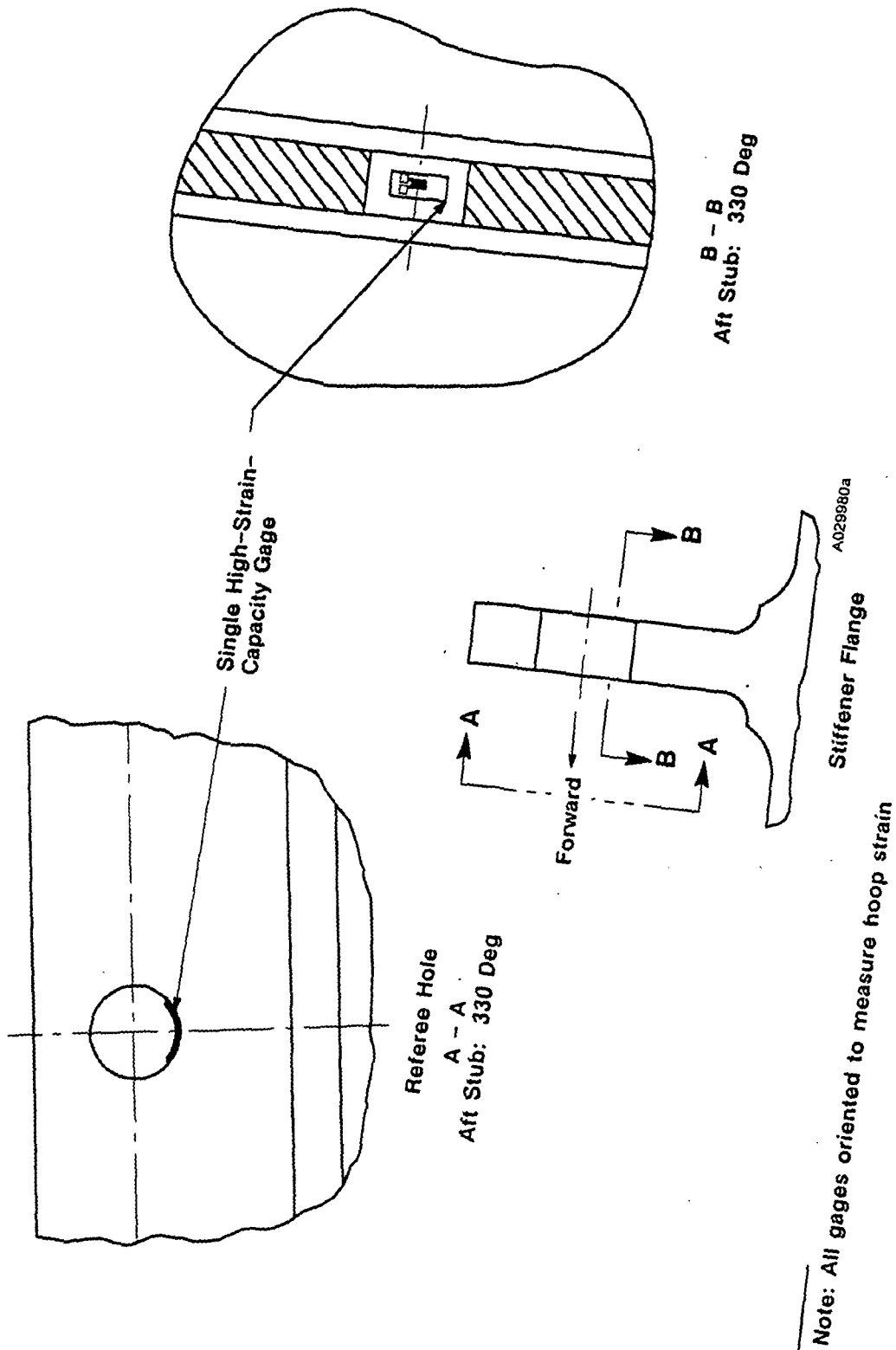
Figure 6-5. Stiffener Stub Outer Ligament Cracks and Instrumentation

insulation configuration, as shown in Figure 6-6. The nozzle-to-case joint had the standard HPM nozzle joint insulation configuration, as shown in Figure 6-7.

The assembly and joint configuration were as follows:

A. The forward segment and forward center segment were mated to form the forward field joint. The forward center segment and aft center segment were mated to form the center field joint. The aft center segment and aft segment were mated to form the aft field joint. The field joints which connected these segments were configured with:

- Tang and clevis with long pins (Drawing 1U51055), custom-fit shims (Drawing 1U51899), and hat band pin retainers (Drawing 1U82840).
- Standard HPM insulation configuration with putty joint filler (STW4-3266), as shown in Figure 6-6.
- Primary and secondary O-rings were fluorocarbon (STW4-3339).
- Leak check port plugs (Drawing 1U100269)
- Improved field joint heater (Drawing 1U77252).
- Baseline TEM field joint protection system (Drawing 7U77328).

B. Factory joints were configured with the following:

- HPM tang and clevis hardware design.
- Insulation overlaid and cured over interior of the joint.
- HPM pin retainer centered over the short (HPM) pins. Standard shim clips were used between the clevis outer leg and the tang outside diameter (OD).

C. The nozzle to case joint was configured with:

- Primary (larger diameter RSRM) and secondary O-ring seals were fluorocarbon (STW4-3339).
- Standard HPM nozzle joint insulation configuration with putty joint filler (STW4-3266), as shown in Figure 6-7.
- RSRM-configuration ultrasonic preload axial bolts installed in accordance with Drawing 7U76882.

A017952aR1

NBR Inhibitor

Inmont Canada Putty

NBR

Castable Inhibitor

Propellant

NBR

CF/EPDM (center segment only)

NBR

Heater

Sensor

Cork

Teflon® Tape

Strap
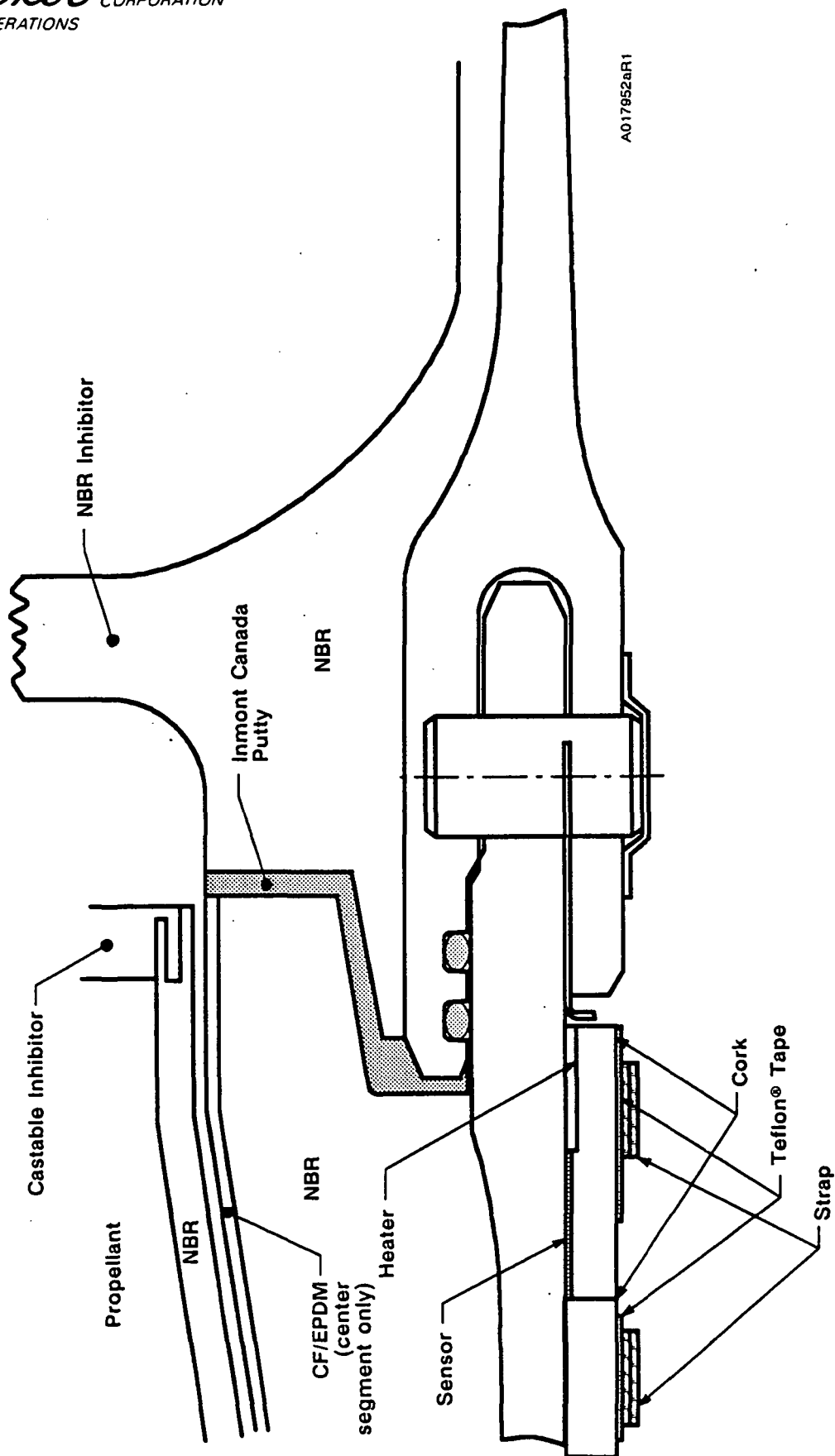
Figure 6-6. TEM-7 Field Joint Configuration
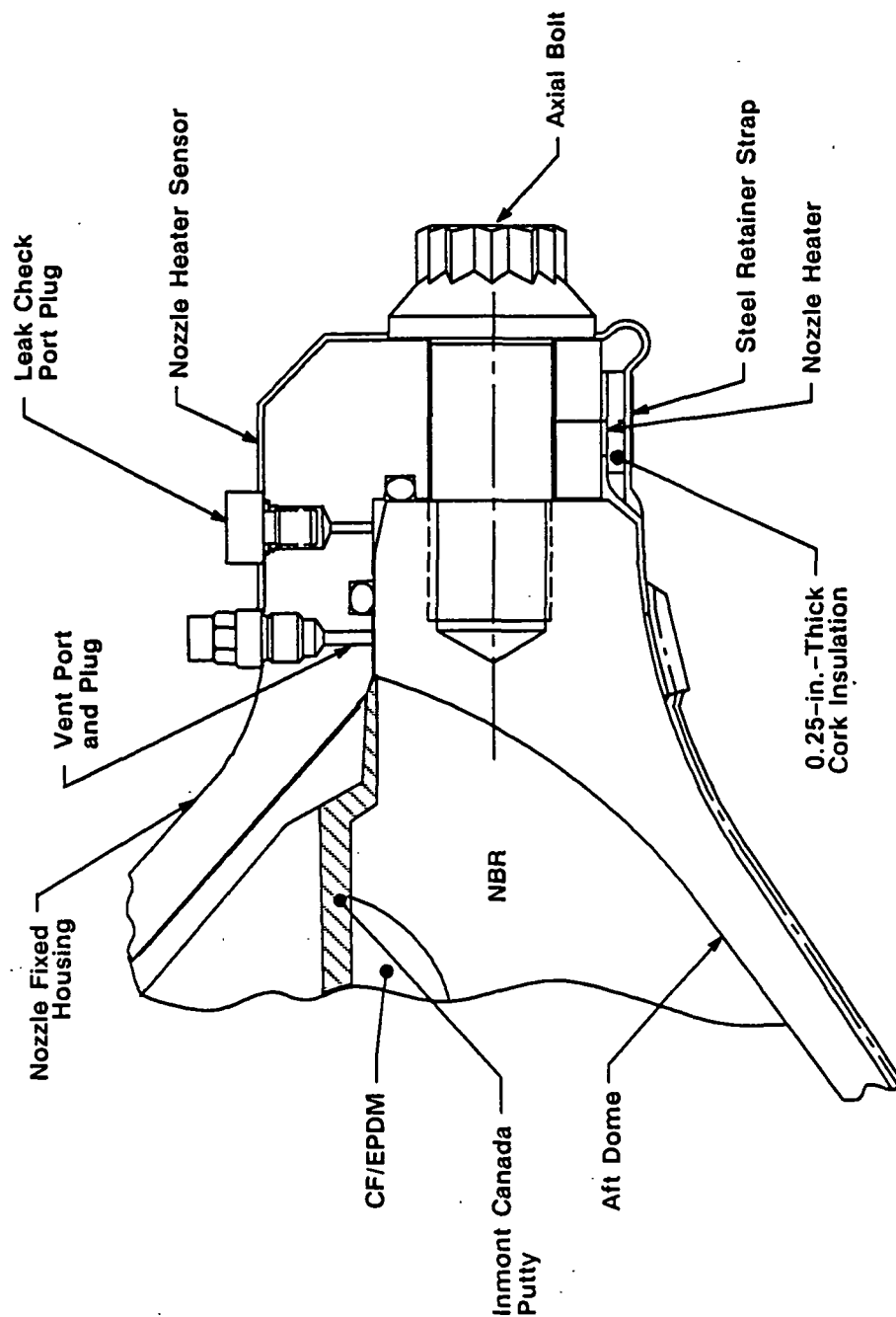
Figure 6-7. TEM-7 (HPM modified) Nozzle-to-Case Joint Configuration

- MS16142 vent ports at 15, 105, 195, and 285 deg in the fixed housing (7U76865-02) upstream of the primary O-ring.
- Adjustable vent port plugs and closure screw (Drawings 1U76425 and 1U50159).
- Leak check port plug (Drawing 1U100269).
- Redesigned nozzle-to-case joint heater (7U77118-04).

D. Igniter-to-forward dome joint was configured with:

- Primary and secondary seals of the outer gasket (Drawing 1U51927) are fluorocarbon.
- Improved igniter-to-case joint heater (Drawing 1U77253).
- Putty joint filler (STW4-3266).
- Ultrasonic bolts (Drawing 1U76598) inner and outer bolt circle.

Corrosion protection consisted of full external paint and a film of grease applied as specified in Drawing 7U76881 and STW7-3688 (including O-rings, sealing surfaces, and pin holes).

Case assembly procedures proved adequate, and chamber pressure was contained during the static test.

6.3.2 <u>Objectives/Conclusions</u>

The objectives and corresponding conclusions from Section 2 regarding case performance were:

<u>Objective</u>	<u>Conclusion</u>
F. Recover case and nozzle hardware for RSRM flight and static test programs.	Case and nozzle hardware is available for refurbishment.
M. Obtain additional data on the performance of the aft stiffener segment with known outer ligament cracks in the stiffener stubs.	The instrumented stiffener stub holes strain gages all recorded data except for the lone referee strain gage mounted inside a stiffener stub hole. There was a large variation between measured and predicted strains at holes with outer ligament cracks. Measured strains at holes with intact outer ligaments correlated well to predicted strains.

6.3.3 Recommendations

It is recommended that the immediate future of stiffener stub testing be refocused around a hydroproof-type test setup. This would offer several distinct advantages:

1) Slower pressure rise rates
   a. Allows much better strain gage performance evaluations.
   b. The nonlinear stress/strain behavior at onset of yielding would be easier to define.
2) A matrix of tests could be performed on the same test setup, including:
   a. T-ring installed versus nonring comparisons, to help determine possible ring influences.
   b. Instrumenting and proof testing a new (never proof tested) segment; monitor initial plastic strains at intact holes.

These types of tests would help to substantiate some of the theories covered in this report and help to fully understand the seemingly erroneous data measured on several of the severed outer ligament holes during the TEM-7 firing.

TEM aft segments should have T-rings installed on stiffener stubs with known outer ligament cracks to minimize risks associated with this condition.

6.3.4 Results/Discussion

6.3.4.1 Cracked Stiffener Stub Holes

Special Issue (TWR-61209, Para 3.2.1, Item 1)

The TEM-7 static test provided an opportunity to gain information concerning the behavior of stiffener stub outer ligament cracks during an actual motor firing. Thiokol Corporation has decided not to allow RSRM stiffener case segments with outer ligament cracks into the flight rotation. This decision was based in part on a lack of knowledge about the structural effect of the severed outer ligament on the T-ring/case assembly. In an effort to help fully understand this interaction, the

severed stub holes as well as several intact stub holes were instrumented with strain gages to help characterize the strain gradient at the holes. This testing was requested to help verify analytical models of the region and to provide a better overall understanding of the problem.

The testing was successful, with only one of the 44 channels of stiffener stub instrumentation being lost during the test. Each of the gages appears to have performed well, following the pressure trace and returning fairly close to the zero mark at the completion of the firing. The maximum measured strain at an intact hole was 5,600 microstrain, while the maximum strain at a severed hole was measured at 7,250 microstrain. The strains were generally less than anticipated, and several unusual data points were found. The strain-versus-pressure plots for each gage (by gage number) have been included in Appendix D. Drawing 7U77011 provides a convenient cross reference for gage number versus gage locations.

The testing has provided further insight into the behavior of the intact as well as the severed outer ligaments of the stiffener flange hole. The severed hole and the intact hole are fairly well characterized by the elastic strain predictions. This indicates that the local residual compressive strains induced in the material during proof test seem to limit the subsequent test/flight load strains within the elastic range. Formalized documentation of analogue and X-ray diffraction tests need to be completed to add further credibility to this theory.

The test also establishes that more work must be performed to totally understand the problem. All predictions, even the elastic strain predictions, were inflated. Data points from several of the holes are, at this point, unexplainable, and more testing is required before the results can be totally discounted.

Strip-type strain gages were used to provide added definition to the rapidly changing strain gradient around stiffener stub holes. Conservative predictions showed strains approaching the maximum capacity of the strip strain gages; therefore, several

holes were instrumented with higher capacity single gages strategically positioned to envelope the possible high-strain regions. The distance of the gage from the hole was measured and recorded to provide improved accuracy. In all cases the gages were installed on the forward face of the stub flange, which models have indicated to be the maximum stress region. Shims were installed between the T-ring and stub to prevent the ring from crushing the gages during T-ring installation and internal pressure loading. Figure 6-8 shows the instrumentation layout by illustrating typical gage locations for severed as well as intact outer ligament holes.

All gages were oriented to measure hoop strains. The severed holes had gages on the inboard side of the holes only, while the intact holes had both inboard and outboard gages. The outboard gages on the intact holes provide additional information on how loads are redistributed around the severed outer ligament. The test configuration and instrumentation are defined in detail on Drawings 7U76881 and 7U77011, respectively.

<u>Predictions</u>

Several finite element models have been prepared to evaluate this region of the motor case:

1.   Intact outer ligament
     a.   3-D Elastic
     b.   3-D Plastic
2.   Severed outer ligament
     a.   2-D and 3-D Elastic
     b.   3-D Plastic

The models were prepared using minimum material properties for the case and ring, as defined in TWR-18011 RSRM Structural Materials Properties Book. Each also assumes that, maximum expected operating pressure (MEOP) is reached during the test. The models include the T-ring and attachment hardware as in the test
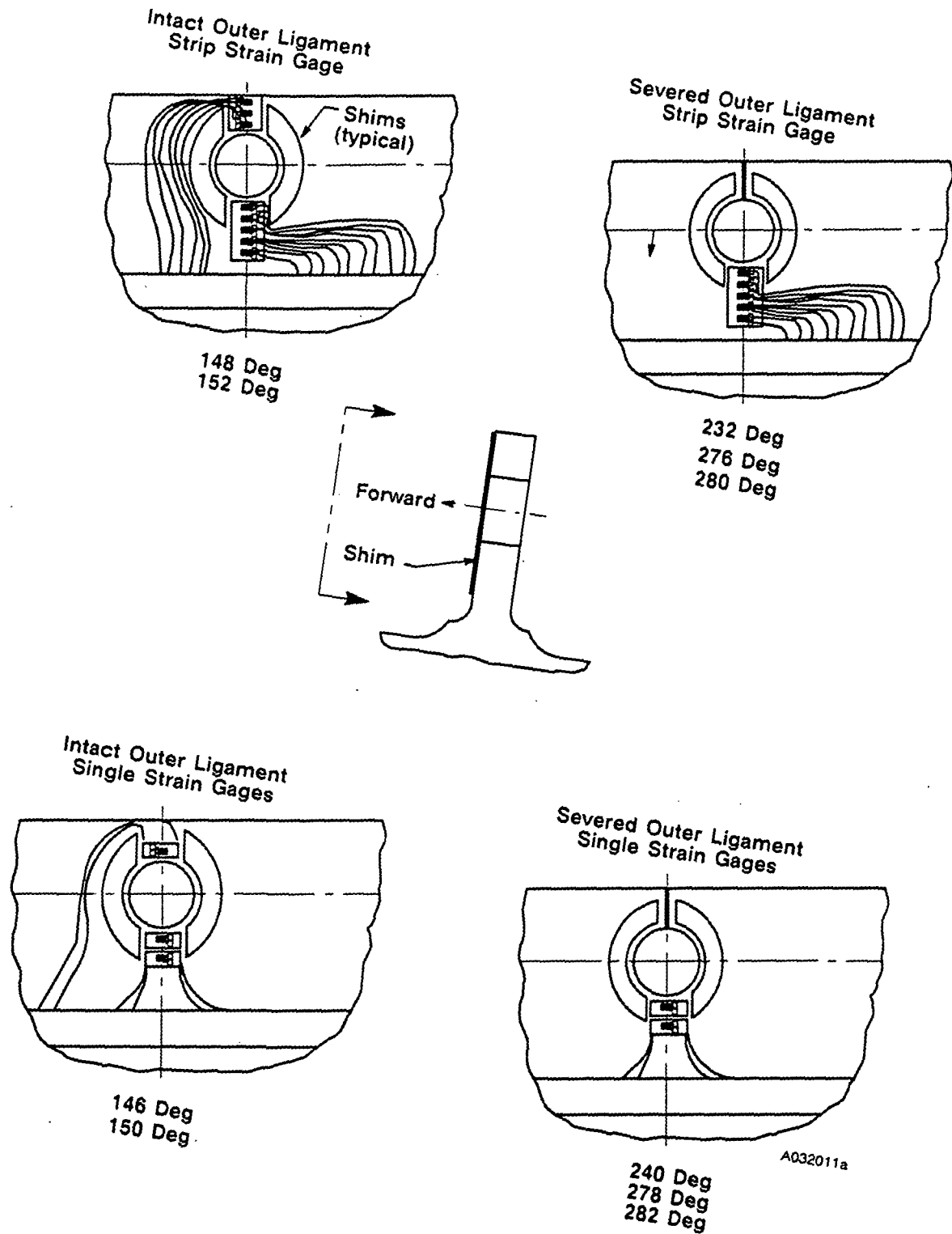
Figure 6-8. Stiffener Instrumentation Configuration

hardware. The interface load is transmitted between the T-ring and the stub through the attach bolts, utilizing gap elements at the ring to stub interface.

The 2-D analysis was chosen for the severed outer ligament elastic predictions because the boundary conditions in the 3-D analysis assume that a crack exists at every hole. This was originally thought to be conservative. However, having a crack at every hole does not permit the load to be channelled through any of the outer ligaments; thus, the stress concentration is not properly realized at the hole. For the intact hole the problem is symmetrical and this concern does not exist; therefore, the 3-D predicted values have been used. To illustrate the changing strain field at the hole, color plots of the results of the elastic analyses (intact and severed holes) are included in Figures 6-9 and 6-10.

Data Evaluation

As alluded to earlier, the overall trend was that strains were much lower than originally anticipated. The measured strains on the intact hole did, however, match more closely with the predicted elastic strains. The severed hole strains fell below the elastic predictions and were much less than the elastic-plastic strain predictions. To illustrate this result, the predicted elastic and elastic-plastic strains have been graphed over the maximum measured strains for both the intact and severed outer ligament holes in Figures 6-11 through 6-14. Since the analytical predictions were based upon reaching MEOP, the data were scaled (by linear interpolation) to reflect the TEM-7 actual headend pressure of 933.5 psig. This resulted in a pressure scaling factor of 0.928.

It should be noted that while all of the models predicted plastic behavior at the edge of the hole for both the severed and intact holes, the models also assumed a zero-stress state at the start of the test. Analogue tests and X-ray diffraction examination have shown in a separate test effort (yet to be formally documented) that the holes, especially the cracked holes, have local residual stresses induced after

ANSYS 4.4A
FEB 18 1991
14:23:28
PLOT NO.   1
POST1 STRESS
STEP=1
ITER=20
EPY (AVG)
SMN =0.612E-03
SMX =0.00895

0.612E-03
0.001153
0.00171
0.002267
0.002824
0.003381
0.003938
0.004495
0.005052
0.005609
0.006166
0.006723
0.00728
0.007837
0.008393
0.00895

OUTBOARD

INBOARD

Figure 6-9. Centroidal Strain—Without Outer Ligament Crack

ANSYS 4.4A
FEB 18 1991
13:23:43
PLOT NO. 1
POST1 STRESS
STEP=1
ITER=20
EPY (AVG)
DMX =0.276897
SMN =-0.197E-03
SMX =0.013223

-0.197E-03
0.686E-03
0.001582
0.002477
0.003373
0.004268
0.005164
0.006059
0.006955
0.00785
0.008746
0.009641
0.010537
0.011432
0.012328
0.013223
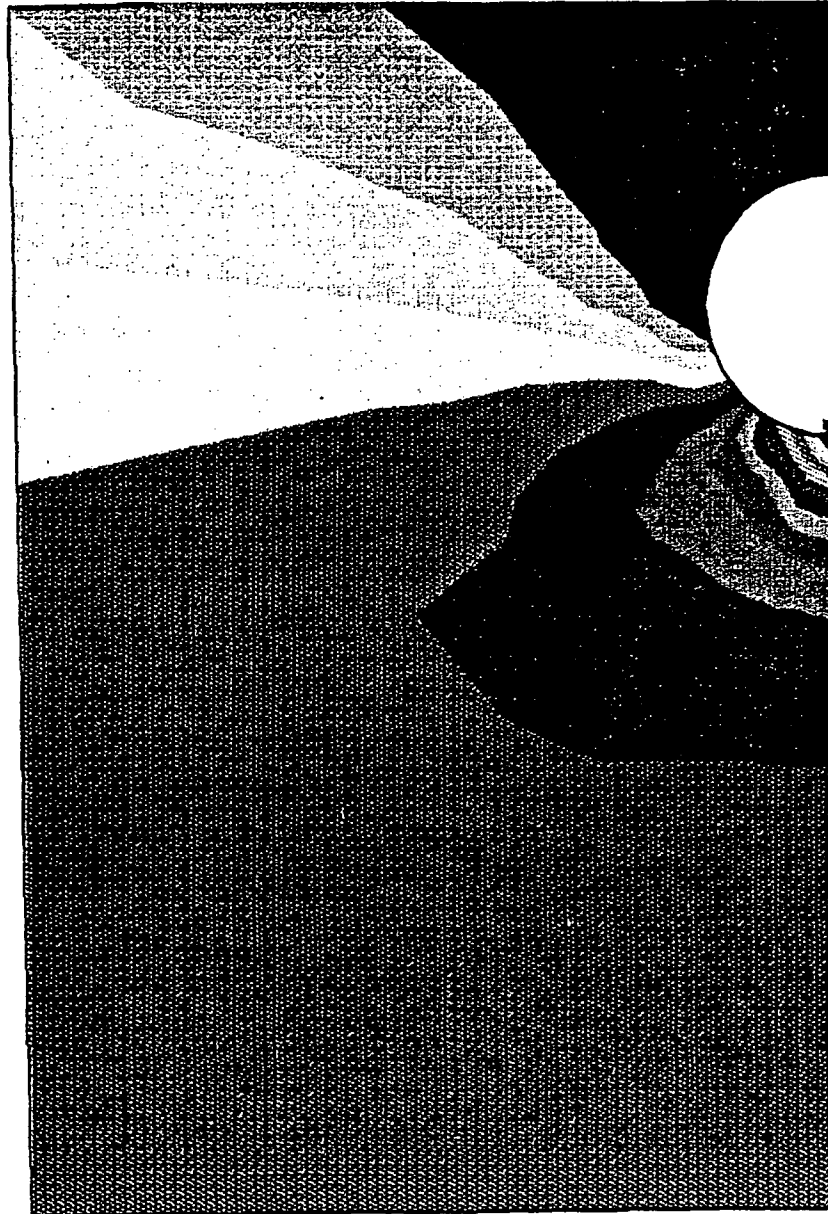
OUTBOARD

INBOARD

Figure 6-10. Centroidal Strain—With Outer Ligament Crack
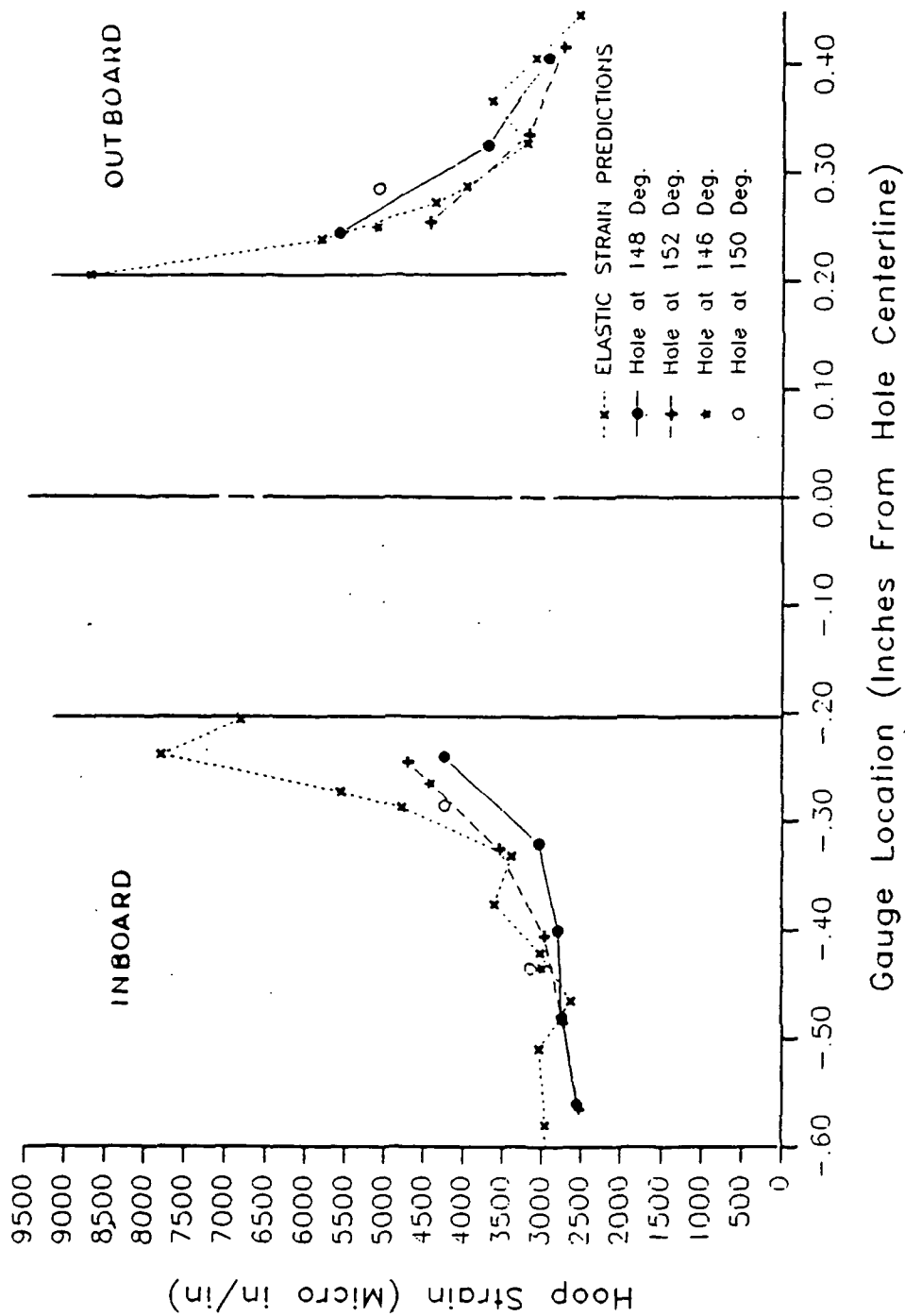
Figure 6-11. Measured Versus Predicted Elastic Stiffener Flange Strains (hoop)—Intact Outer Ligament
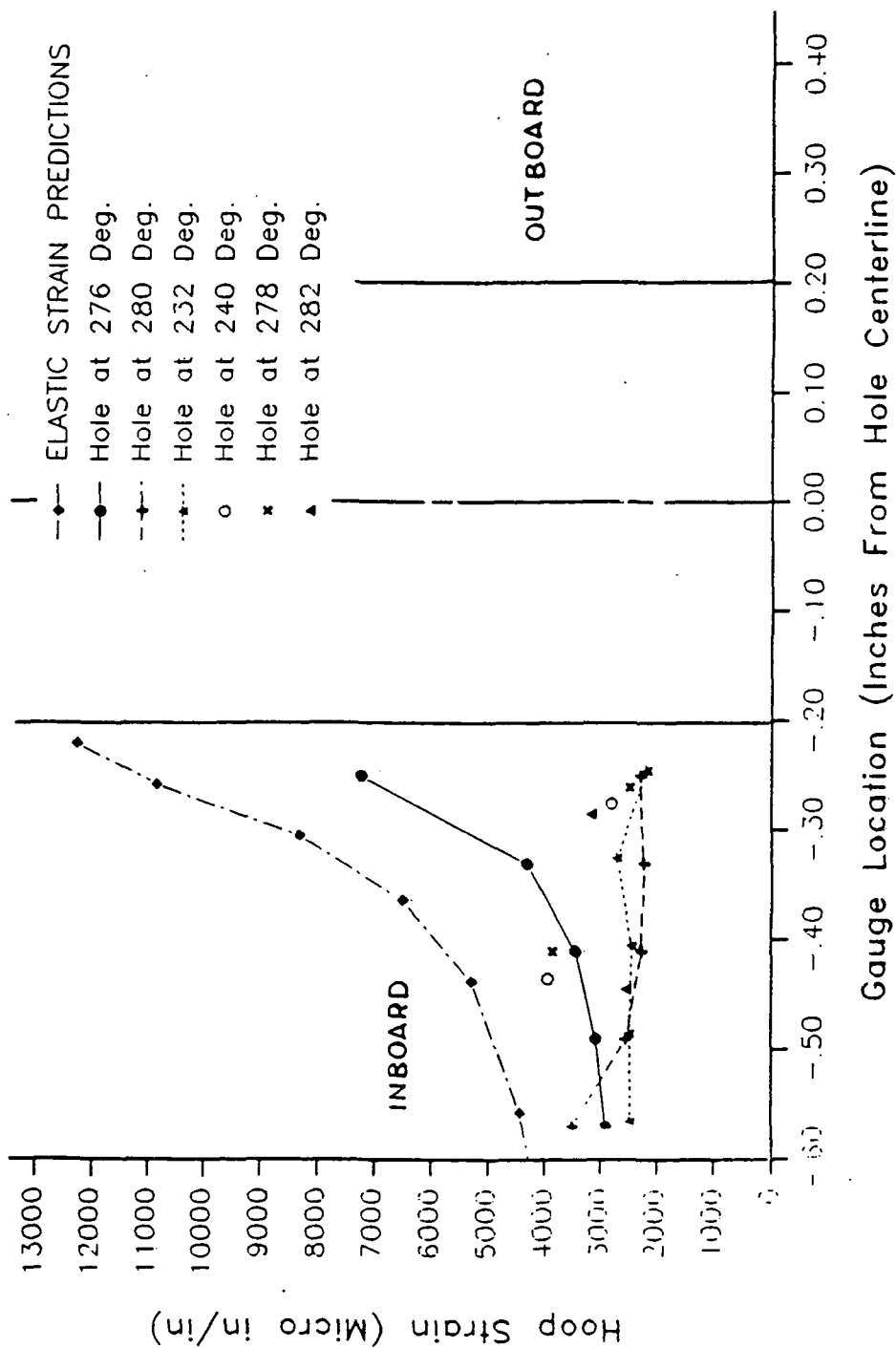
Figure 6-12. Measured Versus Predicted Elastic Stiffener Flange Strains (hoop)--Cracked Outer Ligament
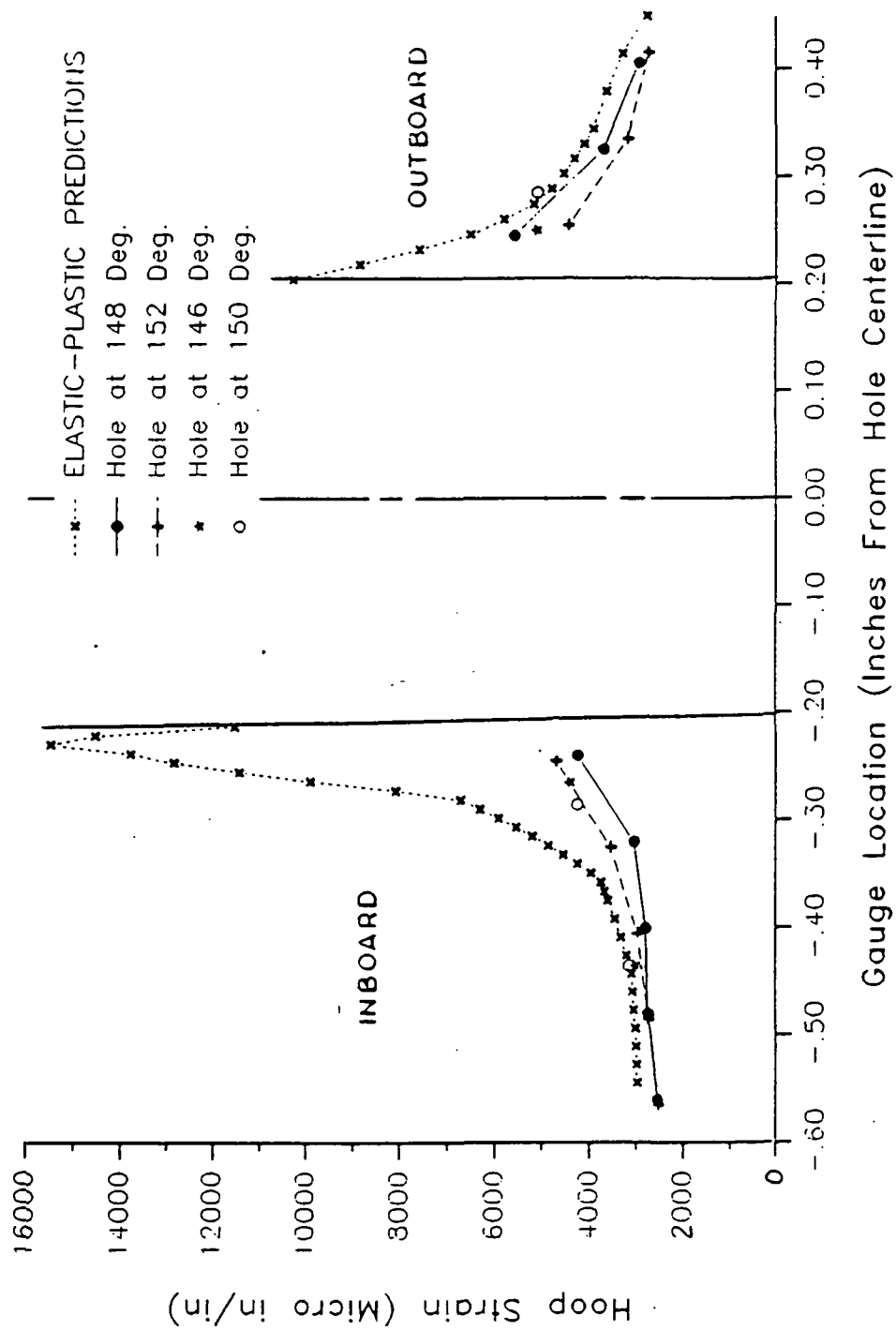
Figure 6-13. Measured Versus Predicted Plastic Stiffener Flange Strains (hoop)—Intact Outer Ligament
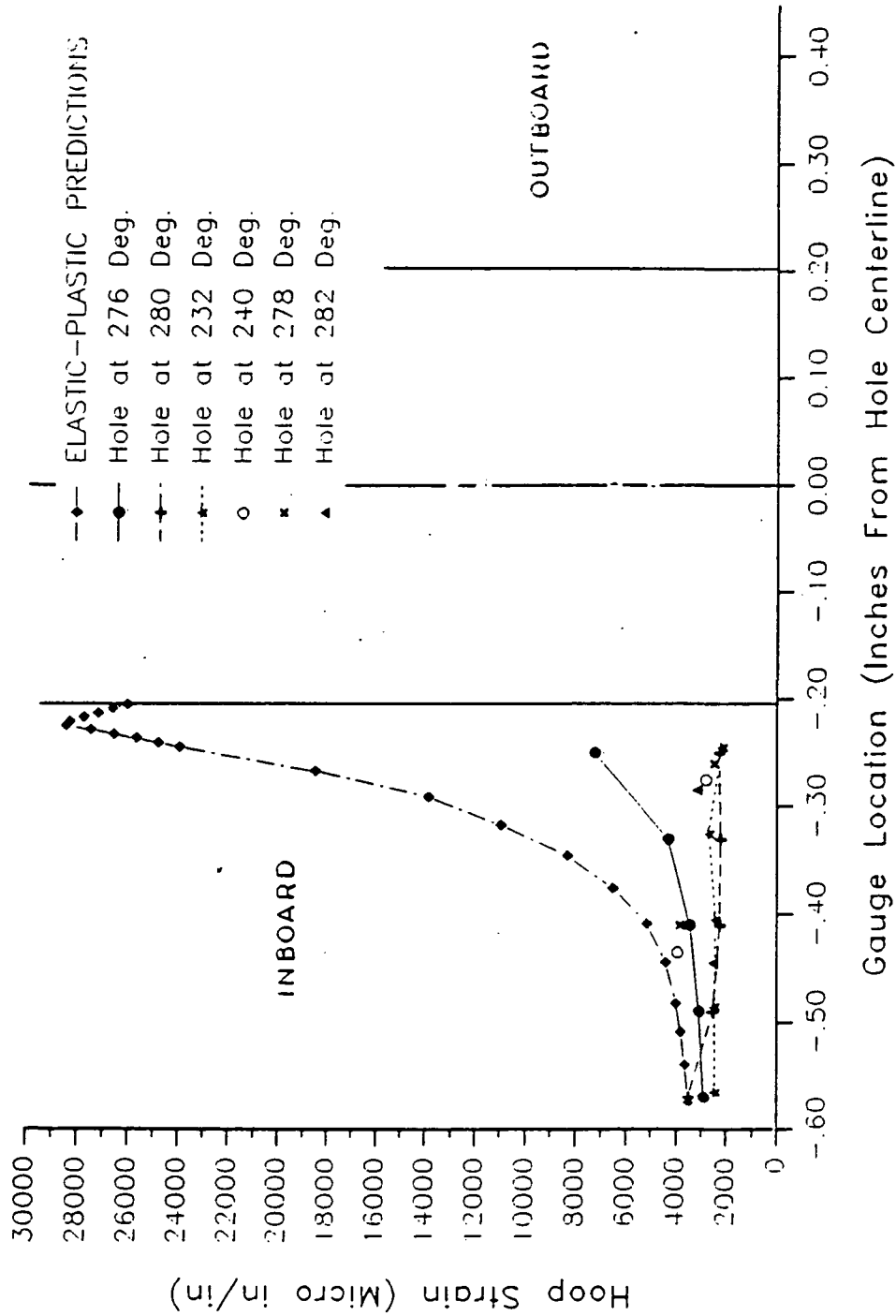
Figure 6-14. Measured Versus Predicted Plastic Stiffener Flange Strains (hoop)–Cracked Outer Ligament

splashdown damage and proof test. The analogue tests also appear to show that despite the prehydro residual stress state (tensile or compressive), the posthydro stresses are compressive and sometimes quite large. The local compressive residual stress at the cracked hole is most likely large enough to ensure that the entire next load cycle (in this case the test) will take place entirely within the elastic range of the material. Figure 6-15 illustrates this concept for a single-yield and postyield load cycle. In reality, however, after several uses these holes may have had numerous yield and postyield cycles.

The previously mentioned testing indicated that the local compressive stresses at the cracked hole may be large enough to induce reverse yielding in the material. Reverse yielding may cause degradation of the material properties at this local region. These results are to be documented and elaborated upon in a future report. This overall effect would explain the large overprediction of strains using the plastic analysis and the reasonable accuracy when compared to elastic strain predictions. The results of this test seem to confirm the analogue testing. However, more work is required to verify this conclusion.

The gages on a number of the severed outer ligament holes resulted in very peculiar output (278, 280, 232, and 240 deg). The strains were very low, compared even with the elastic predictions. Several of these holes also indicated a reverse stress gradient, or, in other words, showed stresses increasing with distance away from the hole. As mentioned in Section 6, Test Description and Results, these gages (as well as all the others) appear to have functioned properly otherwise. This trend, however, does not reflect common engineering experience. There are, as in any test, a number of sources for possible error in the results. Measures were taken, wherever possible, to minimize the variables effecting the results. However, a few sources of error that are worthy of mention in this test are: gage location measurements, the fact that predictions were based on minimum material properties, and gage accuracy.

1-2: Loading Induces Plastic Strain

2-3: Load Release—Results in Compressive Residual Stress

3-4: Post-Yield Loading—Remains Entirely Within the Elastic Range of the Material
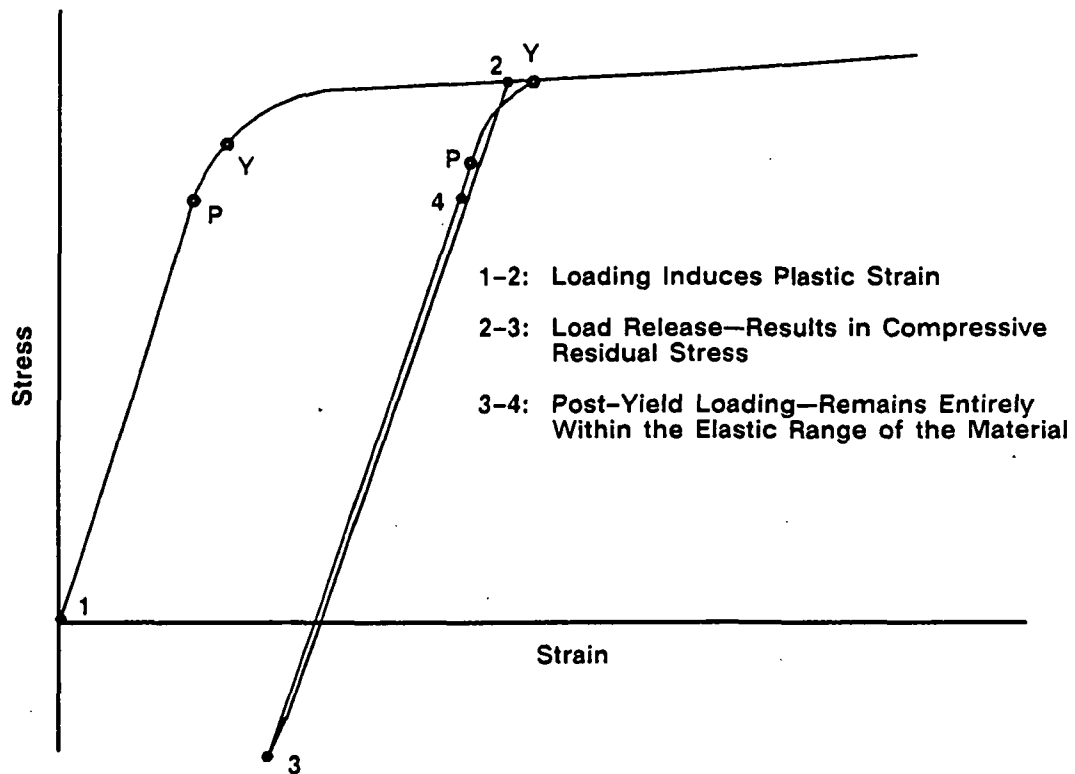
Figure 6-15. Post-Yield Behavior

A032087a

These alone would not be sufficient to explain the oddities described in the data above. Therefore, the data have not yet been totally discounted, and further testing is required before invalidating these results.

All seven cracked stiffener stub holes were visually examined after the test for new cracks and/or deformation. On several holes (240, 278, and 280 deg), deformations were noted to exist on the aft face of the flange (near the hole). It was determined that this condition was a result of a previous usage and not a result of this test. No new cracks were detected by visual inspection. A gouge was found on the 240-deg hole on the aft flange. The gouge was located at approximate center of the flange cross section and raised metal exists. The exact cause of this condition is not known; however, there is no indication that it was caused by the static test.

6.3.4.2 Forward Field Joint. The TEM-7 forward field joint was disassembled on 16 Jan 1991. Light corrosion was observed in and around the leak check port hole and on the case at the joint heater region at 280 through 294 deg. Typical pin hole slivers were found intermittently around the circumference of the clevis and tang pin holes. This is caused by installation of the pins at assembly. Putty was observed in intermittent contact with the primary O-ring for approximately 60 percent of the joint. Putty in contact with the primary O-ring is a typical condition. The grease on the O-rings and sealing areas was as prescribed in STW7-3688. No anomalous conditions were observed.

6.3.4.3 Center Field Joint. The TEM-7 center field joint was disassembled on 14 Jan 1991. The condition of the joint was nominal. No hot gas or soot reached the primary O-ring. No damage was found on the primary or secondary O-rings while in the groove. No corrosion was observed on the tang or clevis joints. Typical pin hole slivers were found intermittently around the circumference of the clevis and tang pin holes. This is caused by installation of the pins at assembly. The grease on the O-rings and sealing areas was as prescribed in STW7-3688. Putty was found over the

full circumference up to, but not past, the primary O-ring. The leak check plug and port were in nominal condition.

6.3.4.4 Aft Field Joint. The TEM-7 aft field joint was disassembled on 10 Jan 1991. No hot gas or soot reached the primary O-ring. There was no evidence of damage to the O-rings while in the groove. No corrosion was observed on the tang or clevis joints. Pin hole slivers were found at 48, 50, 86, 88, and 228 deg. This is caused by installation of the pins at assembly. The grease on the O-rings and sealing areas was as prescribed in STW7-3688. Putty was found in the leak check through hole obstructing all but a very small portion of the hole. Before port hole assessment the joint had shifted approximately 0.5 inches. (Pin holes were misaligned by approximately 0.5 in. at 0 deg.) The putty apparently extruded into the through hole when the joint shifted because no trace of putty was found on the clevis between the primary and secondary O-rings. PFAR TEM07-05 was written because this condition is outside the engineering limits.

6.3.4.5 Aft Segment Disassembly Assessment. No heat effect or erosion was observed on any of the joint O-rings or metal surfaces. M-clip fretting was observed on each joint. The aft dome-to-stiffener joint had M-clip fretting over the full circumference of the joint. The stiffener-to-stiffener joint had M-clip fretting from 8 through 28 deg. The ET-to-stiffener joint had M-clip fretting over the full circumference of the joint. Medium to heavy corrosion was observed in the ET-to-stiffener joint downstream of the secondary O-ring groove and upstream of the pinholes at 356 through 0 through 4 deg. No other anomalous conditions were observed.

6.4 CASE INTERNAL INSULATION PERFORMANCE

The internal insulation system included case acreage insulation, joint insulation, and propellant stress relief flaps. The insulation material used for these components was an asbestos-silica-filled acrylonitrile butadiene rubber (NBR) (STW4-2621). Carbon-fiber-filled ethylene propylene diene monomer (CF/EPDM) (STW4-2868) was bonded

to the NBR in a sandwich-type construction under the propellant stress relief flaps in both center segments. CF/EPDM was also used in a sandwich construction in the aft dome. The CF/EPDM was installed to reduce the erosion of the insulator near the submerged nozzle in the aft dome and under the stress relief flaps in the center segments.

The liner material specified in STW5-3224 was an asbestos-filled carboxyl terminated polybutadiene (CTPB) polymer which bonded the propellant to the internal insulation in the SRM. The forward-facing full web inhibitors were made of NBR. They were located on the forward ends of the center and aft segments. The aft-facing partial web castable inhibitors were made of a material (STW5-3223) similar in type (CTPB polymer) to the liner. They were HPM configuration and were located on the aft end of the forward and center segments.

6.4.1 Introduction

The four TEM-7 segments had been insulated and cast with propellant more than five years before the TEM-7 static test.

6.4.1.1 Field Joint Assembly. The case insulation of the three HPM-configuration field joints consisted of asbestos-silica-filled NBR (Figure 6-16). Prior to mating, the joints were inspected per STW7-2831, Rev NC, the flight motor insulation criteria for the HPM joints. Putty was applied to the clevis joints per STW7-3746, as shown in Figure 6-17, and the joints were mated. After mating, each joint (Figure 6-18) was inspected from the bore for discontinuities and the putty was tamped.

6.4.1.2 Nozzle-to-Case Joint Assembly. The putty layup for the nozzle-to-case joint, shown in Figure 6-7, was performed to the dimensions of STW7-3745, as were previous TEMs. Figure 6-19 shows the putty layup used throughout the HPM program. The TEM-7 nozzle was mated to the aft segment with no apparent anomalies. Because of inaccessibility, the nozzle-to-case joint was not inspected nor ·tamped as the field joints were.

Propellant

EPDM (center segments only)

Castable Inhibitor

Liner

Flap

NBR
Insulation

Tang

A019851a

NBR
Insulation

O-rings

Clevis

A019851a-3R1
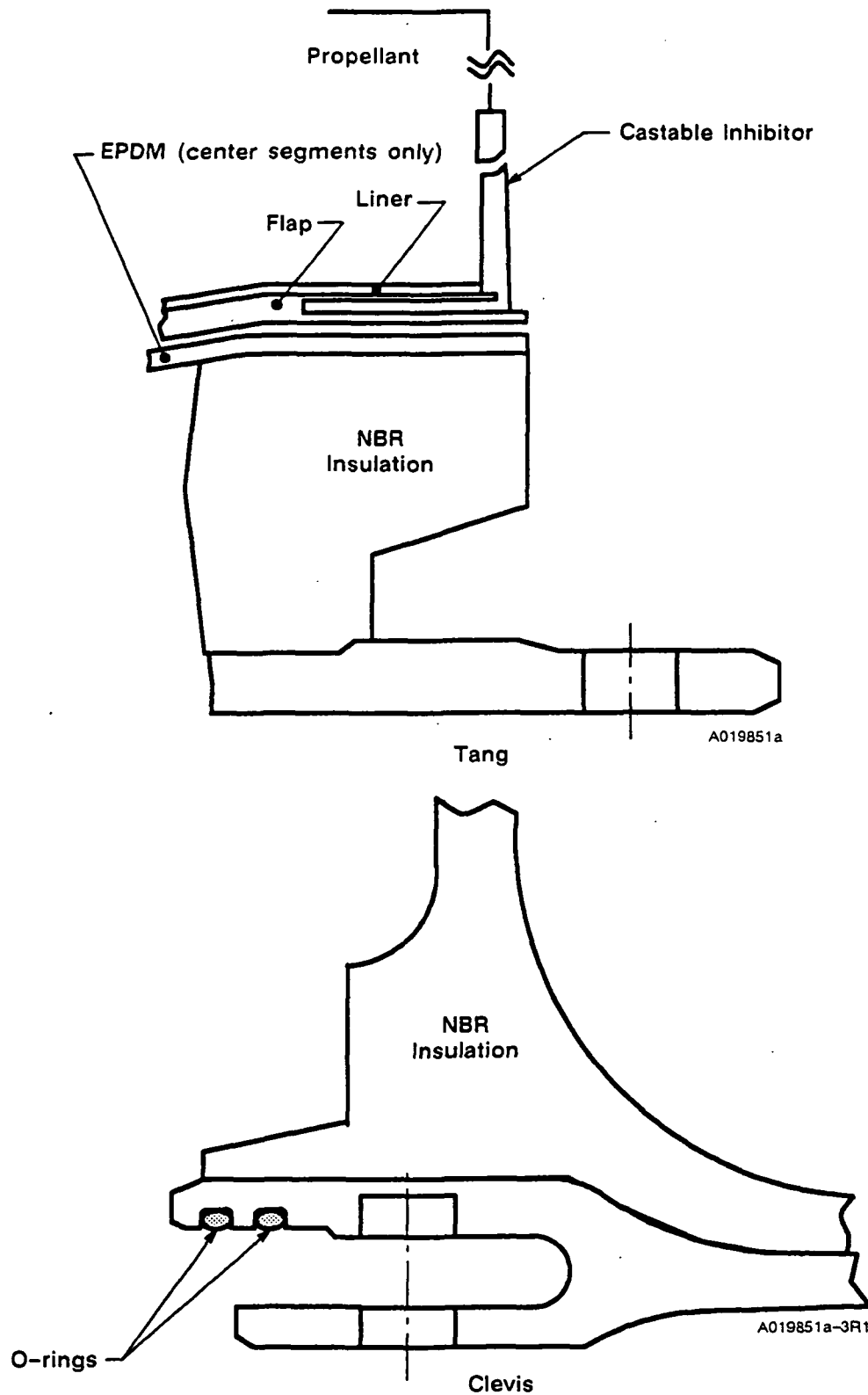
Figure 6-16. HPM Field Joint

0.55
0.45

NBR Insulation

0.50
0.00

0.25
0.20

0.31
0.23

Putty

0.25
0.20

A019851a-2R1

0.15
0.10
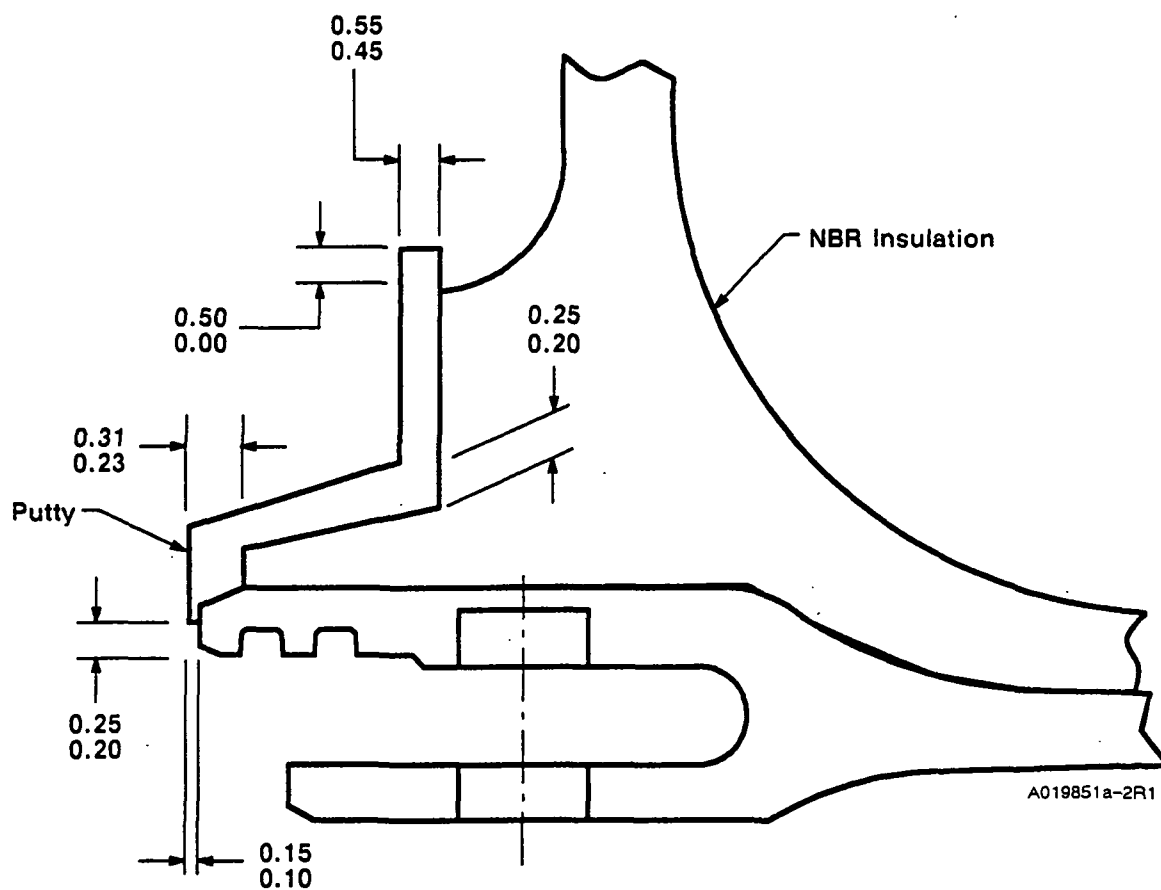
Figure 6-17. Clevis Joint Filler Putty Layup

Propellant

Castable Inhibitor

Putty Squeezeout

Putty Sag

Liner

EPDM (center segments only)

Flap

NBR Insulation

NBR Insulation

A019971a
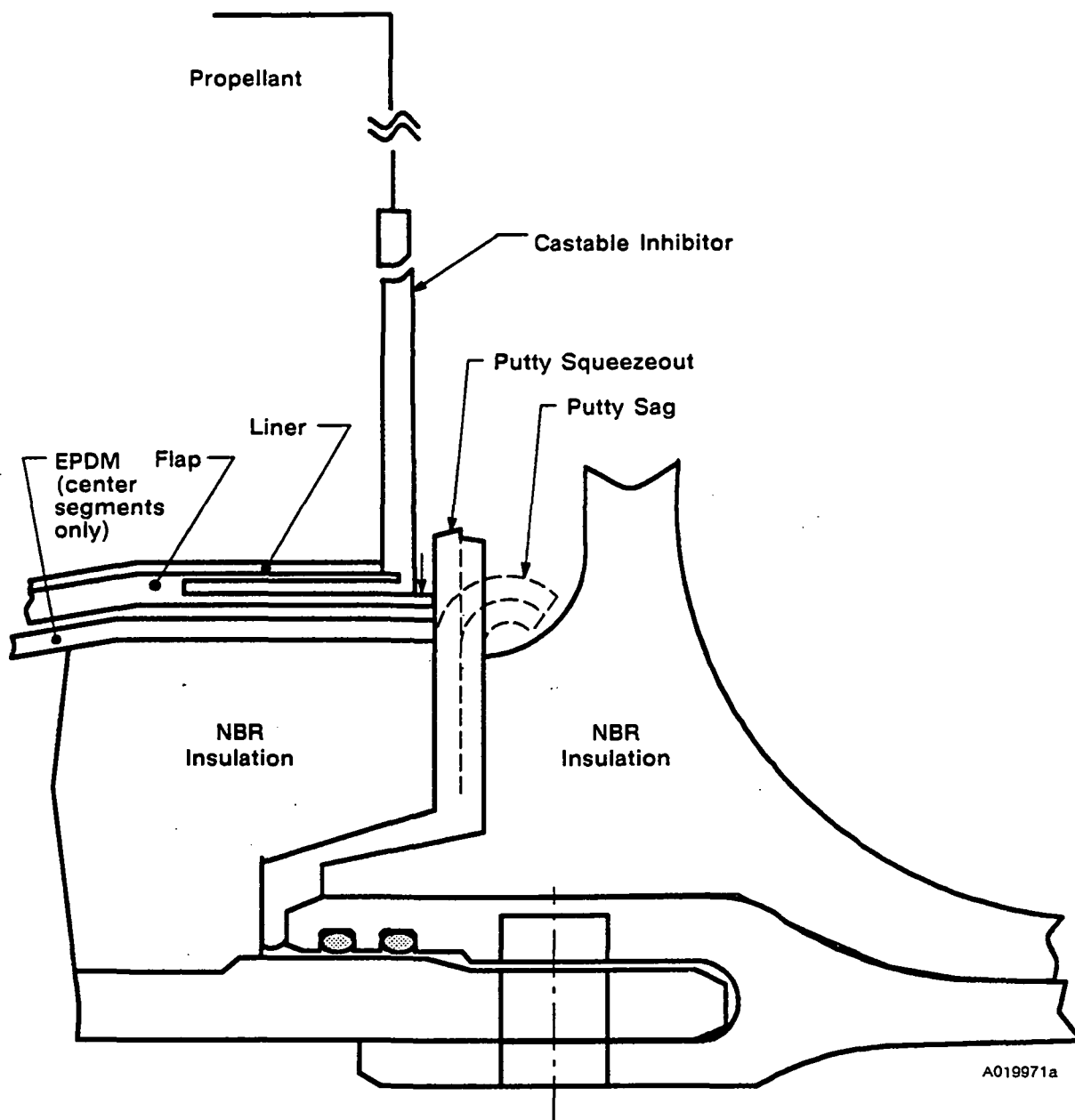
Figure 6-18. Assembled HPM Field Joint
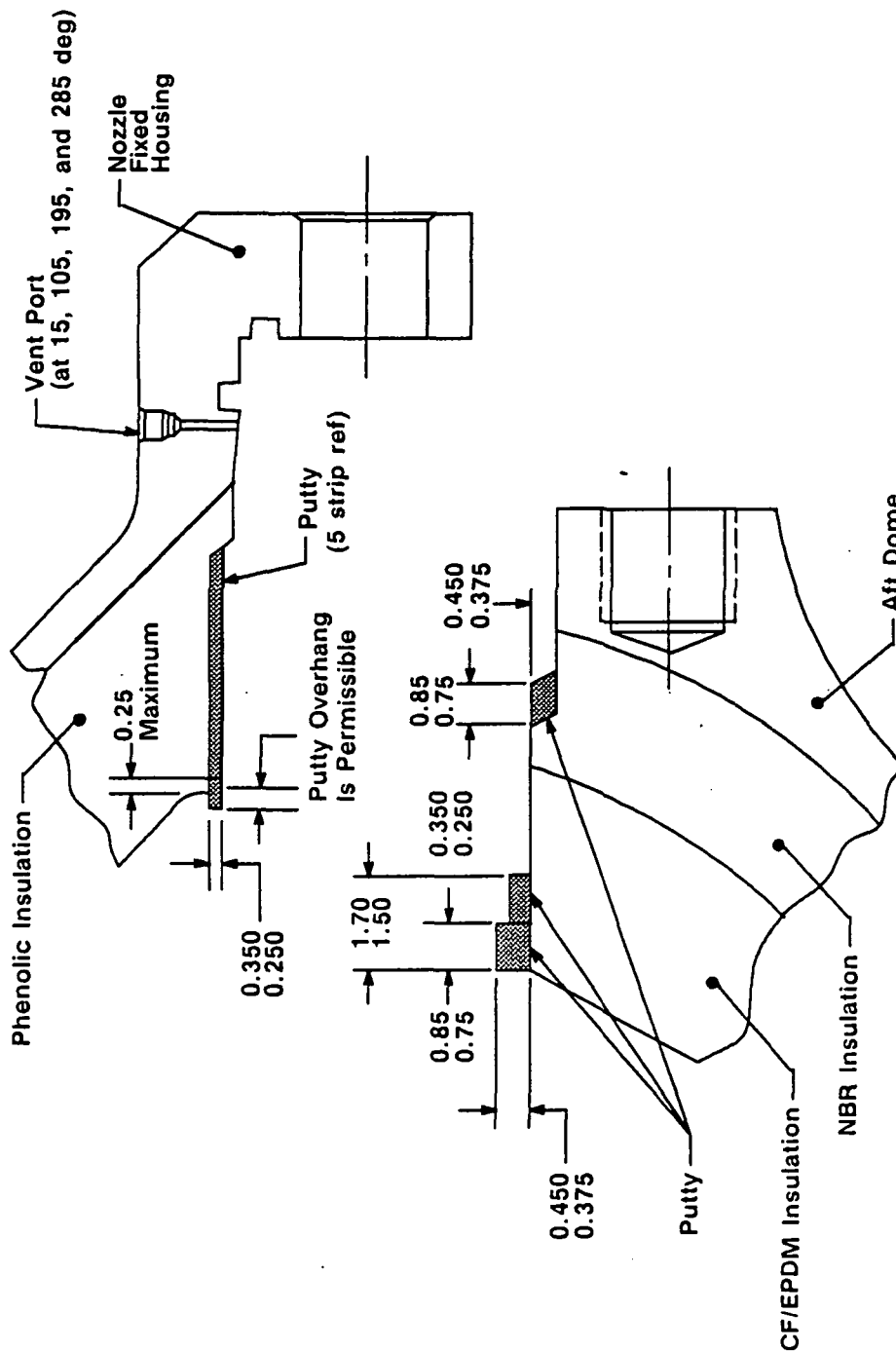
Figure 6-19. TEM-7 (HPM modified) Nozzle-to-Case Joint Configuration—Putty Layup

Similar to TEM-5 and TEM-6, the nozzle-to-case joint incorporated four vent ports in the fixed housing. The vent ports were left open during assembly to exhaust entrapped air from within the joint. This concept was intended to reduce the potential for O-ring damage from gas flow through putty blowholes.

6.4.1.3 Prefire Inspection/Joint Putty Tamping. A prefire bore inspection was performed to assess the putty flow/layup of each field joint. The inspection occurred after the chocks were removed and the final leak check had been performed. This did not include the nozzle-to-case joint, which was inaccessible during this operation. The putty in the field joints was inspected for grease, discontinuities, bubbles, blowholes, etc.

All volcanoes, bubbles, and possible bubbles were tamped closed with a putty tamping tool. No grease contamination was found in any of the joint putty and the field joint putty, condition was nominal. The overall prefire insulation condition of TEM-7 was similar to previous TEMs.

6.4.2 Objectives/Conclusions

There are no objectives from Section 2 concerning case internal insulation. From an insulation standpoint, TEM-7 performed as expected. The performance in all three field joints and nozzle-to-case joint was excellent; no gas penetration to the seals was observed. The joints functioned within the HPM experience.

6.4.3 Recommendations

None.

6.4.4 Results/Discussion

6.4.4.1 Postfire Internal Insulation Inspection. An internal walkthrough inspection was performed. The internal acreage insulation, center and aft segment NBR inhibitors, and stress relief flaps (center and forward segments) appeared to be in normal condition from the walkthrough inspection. A small amount of castable

inhibitor remained attached to the forward center segment flap. Castable inhibitor remained attached intermittently full circumference to the forward segment flap. Two large pieces of castable inhibitor were found lying loose in the middle of the forward and forward center segments. The slag pool extended the full length of the aft segment and 39 in. into the aft center segment. The size of the slag pool and the amount of slag appeared to be typical of previous static test TEMs. The final slag weight in the aft segment was 1,813 lb.

6.4.4.2 Aft Field Joint Insulation. The aft field joint was disassembled and inspected on 10 Jan 1991. The joint insulation and putty were in normal condition, showing normal heat effects, charring, and erosion. The putty exhibited a constant olive green color with normal tack. The putty failure at disassembly was 15 percent adhesive (tang side) and 85 percent cohesive. One terminated blowhole was present at 155 deg measuring 2.1 in. circumferentially by 0.65 in. radially. The blowhole terminated approximately 0.10 in. inboard of the insulation ramp. The gas penetration was between the tang insulation and the putty. Heat effects with slight erosion to the NBR insulation were present on the tang side of the joint in the region of the blowhole. Heat-affected and eroded putty were present on the clevis side. The terminated blowhole is within the experience of the HPM design field joints and had no adverse effect on joint performance. No clevis or tang edge separations were detected. The aft center segment stress relief flap and the aft segment NBR inhibitor were in normal condition. The flap was eroded normally back to the flap bulb full circumference. The NBR inhibitor was eroded uniformly, showing approximately 8 to 10 in. remaining. No tears were present on either the flap or inhibitor.

6.4.4.3 Center Field Joint Insulation. The center field joint was disassembled and inspected on 14 Jan 1991. The joint insulation and putty were in normal condition, showing normal heat effects, charring, and erosion. Gas penetrated into the bondline 0.80 in. maximum outboard of the remaining material on the clevis side from 280 through 0 to 74 deg. Gas did not reach the step in the insulation. The putty

exhibited a consistent olive green color with normal tack. The putty failure at disassembly was 2 percent adhesive and 98 percent cohesive. No clevis or tang edge separations were detected. The forward center segment stress relief flap and the aft center segment NBR inhibitor were in normal condition. The entire flap remained from 270 through 0 to 90 deg. The NBR inhibitor was eroded uniformly, showing approximately 20 to 25 in. remaining. No tears were present on either the flap or inhibitor.

6.4.4.4 <u>Forward Field Joint Insulation</u>. The forward field joint was disassembled and inspected on 16 Jan 1991. The joint insulation and putty were in normal condition, showing normal heat effects, charring, and erosion. Gas penetrated slightly into the joint bondline between the clevis insulation and the putty from 262 to 280 deg. The average depth of the gas penetration was 0.30 in. (0.40 in. maximum) outboard of the remaining material. Heat-affected NBR on the clevis side and heat-affected putty on the tang side were present in this region. The putty exhibited a consistent olive green color with normal tack. The putty failure at disassembly was 2 percent adhesive and 98 percent cohesive. The tang insulation on this joint had several prefire edge separations over 0.50 in. in axial depth (0.75 in. max). These separations were repaired before joint assembly. No clevis or tang edge separations were detected upon postfire inspection, indicating the repair procedure was adequate. The forward segment stress relief flap and the forward center segment NBR inhibitor were in normal condition. The entire flap remained full circumference with heat affected and slightly blistered NBR underneath. Castable inhibitor was present intermittently. The NBR inhibitor was eroded uniformly with approximately 25 to 30 in. remaining. No tears were present on either the flap or inhibitor.

6.4.4.5 <u>Nozzle-to-Case Joint Insulation</u>. The nozzle-to-case joint was disassembled and inspected on 15 Jan 1991. The joint insulation and putty were in normal condition, showing normal heat effects and sooting at the forward edge of the bondline. There was no evidence that gas had penetrated the joint insulation

bondline (putty). The putty exhibited a consistent olive green color with normal tack. The putty failure at disassembly was 5 percent adhesive and 95 percent cohesive. Three voids in the putty were found on the fixed housing at the step extending forward. The largest void was located at 186 deg and measured 2.2 in. circumferentially by 0.7 in. axially.

6.4.4.6 Igniter Outer Joint and Chamber Insulation. Disassembly of the igniter outer joint (igniter adapter-to-forward dome joint) revealed one blowhole through the putty at 272 deg. The blowhole measured 1.90 in. longitudinally and ranged from 0.14 in. wide circumferentially at the forward end to 0.35 in. wide circumferentially near the aft end. The blowhole resulted in sooting forward of the putty from 112 to 272 to 353 deg. The putty was in good condition, exhibiting 100 percent cohesive failure and normal color and tack.

The igniter boss insulation was also in good condition. No tears, ply separations, edge unbonds, or areas of abnormal erosion were identified.

The igniter chamber insulation was in good condition with no tears, gouges, ply separations, or abnormal erosion. Blistering was evident from 320 through 0 through 50 deg on the aft half of the inner chamber insulation. Blistering on the inner chamber insulation is common and is considered to be the result of normal heat effects.

6.4.4.7 Igniter Inner Joint and Adapter Insulation. Disassembly of the igniter inner joint (igniter adapter-to-igniter chamber joint) showed the putty to be in good condition, with no blowhole or voids evident. Slight moist soot was seen in contact with the inner side of the putty, a result of the CO_2 quench blast. The putty exhibited 100 percent cohesive failure and normal color and tack.

The igniter adapter insulation was in good condition. The insulation appeared cleaner than flight adapter insulation because some of the char layer was removed by

the CO_2 quench blast. No tears, ply separations, or areas of abnormal erosion were identified.

6.5 LEAK CHECK PERFORMANCE

6.5.1 Introduction

Leak check port plugs (1U100269-03) with the Nylock® locking feature were installed in the leak check ports of all three field joints and the nozzle-to-case joint.

After each pressure vessel joint was assembled, a leak test was performed to determine the integrity of the seals. The leak tests consisted of a joint volume determination and a pressure decay test. The volume and pressure information was combined with temperature and time data collected during the test and used in the calculation of a leak rate expressed in terms of standard cubic centimeters per second (sccs). Each leak test has a maximum leak rate allowed.

Some specifications require only a maximum pressure decay over time. This method has been determined as sufficient based on the small, constant volumes and the equivalent leak rates, which are conservative when using all worst-case variables.

Table 6-2 lists all joints leak tested on TEM-7, corresponding leak test specifications, and the equipment used. The leak tests are discussed in detail in Section 6.5.4. The case factory joints were tested after the original assembly. This report does not discuss the results of those tests. The majority of the nozzle internal joints (joints No. 1 through 4) were of RSRM configuration and tested to the accompanying requirements. Nozzle internal joint No. 5 was a combination of HPM and RSRM hardware and could not be leak tested because it only contained a single O-ring.

6.5.2 Objectives/Conclusions

There are no objectives from Section 2 concerning seals/leak check.

Table 6-2. TEM-7 Seal Leak Testing

Joint	Specification	Equipment
Case Field Joints	STW7-3682	8U75902
Nozzle-to-Case Joint	STW7-3682	2U129714
Nozzle Joint 1	STW7-2375	8U76248
Nozzle Joint 2	STW7-3476	2U129714
Nozzle Joint 3	STW7-3477	2U129714
Nozzle Joint 4	STW7-3478	2U129714
Ignition System Inner Gasket Outer Gasket	STW7-3632 STW7-3632	2U126714 2U129714
Special Bolt Installation	STW7-3632	2U129714
S&A Device Joint	STW7-3633	8U76500
Transducer Assembly	STW7-2853	2U65686
Barrier-Booster	STW7-2913	2U65848

6.5.3 Recommendations

None.

6.5.4 Results/Discussion

The case field joint leak test results are shown in Table 6-3. The TEM field joints were tested at lower pressures (185 psig) than RSRM field joints (1,000 psig) because of their configuration. These joints were tested with and without the assembly stands (chocks) in place. This was done because previous HPM motors showed the potential for leaking after the stands were removed. The results of the leak tests for the field joints were acceptable.

The field joint tests were performed with a variation of the 8U75902 Ground Support Equipment leak test system. For testing of the TEMs, the equipment was modified to include a pressure relief valve to preclude the possibility of over-pressurizing the joint.

Table 6-3. TEM-7 Case Field Joint Leak Test Results

Pressure (psig)	Maximum Leak Rate (sccs)	Actual Leak Rates (sccs), Prechock/Postchock		
		Forward	Center	Aft
185	0.1	0.0121/0.0084	0.0023/0.0101	0.0128/0.0089
30	0.0082	0.005/-0.002	-0.002/0.0000	0.0003/-0.0001

The ignition system leak test results are shown in Table 6-4. The tests were performed with the new leak test equipment shown in Table 6-2. The equipment was identical to that used to test most of the RSRM joints. All results were within the limits.

Table 6-4. TEM-7 Igniter and S&A Device Leak Test Results

Joint Seal	Allowable Leak Rate (sccs), High/Low*	Actual Leak Rate (sccs), High/Low*
Inner	0.10/0.0082	0.0043/-0.0002
Outer	0.10/0.0082	0.0070/-0.0005
Transducer Installation	0.10/0.0082	0.0085/-0.0001
OPT**	10 psi/10 min/1 psi/10 min	1.0/0.0 2.0/0.0 3.0/0.0 2.0/0.0
Barrier-Booster	1 psi/10 min	Not available
S&A Device	0.10/0.0082	0.0040/-0.0001
*High = 1,000 psig, Low = 30 psig **OPTs tested at 1,024 psig and 30 psig; leak rate units are psi/10 min		

Table 6-5 lists the results of the TEM-7 nozzle-to-case joint leak test. This joint was tested at a maximum pressure of 185 psig. This differs from the RSRM nozzle-to-case joint leak tests, which are performed at 920 psig. The TEM-7 nozzle-to-case leak

test was performed after the first torque sequence, when the axial bolts are torqued to 25 ft-lb. This procedure prevented the occurrence of a metal-to-metal seal between the fixed housing and the aft dome when the axial bolts were fully torqued. All leak test results were within the allowable limits.

Table 6-5. TEM-7 Nozzle-to-Case Leak Test Results

Pressure (psig)	Allowable Leak Rate (sccs)	Actual Leak Rate (sccs)
185	0.072	0.0091
30	0.0082	0.0000

The 2U129714 equipment was used to test the TEM-7 nozzle-to-case joint. This is the new equipment used to test all RSRM nozzle-to-case joints starting with 360L006A.

The nozzle internal joint leak test results are shown in Table 6-6. The tests were performed with the new leak test equipment as shown in Table 6-2. The equipment was identical to that used to test most of the RSRM joints. All results were within the limits.

Table 6-6. TEM-7 Nozzle Internal Joint Leak Test Results

Joint	Maximum Test Pressure	Allowable Leak Rate (sccs), High/Low*	Actual Leak Rate (sccs), High Low*
No. 1	83	0.029/0.0082	0.0025/0.0006
No. 2	920	0.084/0.0082	0.0007/-0.0003
No. 3	740	0.070/0.0082	0.0010/-0.0008
No. 4	144	0.053/0.0082	0.0032/0.0002
* High = 1,000 psig, low = 30 psig			

6.6 NOZZLE PERFORMANCE

6.6.1 Introduction

The nozzle assembly (Drawing 7U76738) was a partially submerged convergent/ divergent movable design with an aft pivot point flexible bearing (Drawing 1U52840). The phenolic liners were RSRM configuration with exceptions defined by the Low Cost Improvement Program Plan, TWR-19524B. All metal hardware was RSRM except for the fixed housing, which was an HPM configuration modified to mate with the HPM aft segment.

The TEM-7 nozzle incorporated many modifications (Figure 6-20). The most significant feature was incorporation of NARC rayon into all CCP liners: forward exit cone, outer boot ring, cowl, fixed housing, nose, aft exit cone, and throat (Drawings 7U76736, 7U76608, 7U76609, 7U76865, 7U77266, 7U77267, and 7U77310).

Metal housings associated with the major nozzle phenolic assemblies (fixed housing, forward exit cone, aft exit cone, nose, throat) were instrumented with strain and temperature sensors.

The nozzle included changes in accordance with Low Cost Improvement Program Plan (TWR-19524B) and MSFC directives as follows:

- Minus 50-deg ply angle change on cowl (Drawing 7U76609) second wrap
- Full cure on CCP first wrap outer boot ring (Drawing 7U76608)
- Delayed pressure cure on glass-cloth phenolic (GCP) inner boot ring (Drawing 7U76608)
- Bearing protector extended belly band (Drawing 7U76864), as shown in Figure 6-21
- Improved nose-to-cowl assembly process (Figure 6-22)
- Boot cavity pressure (Drawings 7U76827, 7U76983) and temperature measurement instrumentation (Figure 6-23)

A032175a

Box Signifies Features Not
Previously Demonstrated
in Full-Scale Motor Firing

Vent Ports
at 15, 105, 195,
and 285 Deg

Aft End Pressure Ports
at 80, 185, 190
and 260 Deg

Fixed Housing Instrumentation
Biaxial Strain (4 ea)
Pressure Oscillation (1 ea)
Teledyne Taber (3 ea)

HPM-Configured
Housing Assembly

Boot Cavity Instrumentation
1 Thermocouple
2 Teledyne Taber
2 Stand-Alone

Inner Boot Ring
Delayed Pressure
Cure/Glass Phenolic

Outer Boot Ring
Full Cure/Carbon
Phenolic/First Wrap

Bearing Protector Belly
Band Extended, Thickened
to 1.0 in. Minimum

Cowl Assembly
Process Change

Cowl Liner Ply
Angle Change
−50 Deg

Cowl Vent Hole
Increased to
0.375 in. Dia

Note: NARC Rayon Used on
All CCP Components

Figure 6-20. TEM-7 Nozzle Configuration

Flex Bearing
Thermal Protector

Increased Length
and Thickness
Was: 0.67 in. Thick Minimum
Now: 1.0 in. Thick Minimum

Was: 2.1 in. Length +/- 0.1
Now: 2.7 in. Length +/- 0.1

Pin

Outer
Boot
Ring

-50 Deg

Cowl

A029981aR1

Cowl Insulation
(silica-cloth
phenolic)

Vent Hole Size Increased: Was 0.312-in Dia,
Now 0.375-in Dia

Cowl Ring Liner
(Carbon Cloth Phenolic)

Ply Angle

Was: 0 Deg
Now: -50 Deg
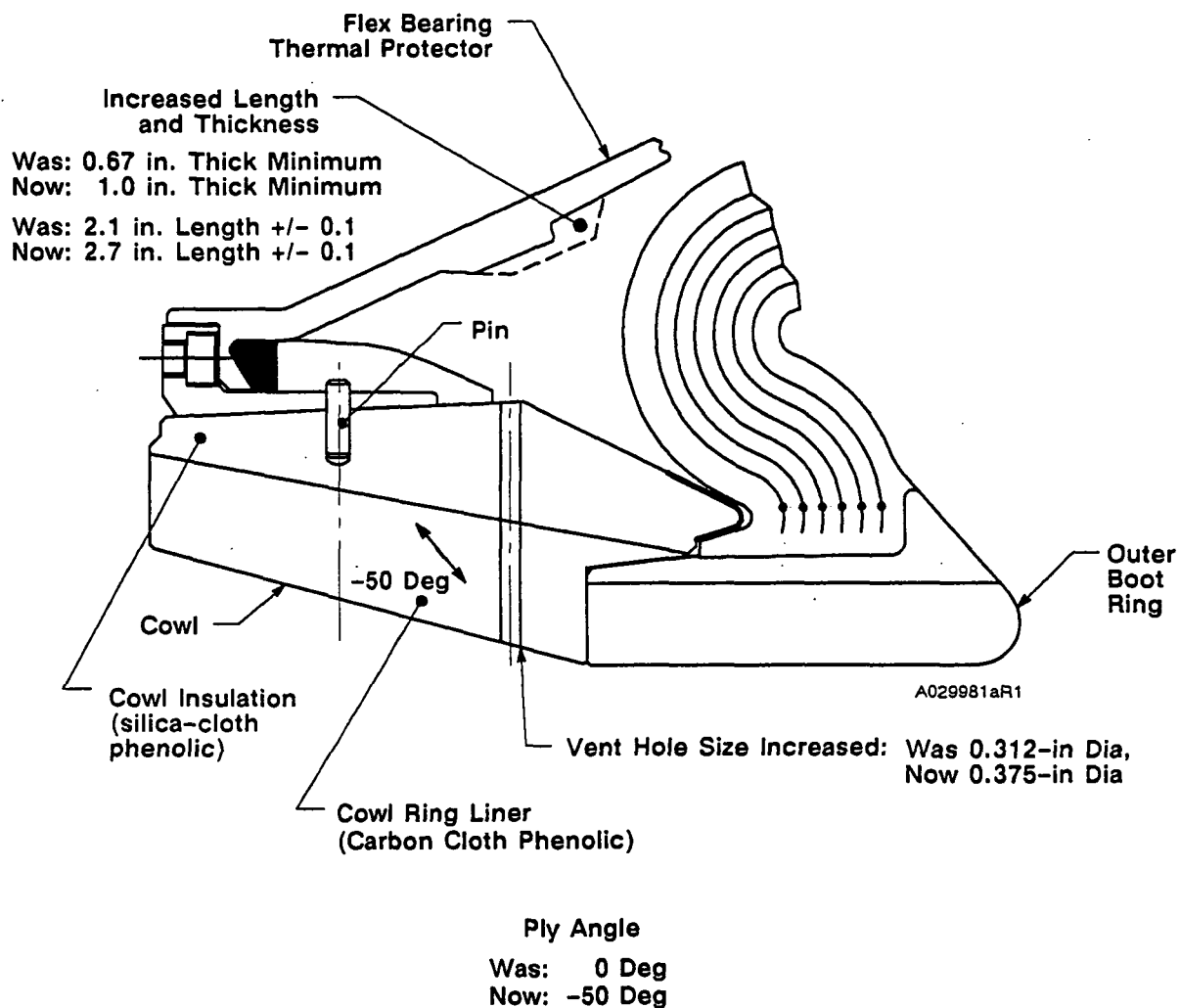
Figure 6-21. Cowl Liner/Flex Bearing Thermal Protector
Area Configuration Changes

A022942a

Improved Assembly Process

Assembly
Fixture

Radial Bondline Backfilled
With RTV

2U65040–01
Assembly
Fixture

Guide Pin
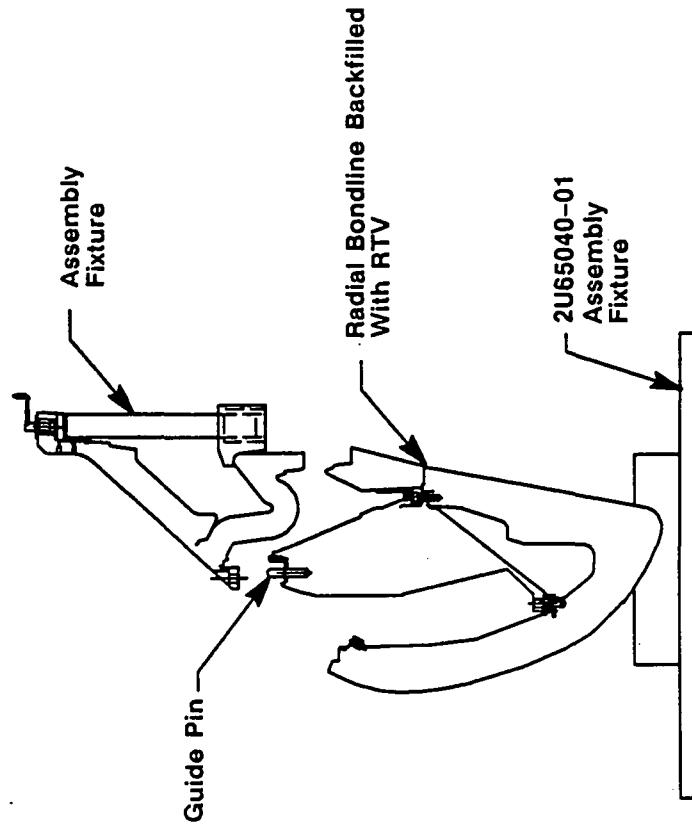
Current Assembly Process

Assembly
Fixture

Radial and
Axial Bondlines

2U65040–01
Assembly
Fixture

Guide Pin
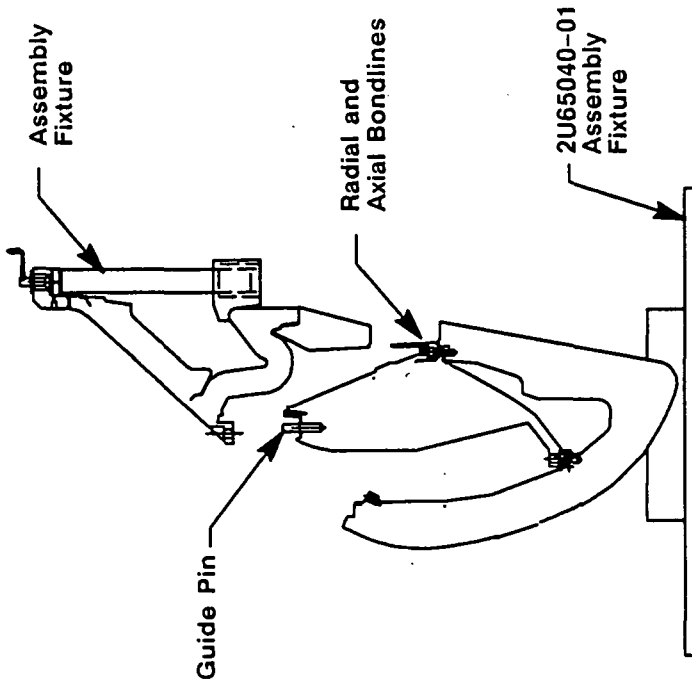
Figure 6–22. Improved Nozzle Cowl Assembly Method

a025667a

SAPMD Activation Wiring

Boot Cavity Output Wiring
(through-flex bearing shims)

4 ea Biaxial
Strain Gages

1 ea 1U50188-07
(pressure oscillation)
3 ea Teledyne Taber
(pressure) 7U76902-01

Vent Ports

1 ea 7U76321-01

3 Pressure Transducers
(2 Teledyne Taber/1 stand alone)

1 Thermocouple
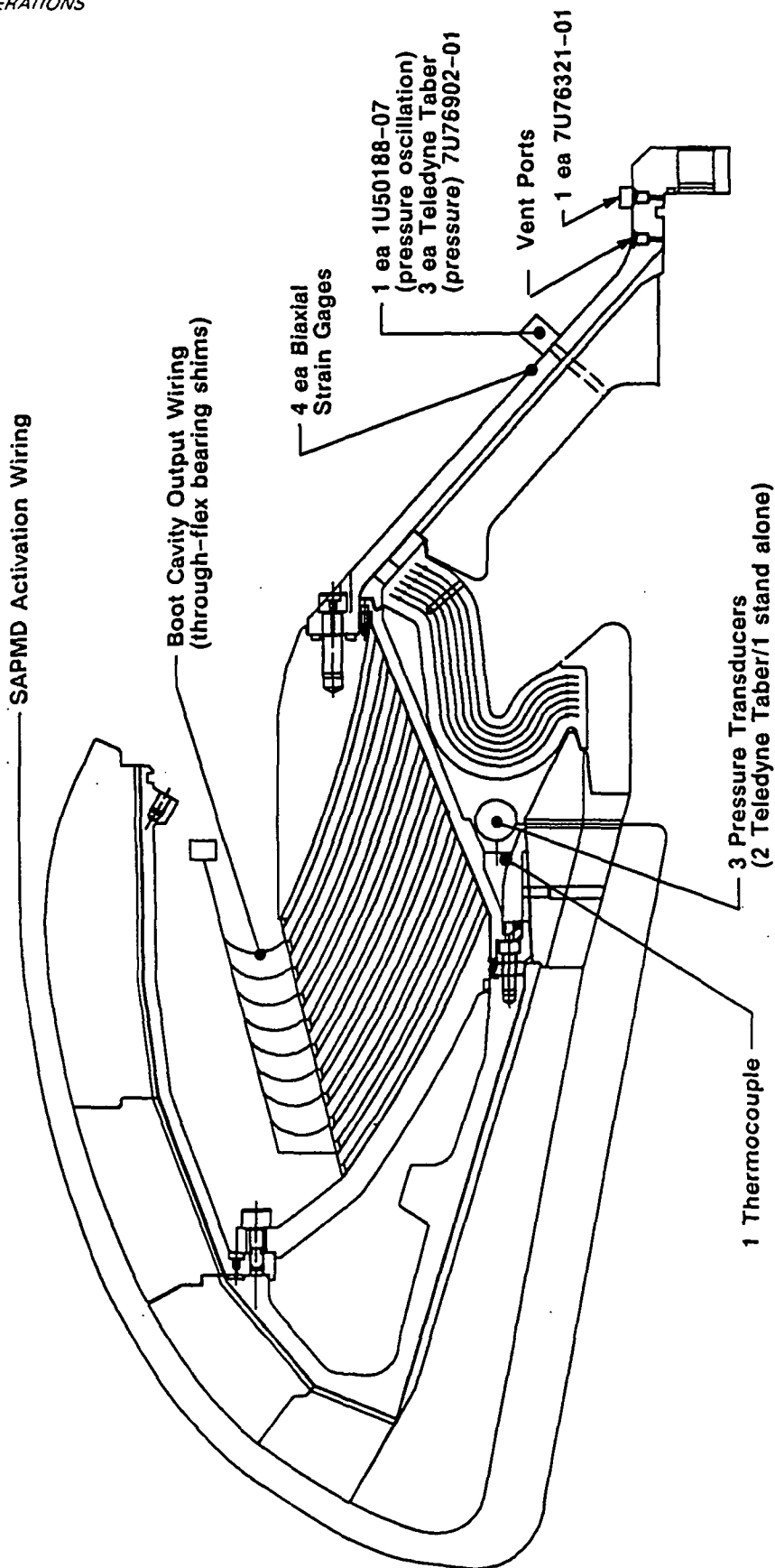
Figure 6-23. Fixed Housing and Boot Cavity Instrumentation

• Fixed housing pressure (Drawing 7U76902) measurement instrumentation (Figure 6-23)

The 36 vent holes in the cowl were increased in size from a nominal 0.312 in. diameter to 0.375 in. diameter to alleviate boot cavity differential pressure. Supporting analyses for this change were documented in TWR-60857, Cowl Vent Hole Study and TEM-2 nozzle boot cavity pressurization.

TEM-7 was configured with a bearing protector in which the extended belly band was also thickened. The belly band was extended to place the region of maximum erosion in the thickened portion of the bearing protector. The belly band was additionally thickened from 0.67 in. minimum to 1.0 in. minimum to accommodate any potential for increased erosion due to the larger vent holes.

A 7U76865-02 nozzle fixed housing was created by machining four MS-16142-type vent ports forward of the primary O-ring to facilitate venting of the cavity between the joint putty and the primary O-ring when assembling the nozzle to the case. Adjustable vent port plugs with the Nylok locking feature (1U76425-03 and -02) and closure plugs (Drawing 1U50159) were installed in the four RSRM vent ports of the nozzle fixed housing.

The nozzle-to-case joint was assembled with RSRM axial bolts with preload measuring capability. The assembly preload was a nominal 120,000 lb.

The linear shaped charge was not added to the aft exit cone (Drawing 7U77267) assembly for this test.

The axial test motor included an SRB aft skirt assembly identified on MSFC-NASA Drawing 14A30649-02. The aft skirt assembly contained the TVC subsystem and the heat shield installation.

The TVA system (Figure 6-24) was comprised of two SRB actuators and two auxiliary power units (APU) located in the aft skirt.
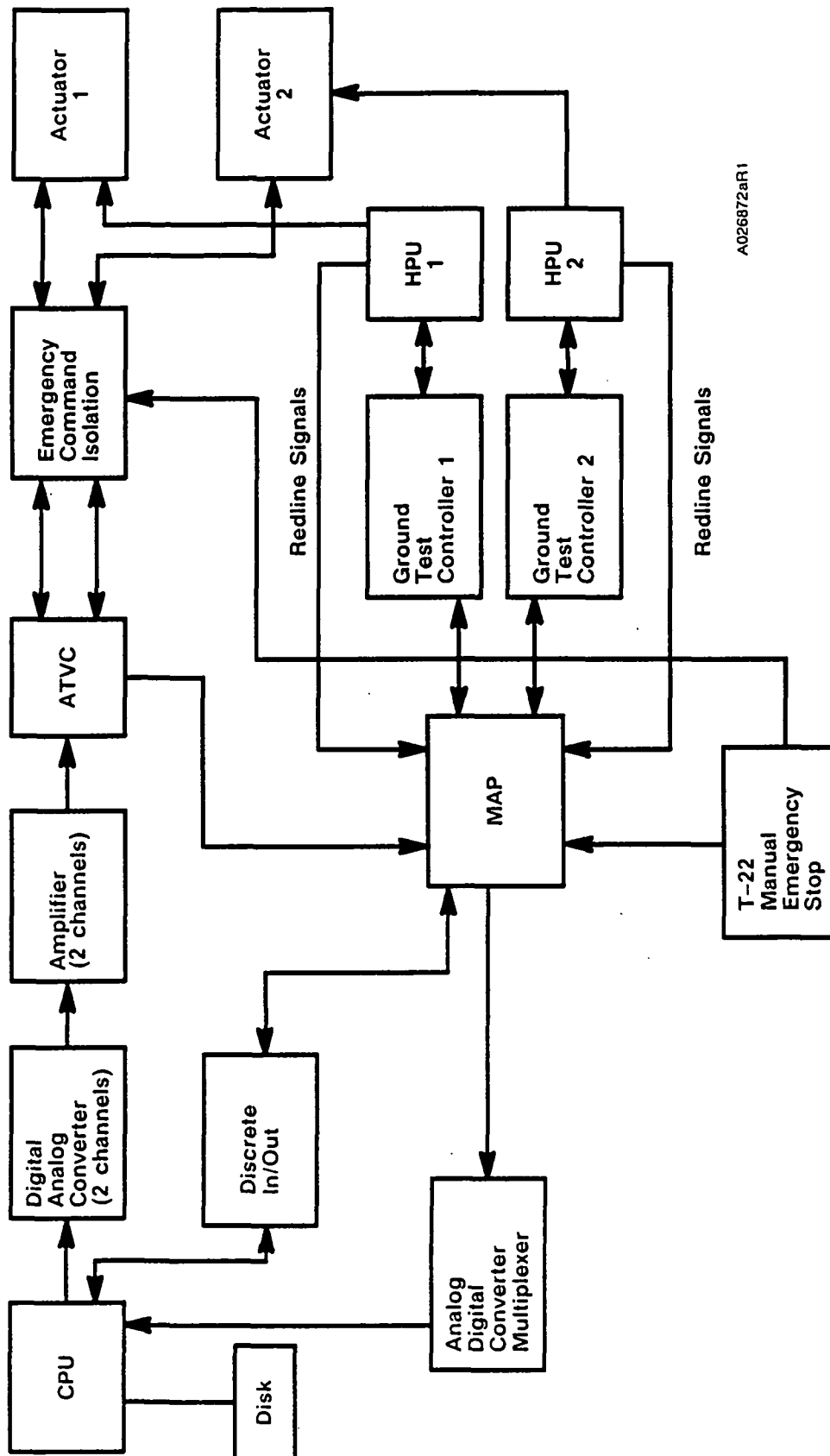
A026872aR1

Figure 6-24. TVA System

The APU ground test controller, APU MAP, and the ATVC served as the control units for the TVC subsystem. This is the first TEM nozzle to have a TVC system for vectoring capability.

6.6.2 Objectives/Conclusions

The objectives and corresponding conclusions from Section 2 regarding nozzle performance were:

Objective	Conclusion
A. Certify NARC rayon for use in nozzle CCP liners (CPW1-3600A, Para 3.2.1.4.13, 3.3.6.1.2.7, 3.3.6.1.2.8).	*Certification requirements for this test were met. First of three full-scale static tests.* The performance of the nozzle liners was nominal. There were no abnormal erosion patterns, and the performance margins of safety were equal to or better than baseline. X-ray results and post test comparisons verified better than average components.
B. Certify nozzle inner boot ring cure cycle improvement (CPW1-3600A, Para 3.3.6.1.2.8).	*Certification requirements for this test. were met. Second of three full-scale static tests.* The inner boot ring performed nominally. A delamination along a GCP ply was due to forward movement of the fixed housing liner and was not cure cycle related. There were no LDIs disclosed by pre-test X-rays.
C. Certify nozzle outer boot ring cure cycle improvement (CPW1-3600A, Para 3.3.6.1.2.8).	*Certification requirements for this test were met. Second of three full-scale static tests.* The outer boot ring performed nominally. The structural support ring remained attached to the overwrap. There were no LDIs disclosed by pretest X-rays.

Objective	Conclusion
D. Certify the nozzle cowl ring with an ablative liner ply angle change (from 0 to -50 deg) (CPW1-3600A, Para 3.2.1.4.13, 3.3.6.1.2.8)	*Certification requirements for this test were met. Second of three full-scale static tests.* The cowl ring surface eroded smoothly and contained none of the wash areas typically seen on present RSRM cowl rings with the 0-deg CCP ply wrap. Performance margins of safety met or exceeded flight baseline.
E. Certify the improved nozzle bearing protector (CPW1-3600A, Para 3.3.6.1.2.8).	*Invalid test due to possible effects of other configuration changes.* The greater erosion areas due to gas impingement were located within the thickened, extended portion and did not overlap into the thinner areas as on RSRM bearing protectors. Configuration changes (see Objective I) may have contributed to more severe erosion than anticipated.
F. Recover case and nozzle hardware for RSRM flight and static test programs.	Case and nozzle hardware is available for refurbishment.
H. Demonstrate the performance of an improved nose assembly to cowl assembly process for the nozzle (CPW1-3600A, Para 3.2.3, 3.2.3.1, 3.3.1.1).	*Demonstrated.* Due to the improved cowl bonding process, EA 913NA adhesive did not squeeze out and mix with the RTV in joint No. 2 as is typically seen. RTV penetrated uniformly all the way into the joint as intended. The RTV was below the char line over the full circumference. No blowpaths were observed.
I. Demonstrate the performance of increased cowl vent hole size (0.375-in. nominal diameter) for reducing boot cavity delta pressure (CPW1-3600A, Para 3.3.6.1.2.8).	*Not demonstrated.* Boot cavity pressure (Objective L) was not obtained to verify performance, although 18 of 36 holes remained open, compared to the postflight average of five open vent holes. However, the increased cowl vent hole size contributed to the severe erosion of the bearing protector (Objective E). The erosion was > 0.4 in. at 230 through 0 through 10 deg and burned through the bearing protector at 280 and 330 deg.

6.6.3 Recommendations

Demonstration and qualification activities should continue for the following nozzle features:

A. NARC rayon in nozzle CCP liners.

B. Nozzle inner boot ring and outer boot ring cure cycle improvements.

C. The nozzle cowl ring with the -50-deg angle CCP ply wrap.

D. The improved (extended) nozzle bearing protector (without the thickened portion).

E. The improved nose assembly-to-cowl assembly process for the nozzle.

The larger cowl vent holes (0.375 in.) are not planned for use on future static test or flight nozzles.

6.6.4 Results/Discussion

Overall, the postburn condition of the nozzle liners was very good. Only two small, shallow wash areas were found on the aft exit cone liner, and no surface ply lifting was observed. The erosion of the throat and throat inlet rings was smooth, with the typical rippled erosion pattern occurring on the aft 6 in. of the throat ring (0.1 in. deep maximum). The postburn mean throat diameter was 56.07 inches. This is within the historical database of RSRM/HPM throat diameters. The throat erosion rate was 9.20 mils/sec. Typical minor wash areas (0.1 in. deep maximum) were observed on the forward portions of the nose cap. The cowl ring erosion was smooth and did not exhibit the typical wash areas as seen on RSRM (0-deg ply wrap) cowls.

All postfire flow surface gaps between phenolic components were uniform around the circumference and were within the historical database.

A discussion of the nozzle subassemblies and joint conditions follows. Design configuration/modifications are in parentheses. All liner performance margins of safety were zero or greater (meets CEI specification Para 3.3.6.1.2.8).

6.6.4.1 Nozzle Subassemblies

Aft Exit Cone (RSRM configuration/linear shaped charge (LSC) removed).
Performance margins of safety were positive for all stations of the aft exit cone. The forward 12 in. showed typical, but less pronounced, dimpled erosion extending from the forward exit cone. The remainder of the liner exhibited smooth erosion with no surface ply lifting and no evidence of subsurface ply lifting. Two minor wash areas were found. The first was at 240 deg and measured 7 in. axially by 5 in. circumferentially by 0.02 in. deep. The second was at 260 deg and measured 12 in. axially by 1 in. circumferentially by 0.1 in. deep. Core samples taken at the wash areas and at other locations showed that no subsurface ply lifting had occurred. There were no wedgeouts observed.

The postburn exit plane diameters (determined from sectioned liner sections) were:

- 0 to 180 deg: 149.76 in.
- 90 to 270 deg: 149.83 in.

Forward Exit Cone (RSRM configuration/no snubber assembly). All performance margins of safety were positive. The forward 17 in. showed smooth erosion. The aft 17 in. had typical dimpled erosion approximately 0.1 in. deep. There were no wedgeouts observed.

Throat/Throat Inlet Rings (RSRM configuration). All performance margins of safety were positive. The throat inlet ring and the forward 10 in. of the throat ring showed smooth erosion. The aft 6 in. of the throat ring had typical rippled erosion measuring approximately 0.1 in. deep. There were no wedgeouts observed. The postfire throat diameters were as follows:

- 0 deg: 56.075 in.
- 45 deg: 56.108 in.
- 90 deg: 55.998 in.
- 135 deg: 56.105 in.

The average throat diameter is 56.07 in. (erosion rate of 9.20 mils/sec based on action time of 120.2 sec). The postfire throat diameters for RSRM and HPM have ranged from 55.787 to 56.124 inches.

Nose Inlet Assembly (RSRM configuration). All performance margins of safety were positive. The forward nose and aft inlet rings exhibited smooth erosion, with no wedgeouts observed. Typical minor wash areas were seen on the nose cap OD forward 8 in. and measured approximately 0.15 in. deep. The remainder of the liner showed smooth erosion. The aft 1.6 in. had typical intermittent postburn popped up, charred CCP, but there were no wedgeouts observed.

Cowl Ring (-50-deg ply wrap; vent holes increased to 0.375 in. diameter). Performance margins of safety were positive. The surface had smooth erosion, with no wash areas observed. Eighteen of the 36 enlarged (from 0.315- to 0.375-in. diameter) cowl vent holes were still open, with diameters ranging from 0.05 to 0.20 inch. Boot cavity pressure was not obtained to verify that the enlarged cowl vent holes successfully vented the boot cavity pressure during motor pressure tailoff. There were no wedgeouts observed. The flow surface gap measurement between the cowl ring and nose cap was 0.1 in., which is typical. This indicates there was no forward movement of the nose cap, as was seen on TEM-6.

Outer Boot Ring/Flex Boot (RSRM configuration/full cure on outer boot ring CCP first wrap). All performance margins of safety were positive. The outer boot ring was intact, and the surface exhibited smooth erosion with no wash areas. The cowl-to-outer boot ring bondline was also intact and showed no evidence of flow or erosion. The flow surface gap measurement between the cowl and outer boot ring was 0.20 in., which is within the historical database. The aft end had typical postburn delaminations along the 35-deg plies. The aft tip adjacent to the flex boot typically fractured off postburn. There were no wedgeouts observed.

Sections of the liner showed the structural support ring intact and attached to the overwrap portion, with no anomalies associated with the full cure cycle.

The flex boot OD eroded evenly around the circumference, leaving three intact NBR plies. The minimum performance margin of safety for the flex boot is 0.19. The inside diameter (ID) side of the flex boot showed typical sooting and minor charring of the NBR near the middle of the boot.

Fixed Housing (four pressure ports drilled through the liner and housing; four pressure transducers installed). The fixed housing liner surface eroded smoothly and, typically, had only a light coat of slag along the aft end. All performance margins of safety were positive.

Examination of the aft end after nozzle-to-case joint demate showed a bondline separation between the EA 913NA adhesive (STW5-3292) and the metal housing of approximately 0.20 in. around the full circumference. Soot was seen extending from the separation. The liner had moved forward approximately 0.20 in., allowing gas to enter the separation through the pressure ports. All pressure ports were found to be plugged with slag during the inspection. The forward movement caused the inner boot ring to delaminate along a GCP ply and also move forward. This condition was written up in PFAR TEM07-07. The aft portion of the inner boot ring was still attached to the fixed housing liner, and the forward portion remained attached to the metal housing. There is no evidence of a cure cycle association with this delamination in the inner boot ring.

The pressure inlet tips of the four pressure transducers were heat affected and eroded due to the gas flow from the pressure ports to the backside of the liner. The primary O-rings on two of the transducers (at 80 and 260 deg) were also heat affected. These conditions were written up in PFARs TEM07-02 and TEM07-04.

The fixed housing unbond failure was attributed to contamination of the fixed housing bonding surface coupled with the stress concentration induced on the housing by gas pressure through the four aft end chamber pressure ports.

Detailed results of the unbond investigation will be documented in TWR-61585.

Bearing Protector (thicker and extended belly band). The bearing protector showed severe erosion at some of the gas impingement points in line with the cowl vent holes. Two locations (280 and 330 deg) were burned through the thickened portion. The erosion was >0.4 in. from 230 to 0 to 10 deg. This condition was written up in PFAR TEM07-11. The impingement points were located within the modified belly band and did not overlap onto the thinner areas of the bearing protector.

The bearing protector burnthrough is considered to be an anomalous condition and not a failure. Performance of the extended belly band was determined to be unique to TEM-7 because of the cowl vent hole and bearing protector thickness changes, which resulted in increased erosion of the bearing protector. The larger cowl vent hole diameter (change from 0.315 to 0.375 in.) resulted in a 44.5-percent increase in flow area. It is hypothesized that vectoring may have created a circumferential flow condition in the boot cavity due to delta pressure. This condition could have contributed to increased erosion, particularly in localized areas. However, boot cavity pressure was not obtained to verify this theory. Also, the increased bearing protector thickness brought the surface of the protector closer to the exit plane of the vent holes. Spreading of the exiting gas jet was reduced due to the decreased distance between the protector and vent hole, resulting in more direct gas impingement and greater concentration on the surface of the bearing protector.

Flex Bearing (RSRM configuration). One flex bearing rubber pad at 280 deg was eroded approximately 0.15 in. due to the burnthrough condition of the bearing protector. The metal shims did not appear heat affected. This was written up in the same PFAR as the bearing protector.

6.6.4.2 Aft Exit Cone Field Joint and Nozzle Internal Joints. A discussion of observations made after each nozzle joint disassembly follows. Figure 6-25 shows the joint configurations and designations.

Joint 2 — Nose Inlet Assy-to-Flex Bearing-to-Cowl Assy
Joint 3 — Nose Inlet Assy-to-Flex Bearing Forward End Ring
Joint 4 — Throat Assy-to-Forward Exit Cone
Joint 5 — Flex Bearing-to-Fixed Housing Assy
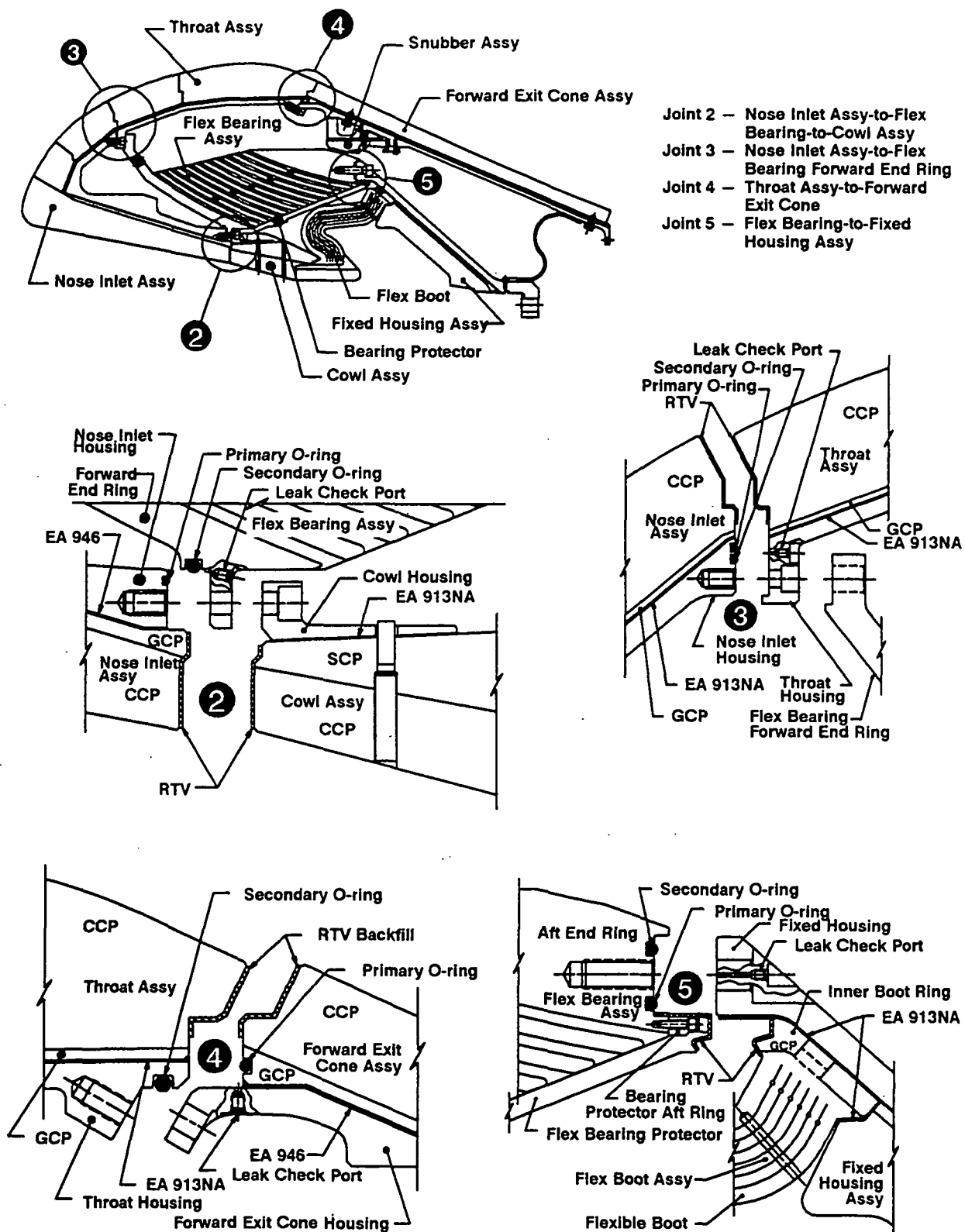
Figure 6-25. TEM Nozzle Internal Joints

A032174a

<u>Forward Exit Cone-to-Aft Exit Cone Field Joint (joint No. 1)</u>. The postfire evaluation of the TEM-7 aft exit cone-to-forward exit cone joint was conducted on 3 Jan 1991. The sealing surfaces were visually inspected and found to be in good condition with no evidence of damage, corrosion, or excess grease coverage. No damage was found on the primary or secondary O-rings. RTV backfill extended below the joint char line and was found up to the primary seal but not past the primary O-ring over the full circumference. No pressure path (blowpath) was found through the RTV rubber.

A postburn cohesive separation in the aft exit cone polysulfide occurred over a 242 deg circumferential arc. The maximum radial width of the separation was 0.14 in., which is within the static test historical database.

A metal-to-EA 946 adhesive (STW5-2931) postburn separation of 0.08 in. maximum was observed on the aft end of the forward exit cone over the full circumference.

There was no corrosion on the joint metal surfaces.

<u>Forward End Ring-to-Nose Inlet Housing Joint (joint No. 2)</u>. The TEM-7 forward end ring-to-nose inlet housing joint was disassembled on 17 Jan 1991. No anomalous conditions were observed. Light to medium corrosion was observed intermittently around the circumference from 348 through 0 to 36 deg and 84 to 210 deg on the forward end ring forward face upstream of the primary sealing surface area. Grease partially plugged the leak check port through hole and was also observed on the bottom tip of the port plug.

The RTV backfill extended below the char line over the full circumference of the joint. The RTV extended to the nose inlet housing/glass cloth phenolic interface. No blowpaths were observed in the joint.

No bondline separations were observed on this joint.

Intermittent light to medium corrosion was present on the forward end ring joint flange. Minor scratches caused by jacking screws during disassembly were located in four equally spaced locations on the nose inlet housing aft surface.

Nose Inlet Housing-to-Throat Support Housing Joint (joint No. 3). The TEM-7 nose inlet housing-to-throat support housing joint was disassembled on 17 Jan 1991. A 0.15-in.-long radial scratch at 130 deg was seen on the primary O-ring sealing surface on the forward end of the throat support housing. The scratch could be felt with a 5-mil brass shim stock. PFAR TEM07-08 was written on this anomaly.

The RTV backfill extended below the char line over the complete circumference. There was no evidence of grease interfering with the flow of RTV into the joint. No blowpaths were present.

There were no bondline separations present on either the nose inlet (-504 ring) or throat inlet.

No corrosion was observed.

Forward Exit Cone-to-Throat Support Housing Joint (joint No. 4). The TEM-7 forward exit cone-to-throat support housing joint was disassembled on 16 Jan 1991. The RTV backfill extended below the char line over the complete circumference of the joint. Scalloping of the RTV was present, with evidence of grease on the throat phenolic surface interfering, up to 0.75 in. upstream of the primary seal, with the flow of RTV into the joint at 22 to 42, 220 to 225, and 275 to 300 deg, circumferentially. PFAR TEM07-09 was written on this condition. The RTV reached the primary O-ring except where grease was present on the phenolics. There were no blowpaths present.

No bondline separations were present on the aft end of the throat housing assembly. A metal-to-adhesive separation of 0.05 in. maximum was observed on the forward end of the forward exit cone assembly over the full circumference.

No corrosion or damage to the metal components was observed.

<u>Fixed Housing-to-Aft End Ring Joint (joint No. 5)</u>. The TEM-7 fixed housing-to-aft end ring joint was disassembled on 16 Jan 1991. RTV reached the primary O-ring at 210 to 215 deg and was found past the primary O-ring footprint area, for a length of 1 in. at 210 deg, on the corresponding sealing area of the mating surface on the fixed housing. It was determined that this anomaly occurred during the assembly process. PFAR TEM07-10 was written on this condition. No RTV adhered to the fixed housing seal surface, indicating that the RTV did not inhibit the sealing action of the O-ring. The only evidence of RTV across footprint was a red stain on the O-ring. Intermittent voids were present in the RTV from the assembly process, but there were no blowpaths. Grease coverage was nominal and did not interfere with the RTV fill in the joint.

Joint No. 5 packing with retainers had typical seal damage due to the disassembly process.

There were no bondline separations seen at the forward end of the inner boot ring. However, the inner boot ring had sheared along a GCP ply and moved forward approximately 0.30 in., although the bondline gap opened up to 0.20 inch. The shearing of the ring was associated with the fixed housing liner separation.

No corrosion or metal damage was present.

6.6.4.3 <u>Results of Special Issues (TWR-61209, Para 3.3)</u>. The following items were designated Special Issues unique to the TEM-7 nozzle that were to be evaluated in conjunction with the standard postfire evaluation. This section lists the condition as written in TWR-61209 and the resulting evaluation.

3.3.8--Condition: 0.15 in. of insulation was removed from the SAPMD to eliminate interference with the bearing protector.

--Results: The thin areas of the insulation were found to be heat affected as a result of the insulation separating along the laminated bondlines, and opened up, allowing soot to reach the SAPMDs. The SAPMDs were not heat affected.

3.3.9--Condition: A pre-1980 process was used to seat the aft exit cone shell onto the aft exit cone liner.

--Results: No anomalies were identified to show that this was an inadequate process.

3.3.10--Condition: 1) One of four rolls of CCP had shear strength in excess of 8,000 psi. 2) Two of four rolls of CCP had compressive strength in excess of 65,000 psi.

--Results: The aft exit cone liner performance was very good. There were no severe wash areas and no ply lifting observed. The higher shear and compressive strengths were not detrimental to the performance of the CCP.

3.3.11--Condition: LDIs in the aft exit cone GCP.

--Result: The LDIs were found not to be delaminations or separations, but were resin-rich areas.

3.3.12--Condition: LDIs (voids) in the nose cap-to-forward nose ring bondline at 273 and 343 deg.

--Result: These voids were contained within the char depth region of the joint and therefore were no longer present. Char depths were normal and there were no anomalies seen which could be associated with the voids.

6.6.4.4 NCPT Assessment and RPRB Recommendations. The NCPT reviewed all observations documented in this report. Violations of the nozzle postfire engineering evaluation limits contained in TWR-60273, Vol II and III were documented on PFAR forms and presented to the RPRB on 30 Jan 1991 for concurrence (refer to memo E623-FY91-161). The RPRB agreed with the classifications and recommendations of the NCPT. A list of the PFARs is included in Appendix A.

6.6.4.5 TEM-7 Nozzle Strain Gage Response Summary. The TEM-7 nozzle metal parts were RSRM configuration except for the fixed housing, which was SRM design. Review of strain gage data shows expected performance except for the fixed housing assembly.

TEM-7 hoop (circumferential) and meridional (axial) strain gages were located as follows:

Motor Station	Circumferential Location (deg)	Assembly
1962.8	0, 90, 180, 270	Aft exit cone
1902.2	0, 90, 180, 270	Aft exit cone housing
1865.0	0, 90, 180, 270	Forward exit cone housing
1839.39	0, 90, 180, 270	Throat housing
1839.0	0, 90, 180, 270	Nose inlet housing
1842.5	0, 90, 180, 270	Nose inlet housing
1867.0	80, 170, 260, 350	Fixed housing

Figures 6-26 through 6-37 show measured strain data (mean value of four gages) versus the RSRM predicted values for those gage locations. Overall, the data correlated very well. Figures 6-38 and 6-39 show the actual strain data for the fixed housing.

Hoop strain at aft exit cone Stations 1962.8, 1902.2, and forward exit cone Station 1865.0 (Figures 6-26, 6-28, and 6-30) match predicted values for 10- and 20-sec time slices. Subsequent time slices do not match predicted magnitudes as well; however, the strain profile and magnitude are indicative of strains from previously observed test motors. The meridional strain profiles for the same station locations (Figures 6-27, 6-29, and 6-31) match predictions very well. The meridional strain profile at Station 1962.8 is shifted down slightly from the predicted. Gage preload is one possible explanation for this; however, the 100-microstrain shift is negligible.

Hoop strain data for throat housing Station 1839.39 (Figure 6-32) match predicted values extremely well. The meridional strains for this same location are, once again, shifted down approximately 80 microstrain maximum (Figure 6-33). This shift is not a problem because the hoop strains match so well and the actual data profile follows the predicted profile.

Strain data from the nose inlet housing aft end (Station 1842.5) was comparable to previous test measurements. Hoop strain (Figure 6-34) matched predictions.

Thiokol CORPORATION
SPACE OPERATIONS
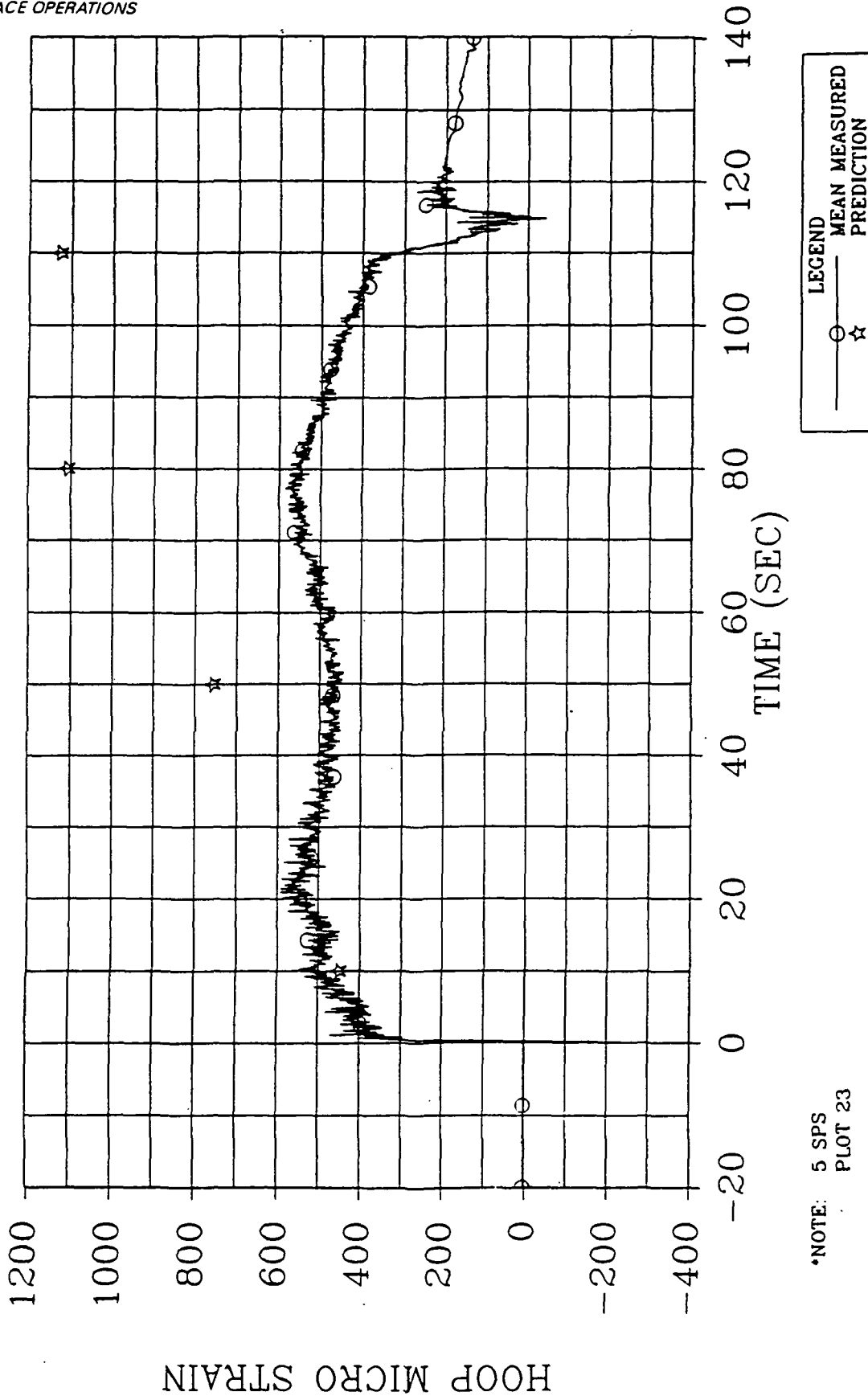
Figure 6-26. Aft Exit Cone Housing Sta 1962.8 Hoop Strain (mean value)
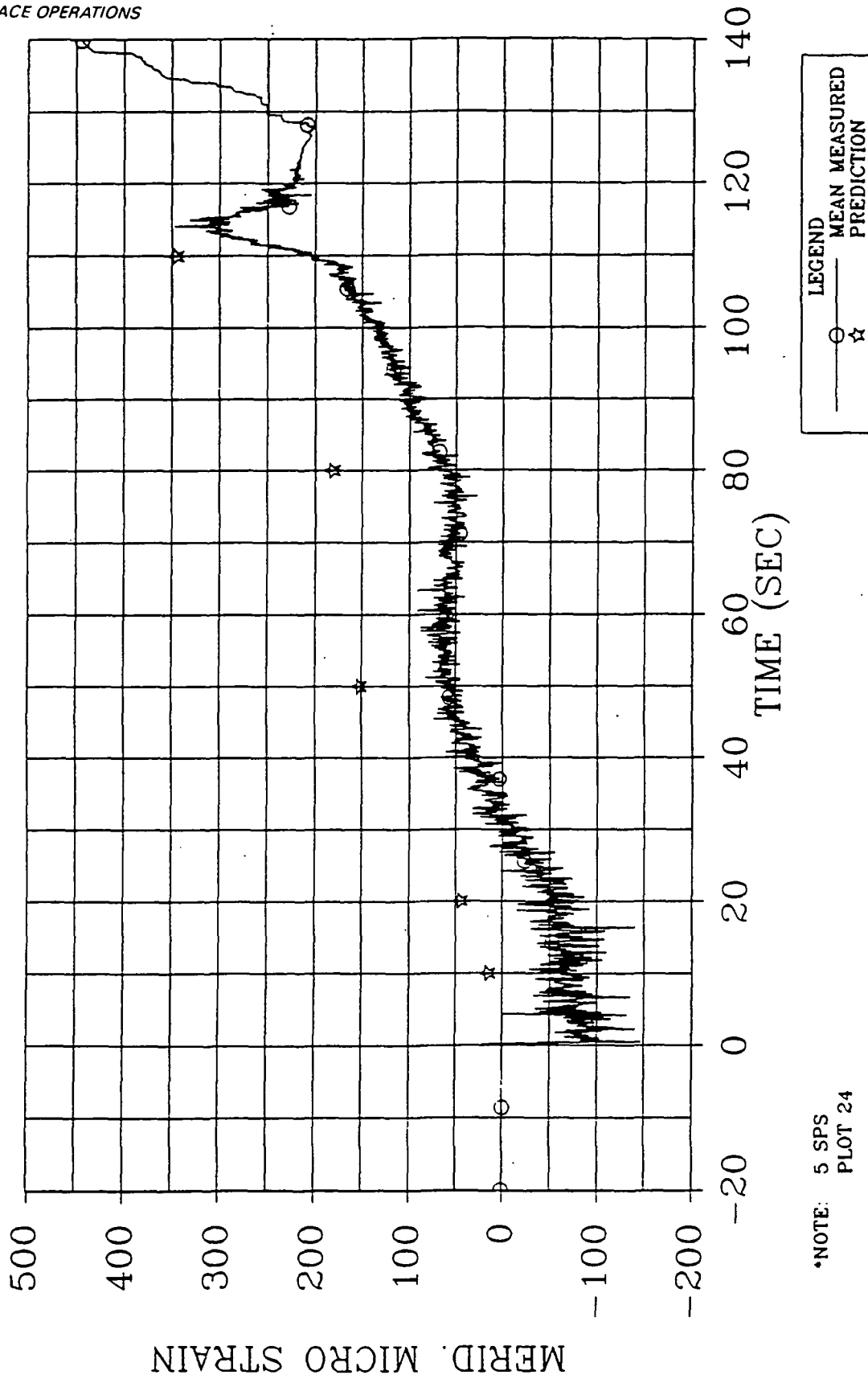
Figure 6-27. Aft Exit Cone Housing Sta 1962.8 Meridional Strain (mean value)

Thiokol CORPORATION
SPACE OPERATIONS

*NOTE: 5 SPS
PLOT 24
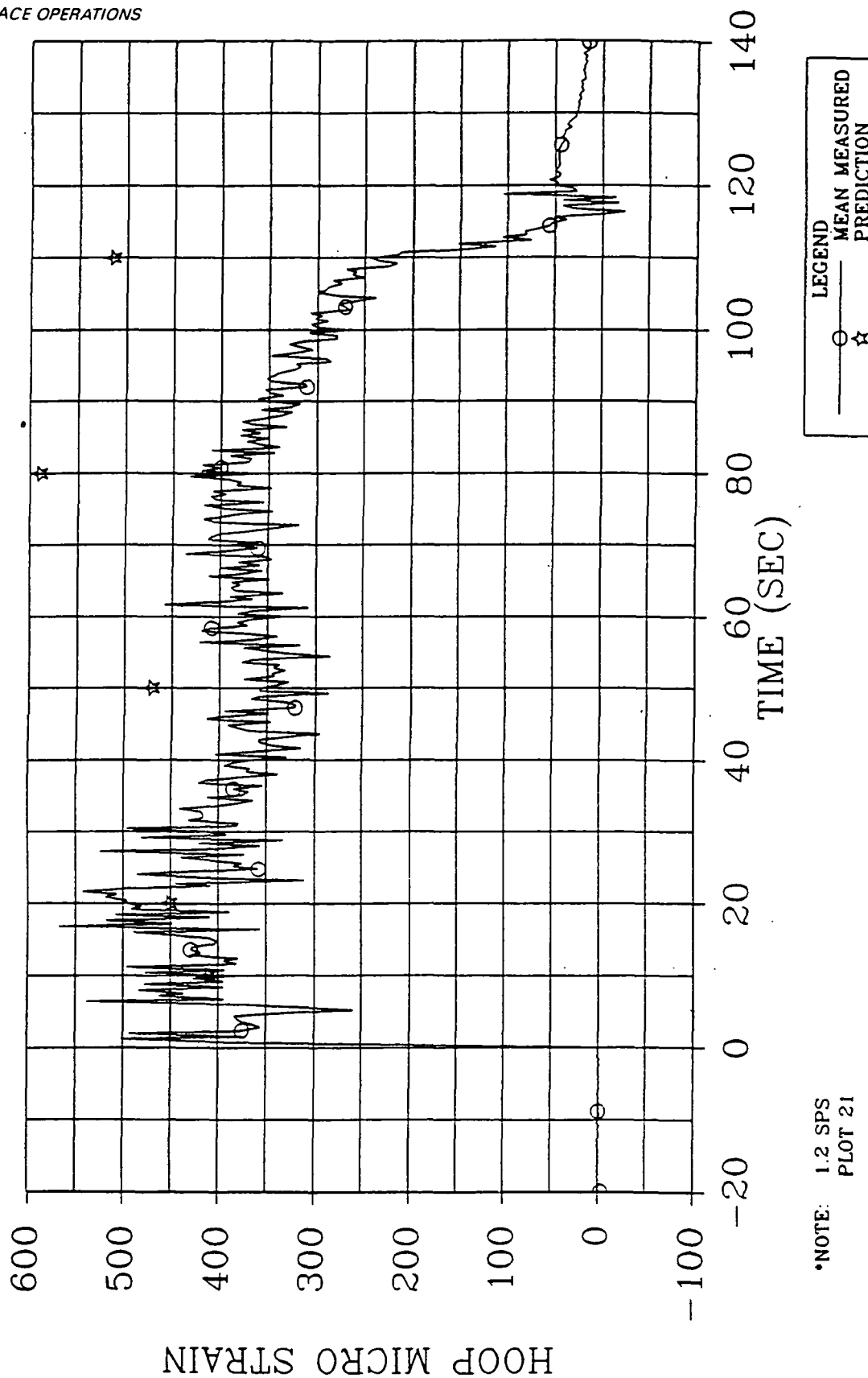
Figure 6-28. Aft Exit Cone Housing Sta 1902.2 Hoop Strain (mean value)
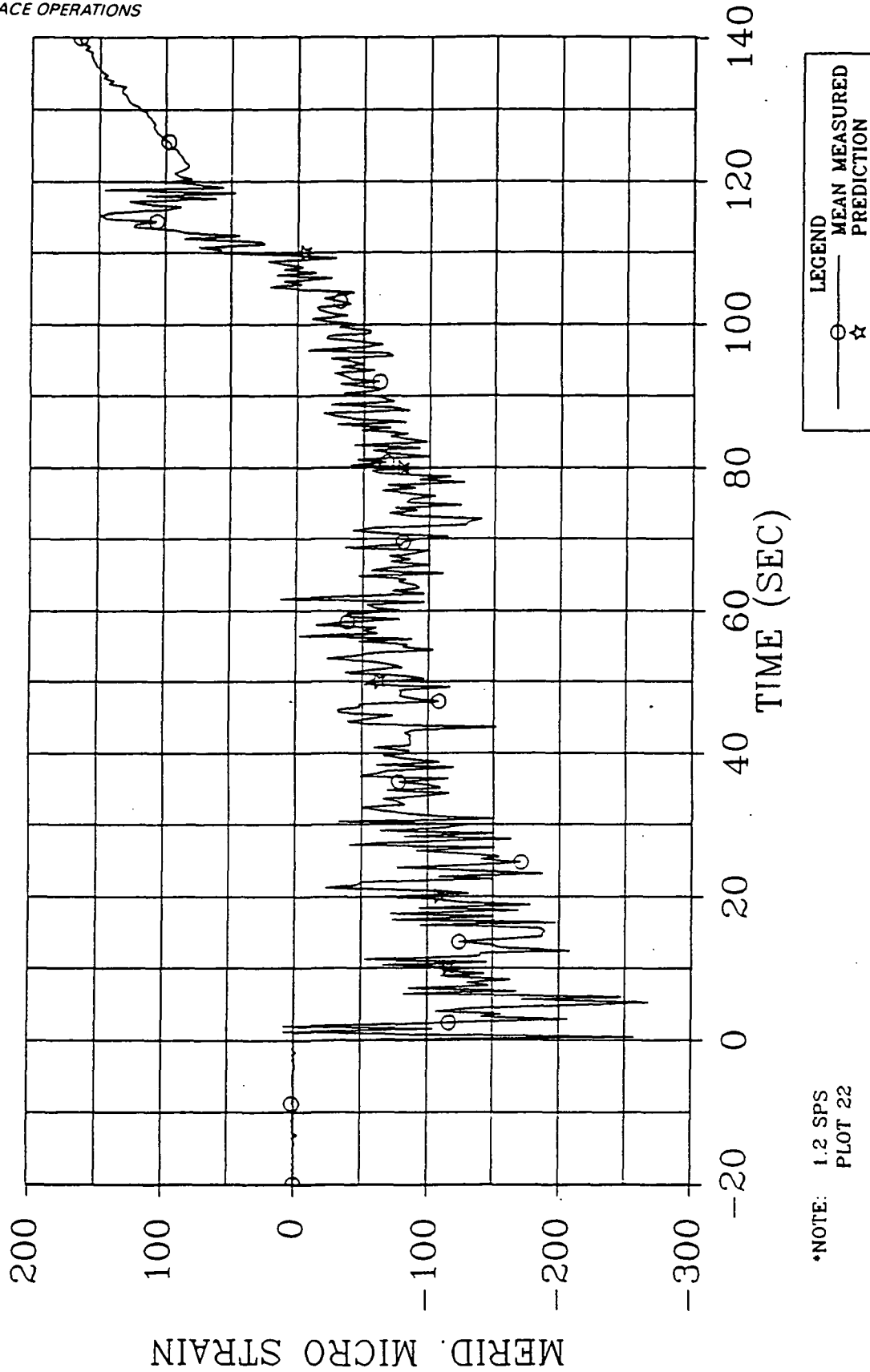
*NOTE: 1.2 SPS
PLOT 21

Figure 6-29. Aft Exit Cone Housing Sta 1902.2 Meridional Strain (mean value)
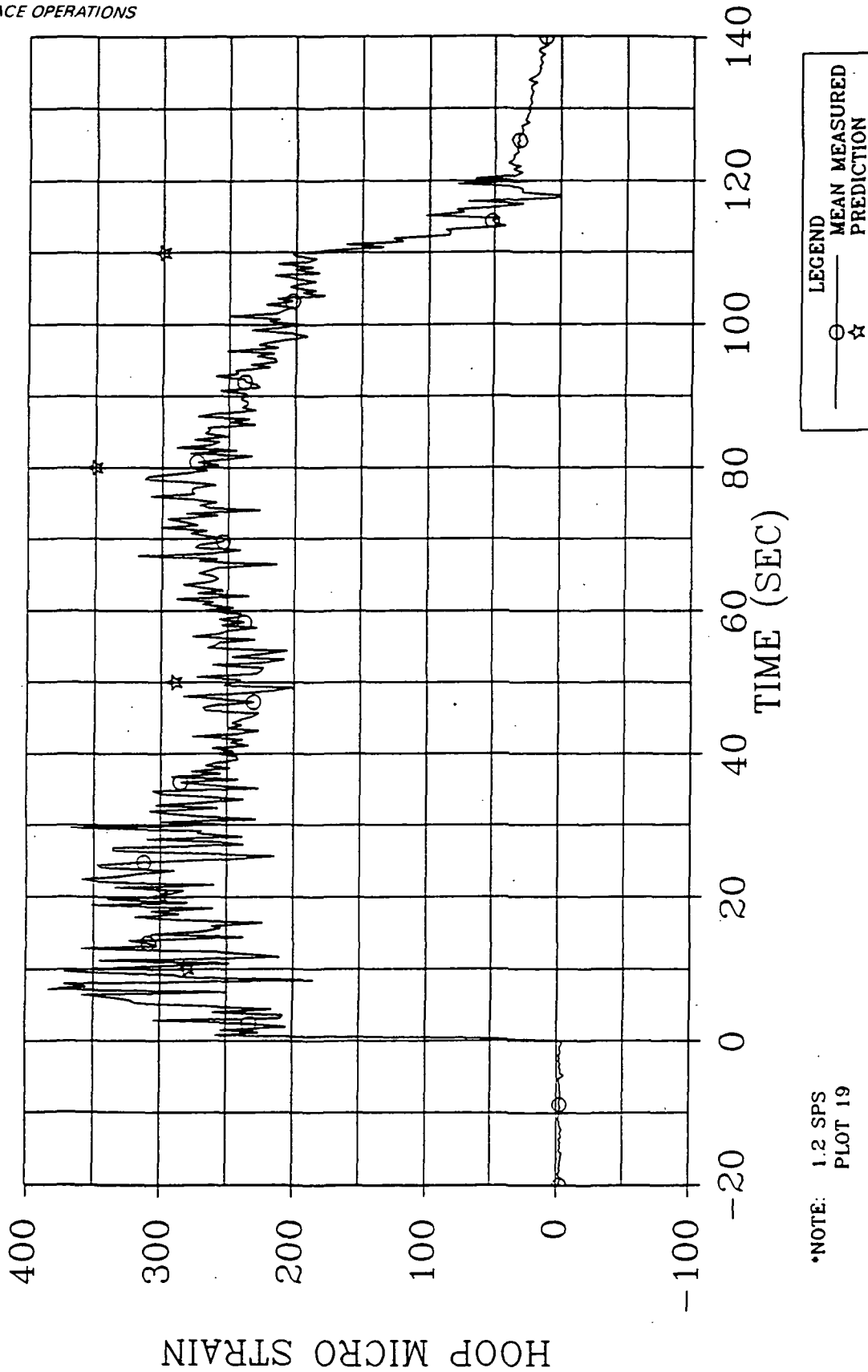
*NOTE: 1.2 SPS
PLOT 22

Figure 6-30. Forward Exit Cone Housing Sta 1865.0 Hoop Strain (mean value)

*NOTE: 1.2 SPS
PLOT 19

NOTE: 1.2 SPS
PLOT 20

LEGEND
MEAN MEASURED
PREDICTION
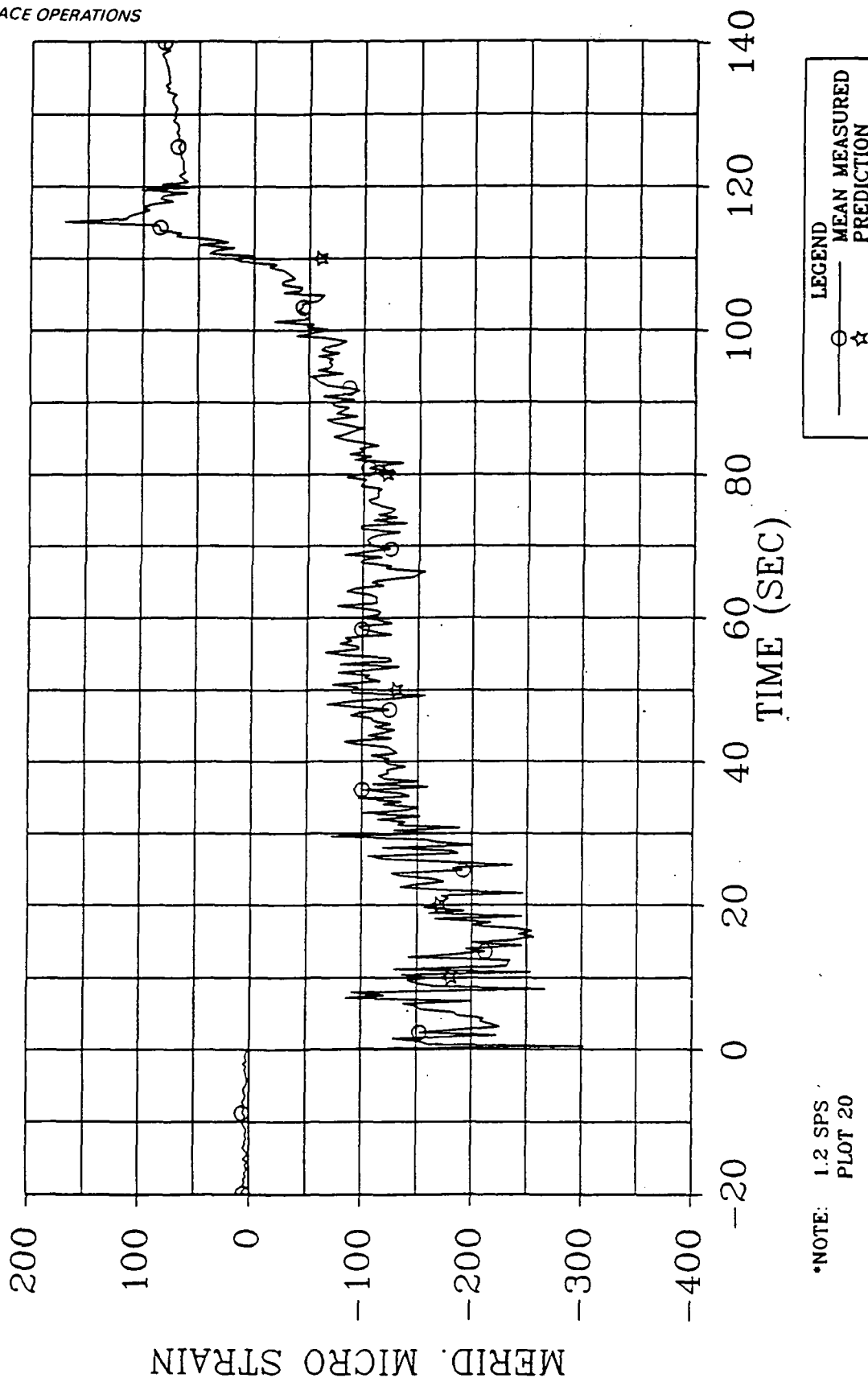
Figure 6-31. Forward Exit Cone Housing Sta 1865.0 Meridional Strain (mean value)
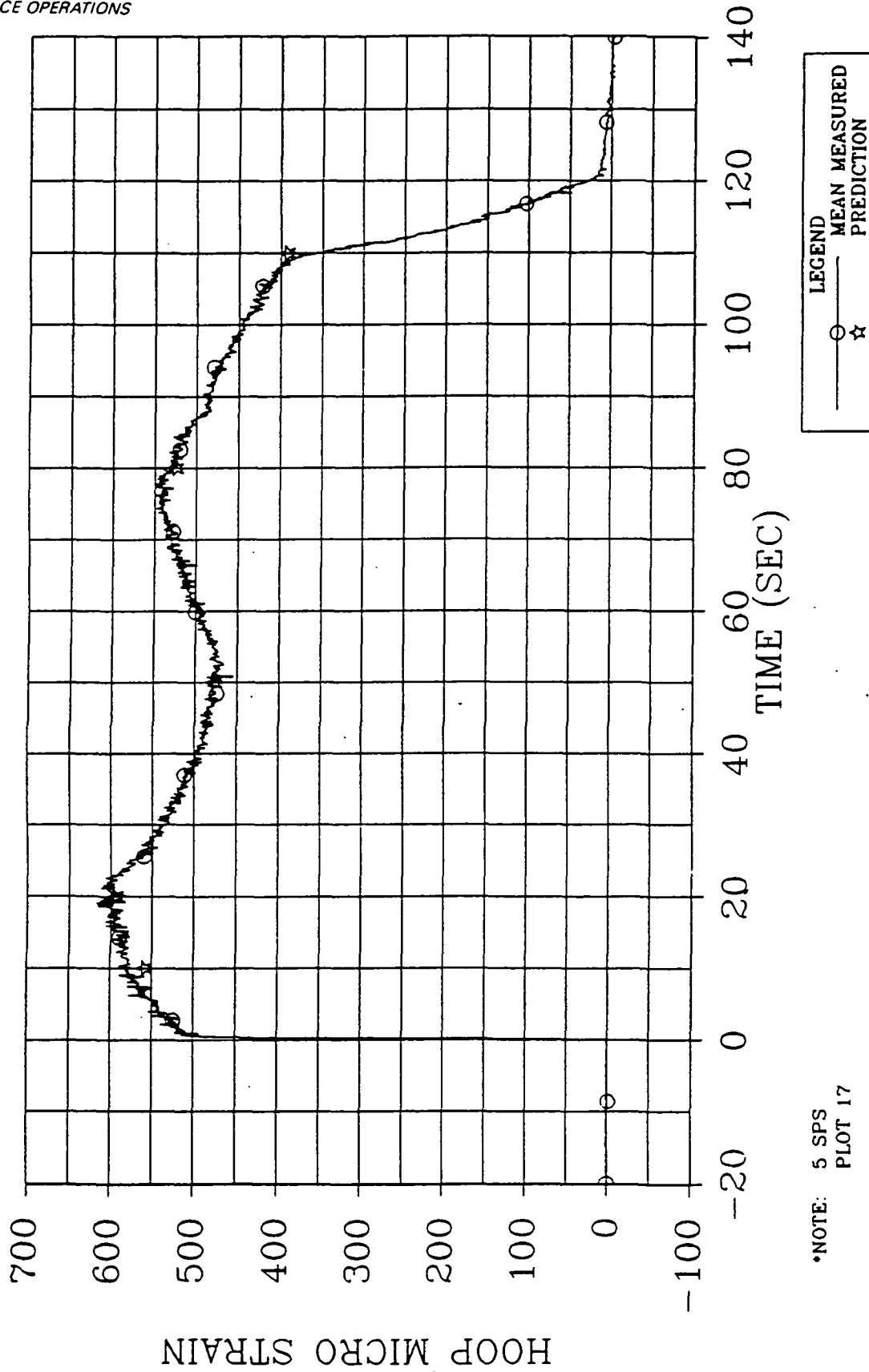
Figure 6-32. Throat Housing Sta 1839.39 Hoop Strain (mean value)

*NOTE: 5 SPS
PLOT 17

Thiokol CORPORATION
SPACE OPERATIONS
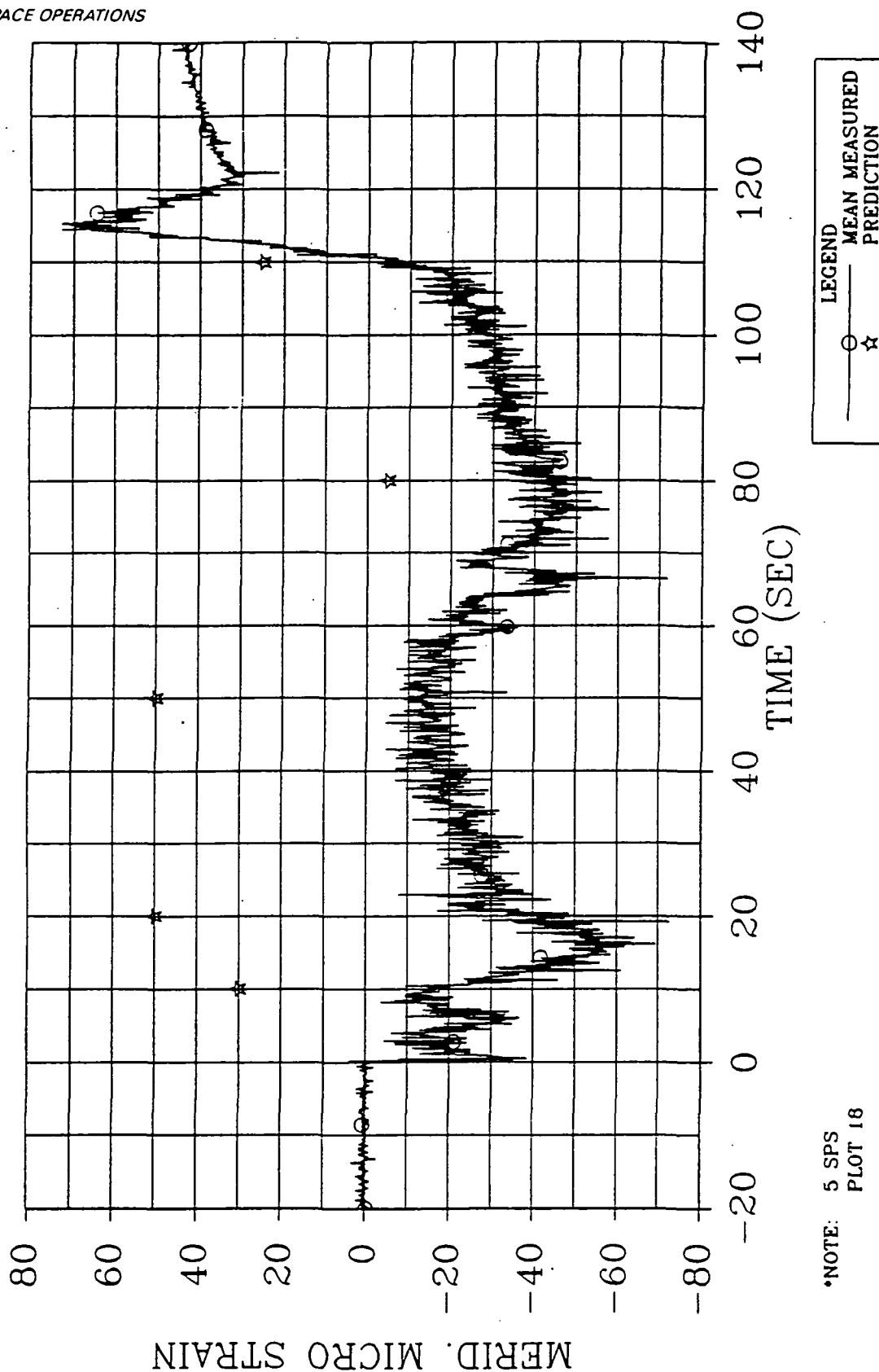
Figure 6-33. Throat Housing Sta 1839.39 Meridional Strain (mean value)
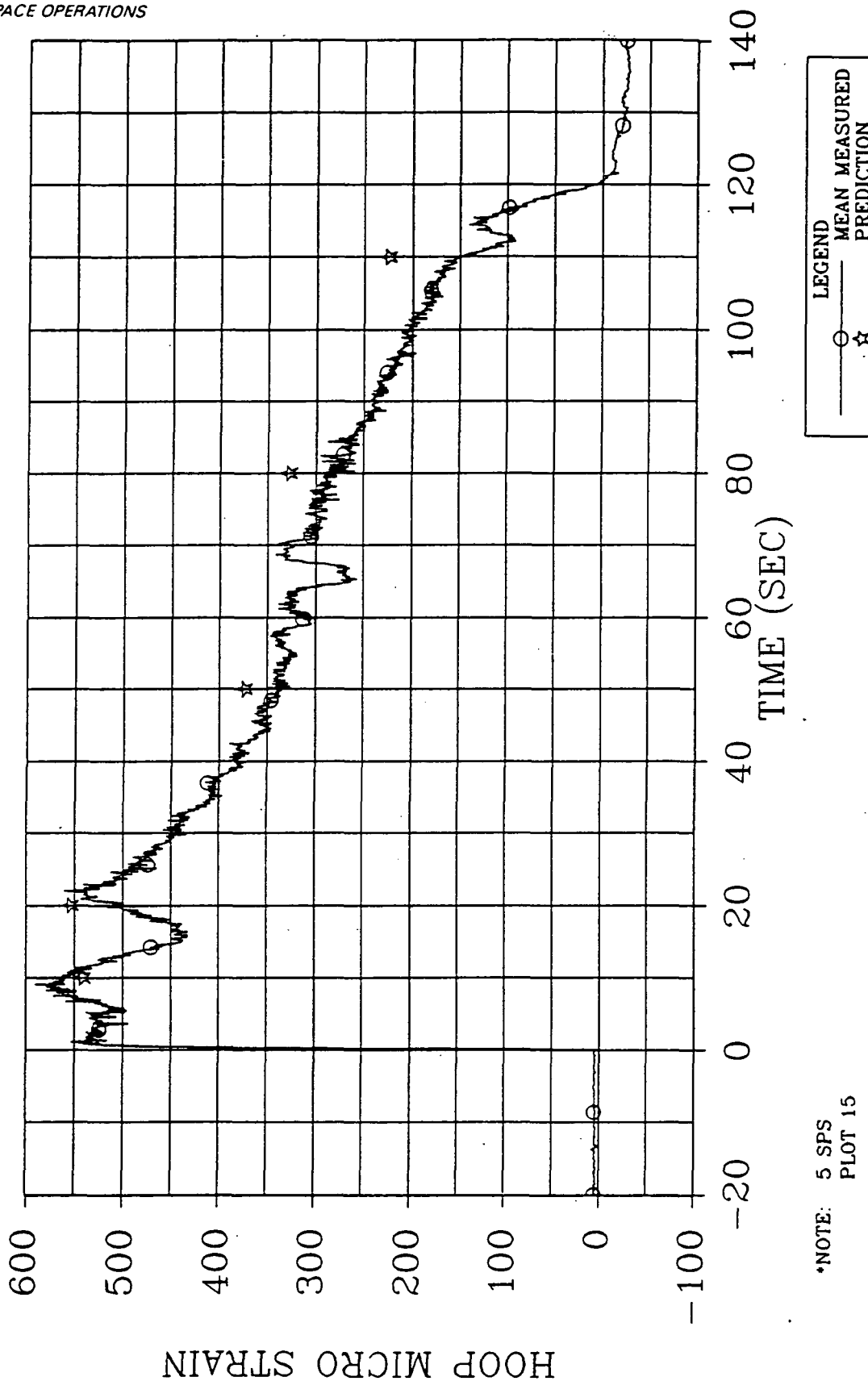
•NOTE: 5 SPS
         PLOT 18

Figure 6-34. Nose Inlet Housing Sta 1842.5 Hoop Strain (mean value)

*NOTE: 5 SPS
PLOT 15

Figure 6-35. Nose Inlet Housing Sta 1842.5 Meridional Strain (mean value)
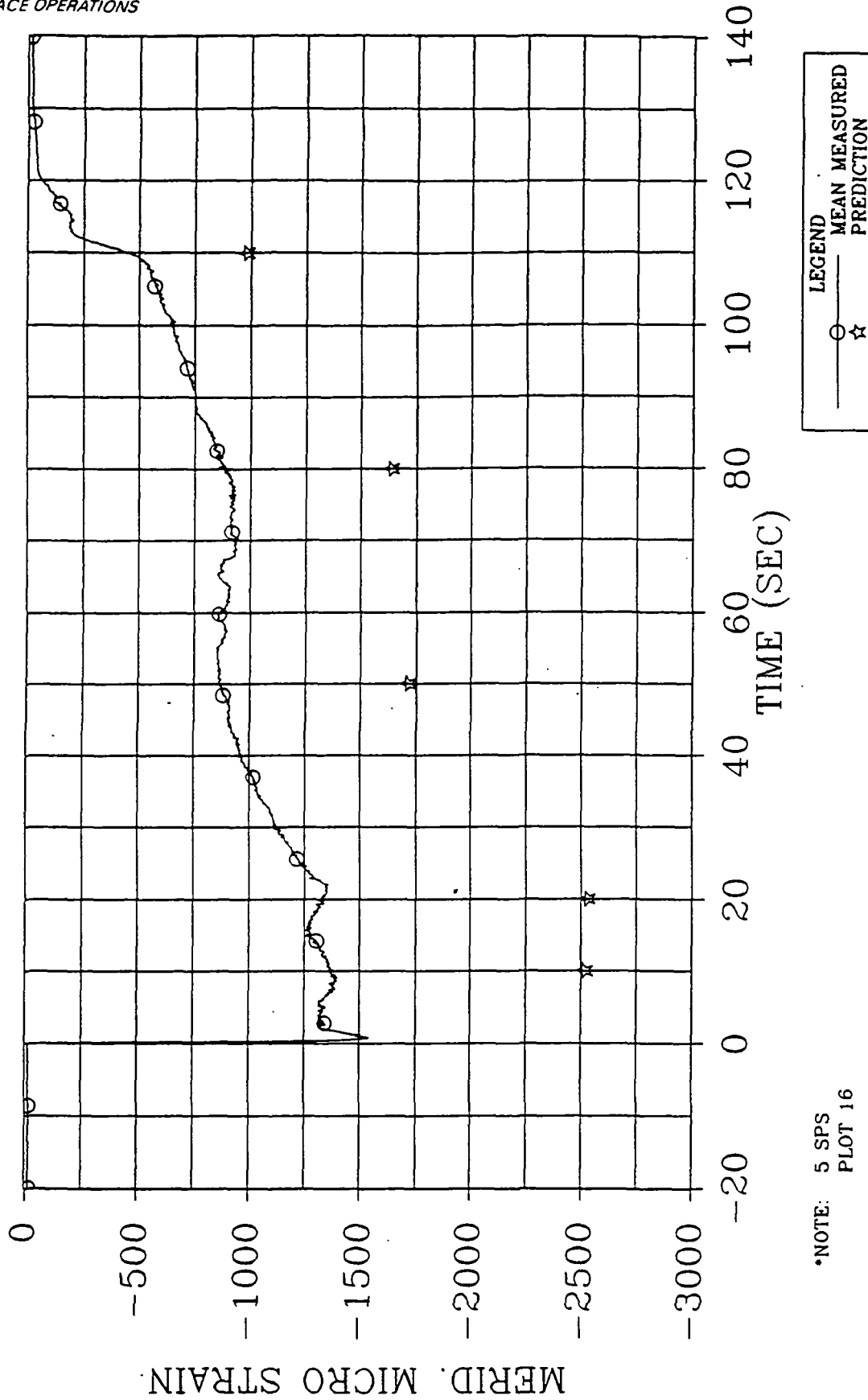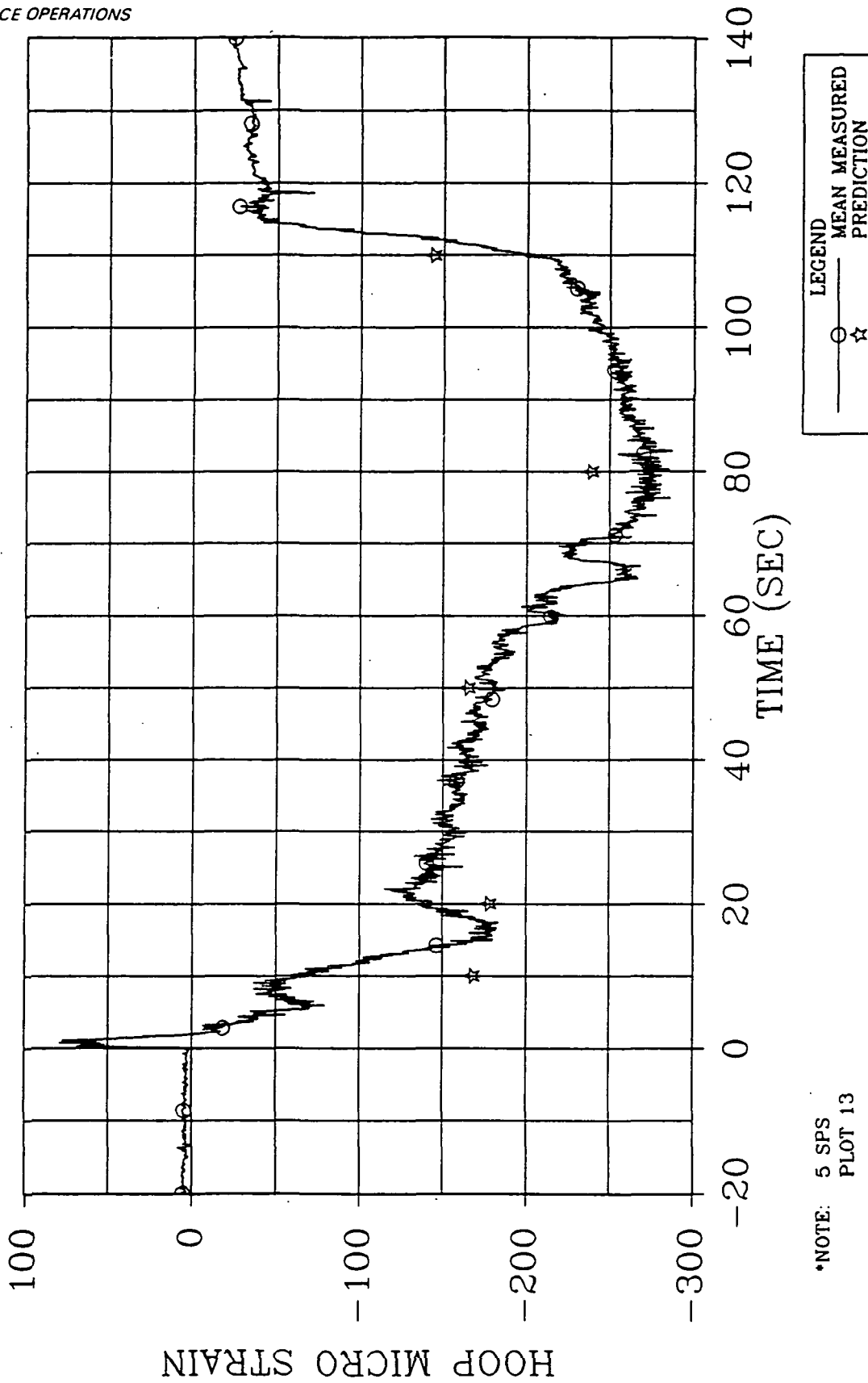
*NOTE: 5 SPS
PLOT 16

Figure 6-36.   Nose Inlet Housing Sta 1839.0 Hoop Strain (mean value)

HOOP MICRO STRAIN

*NOTE: 5 SPS
        PLOT 13

LEGEND
MEAN MEASURED
PREDICTION

Thiokol CORPORATION
SPACE OPERATIONS
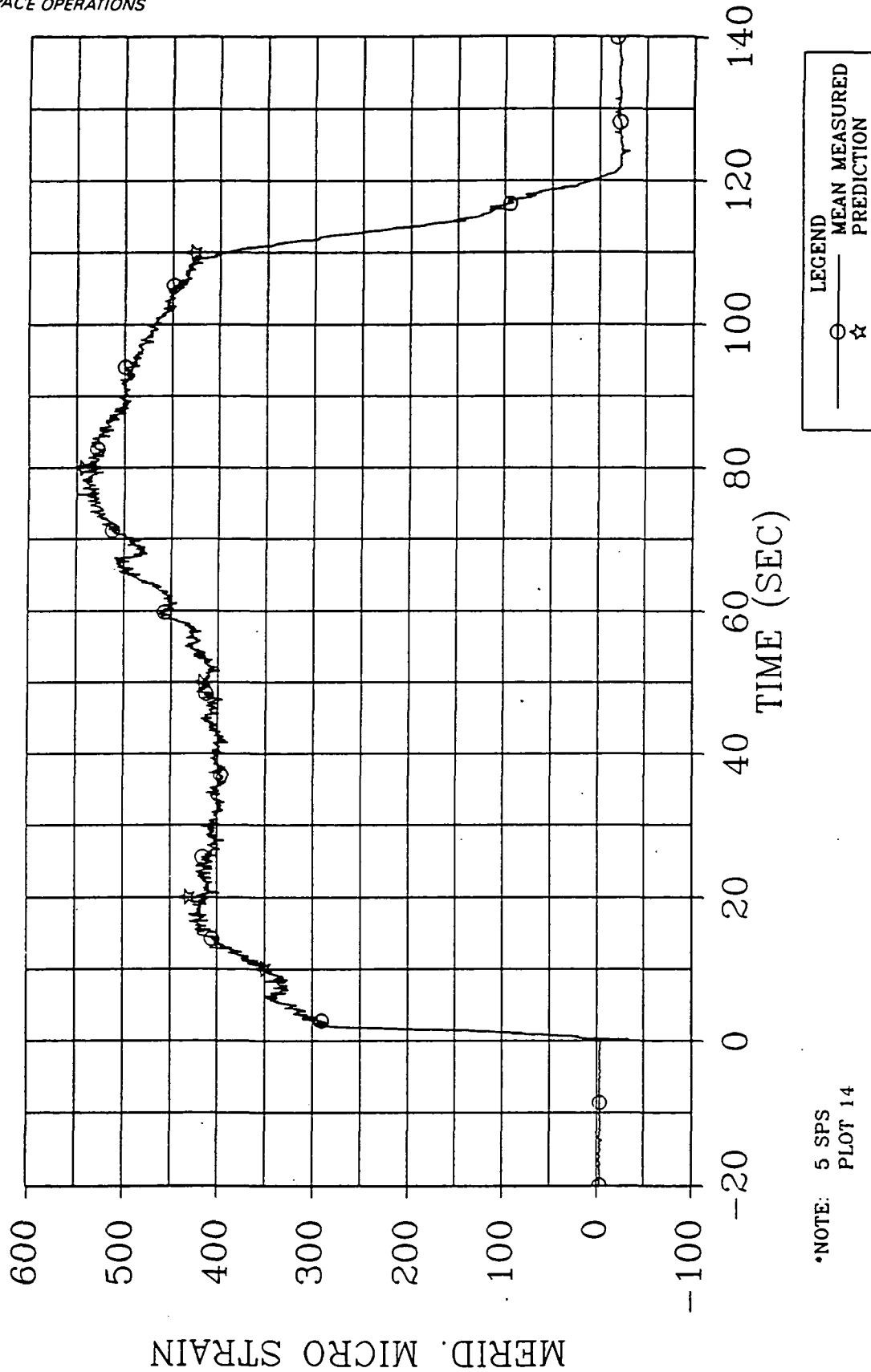
Figure 6-37. Nose Inlet Housing Sta 1839.0 Meridional Strain (mean value)

Figure 6-38. Fixed Housing Sta 1867.0 Hoop Strain
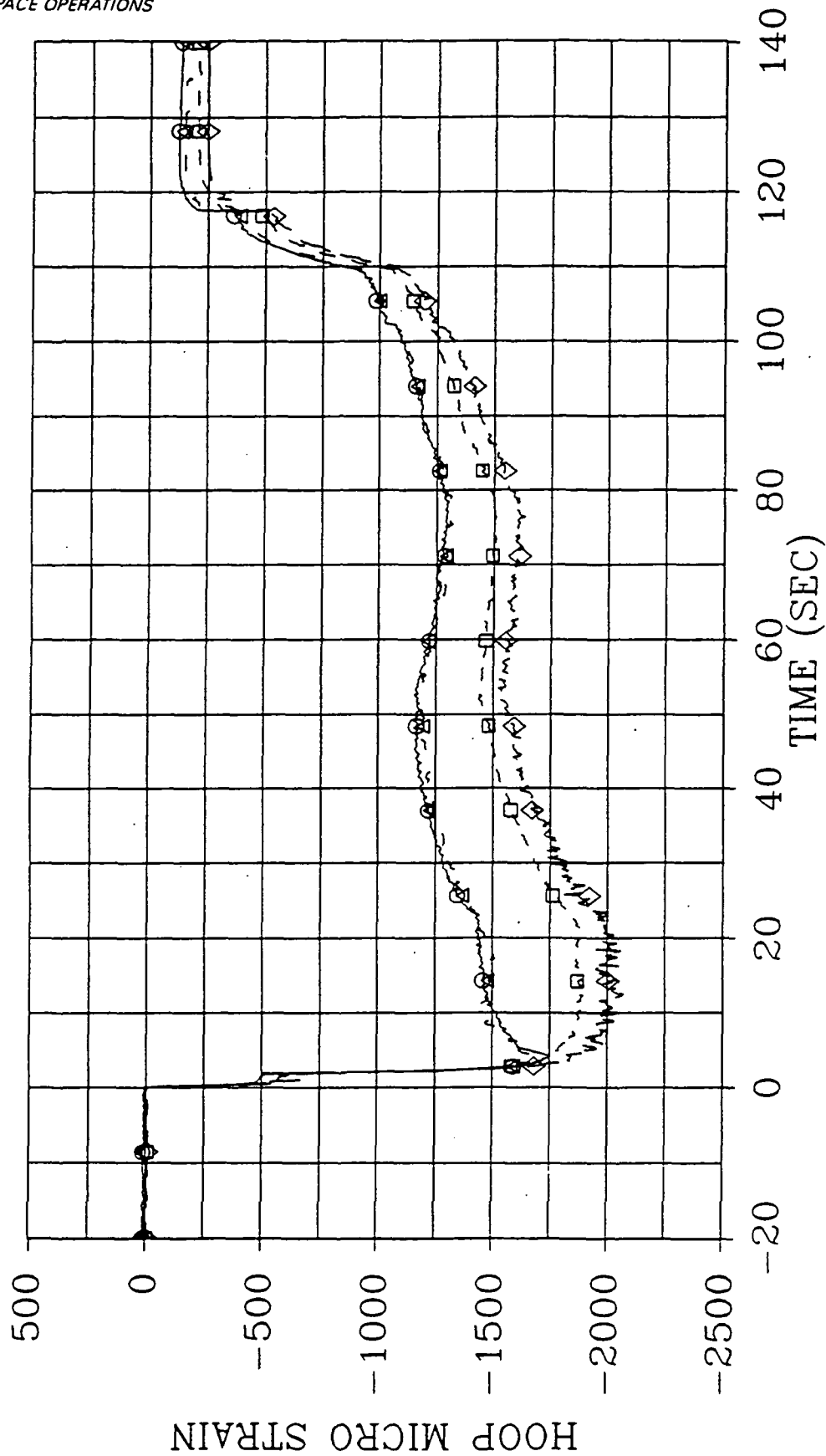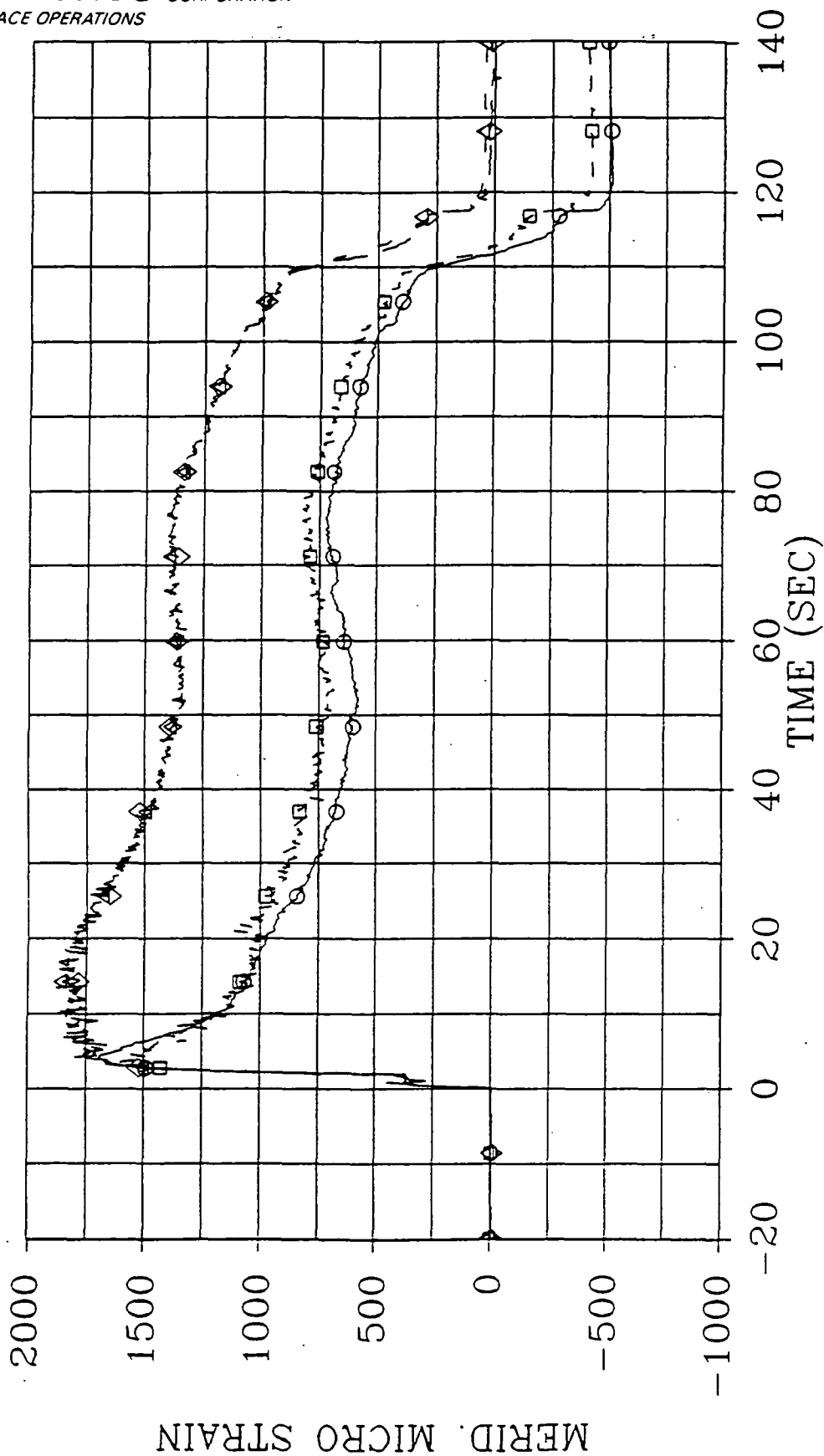
NOTE: 5 SPS
PLOT 25

Figure 6-39. Fixed Housing Sta 1867.0 Meridional Strain

*NOTE: 5 SPS
PLOT 26

Meridional strains at Station 1842.5 (Figure 6-35) were less severe than predicted values, which is typical for this location.

Nose inlet housing hoop strain at Station 1839.0 (Figure 6-36) showed a tensile shift of approximately 60 to 130 microstrain. Hoop strain at this location on the nozzle nose inlet housing is compressive. The shift occurred at ignition and was tensile, which would indicate that the instrumentation experienced a problem not impacting the nozzle hardware itself. Meridional strains at Station 1839.0 (Figure 6-37) matched predicted values.

Strain data at Station 1867.0 on the fixed housing shows an anomalous occurrence approximately 2 sec into motor burn. Both the hoop and meridional strains (Figures 6-38 and 6-39) increased sharply in magnitude at 2 sec. Extensive structural analysis, fracture mechanics analysis, and postfire observations showed that the EA 913NA adhesive bondline failed between the fixed housing and the GCP insulation. This failure was attributed to contamination of the fixed housing bonding surface coupled with the four pressure transducers installed through the fixed housing (test configuration only). This configuration created both a stress concentration and a gas path to the adhesive bond interface. Predicted strains at the gage location, prior to 2 sec, match TEM-7 measurements; also, predicted strains with pressure in the bondline match the strain data after 2 sec (Figures 6-40 and 6-41).

6.6.4.6 Nozzle TVC Performance. The TVC system performed as planned and followed the specified duty cycle.

6.7 IGNITION SYSTEM PERFORMANCE

6.7.1 Introduction

The SRM ignition system was a modified HPM igniter assembly (Drawing 1U50776). It contained a single nozzle, steel chamber, external and internal insulation, and solid propellant (TP-H1178 (STW5-2833)) igniter containing a case bonded 40-point star grain (Figures 6-42 and 6-43).

HOOP MICRO STRAIN

DISTANCE FROM FWD END

STATION 1867.0

LEGEND
PRED. W/PHENOLICS
PRED. NO PHENOLICS
TEM-07 @ 2 (STA 1867.0)
TEM-07 @ 3 (STA 1867.0)
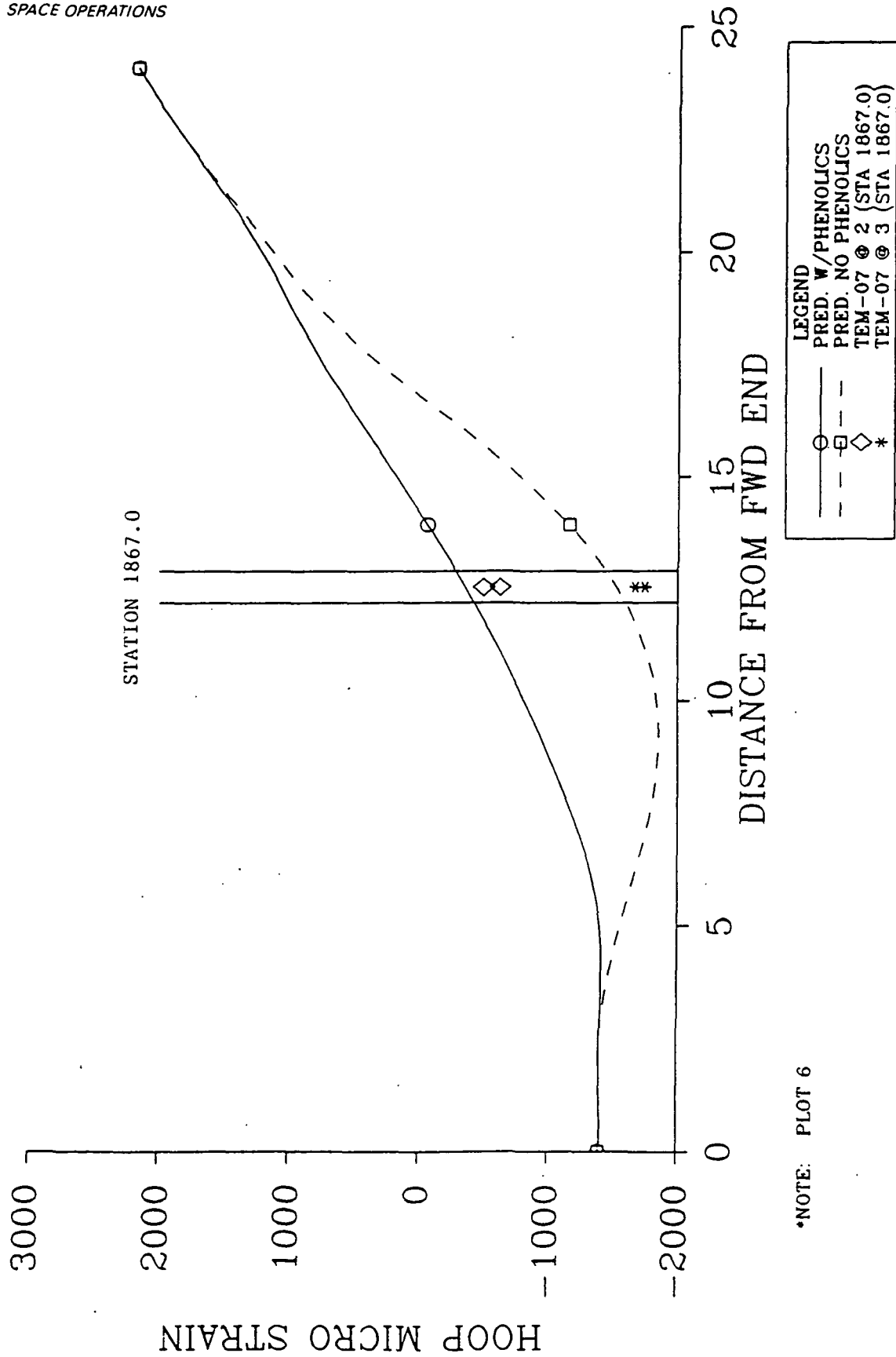
*NOTE: PLOT 6

Figure 6-40. HPM Fixed Housing Assembly–Hoop Strain at 2 Sec (actual versus predicted)
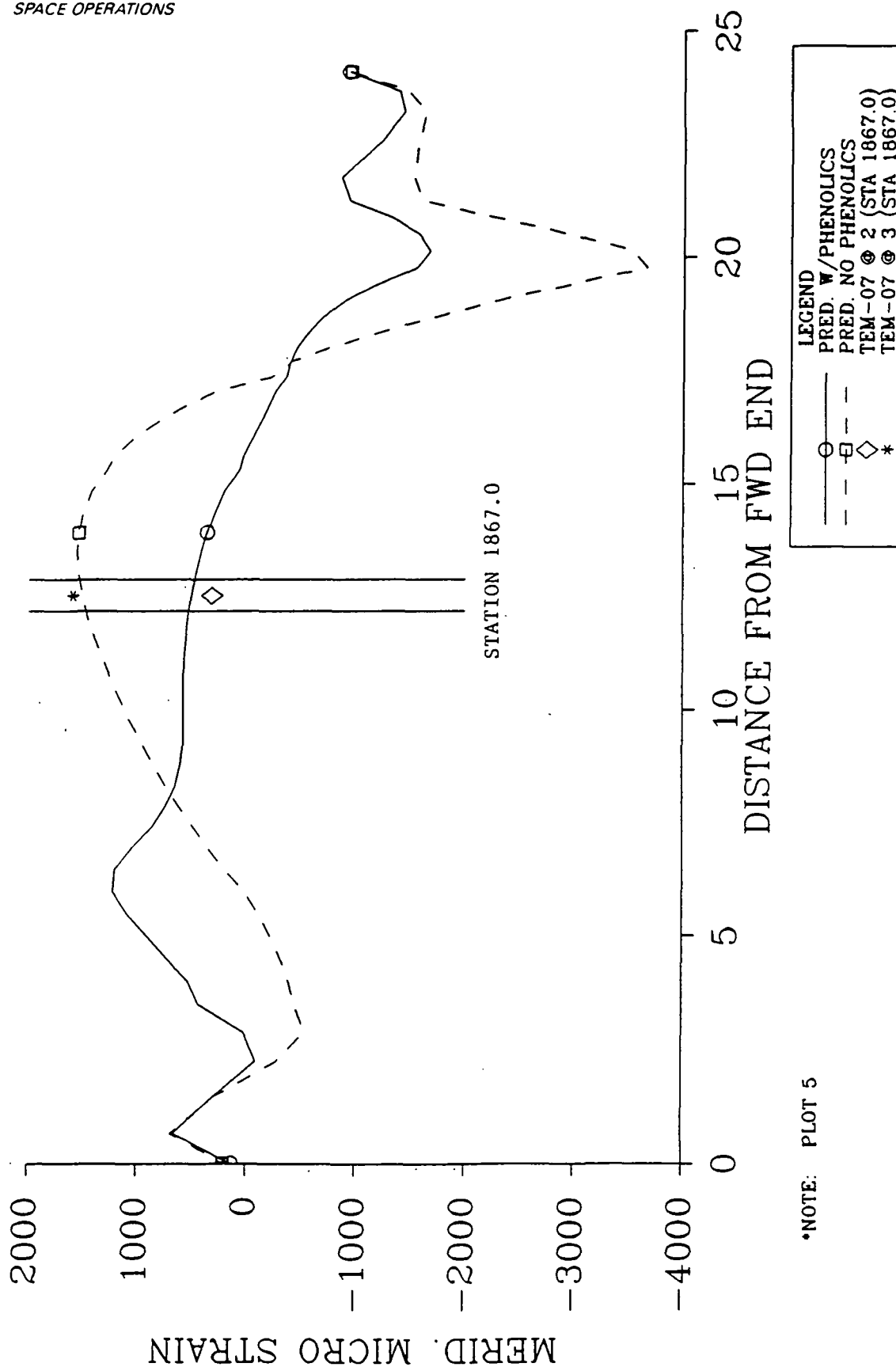
Figure 6-41. HPM Fixed Housing Assembly–Meridional Strain at 2 Sec (actual versus predicted)

*NOTE: PLOT 5

Outer Gasket

Inner Gasket

Special Bolt

OPT

Packing With
Retainers and
Special Washer

S&A Gasket

S&A Device

Igniter Adapter

Inner Gasket

Packing With Retainers

Inner Bolt

Inner Gasket
Leak Check Port

Outer Gasket
Leak Test Port

Outer Bolt

Outer Gasket

Forward Segment
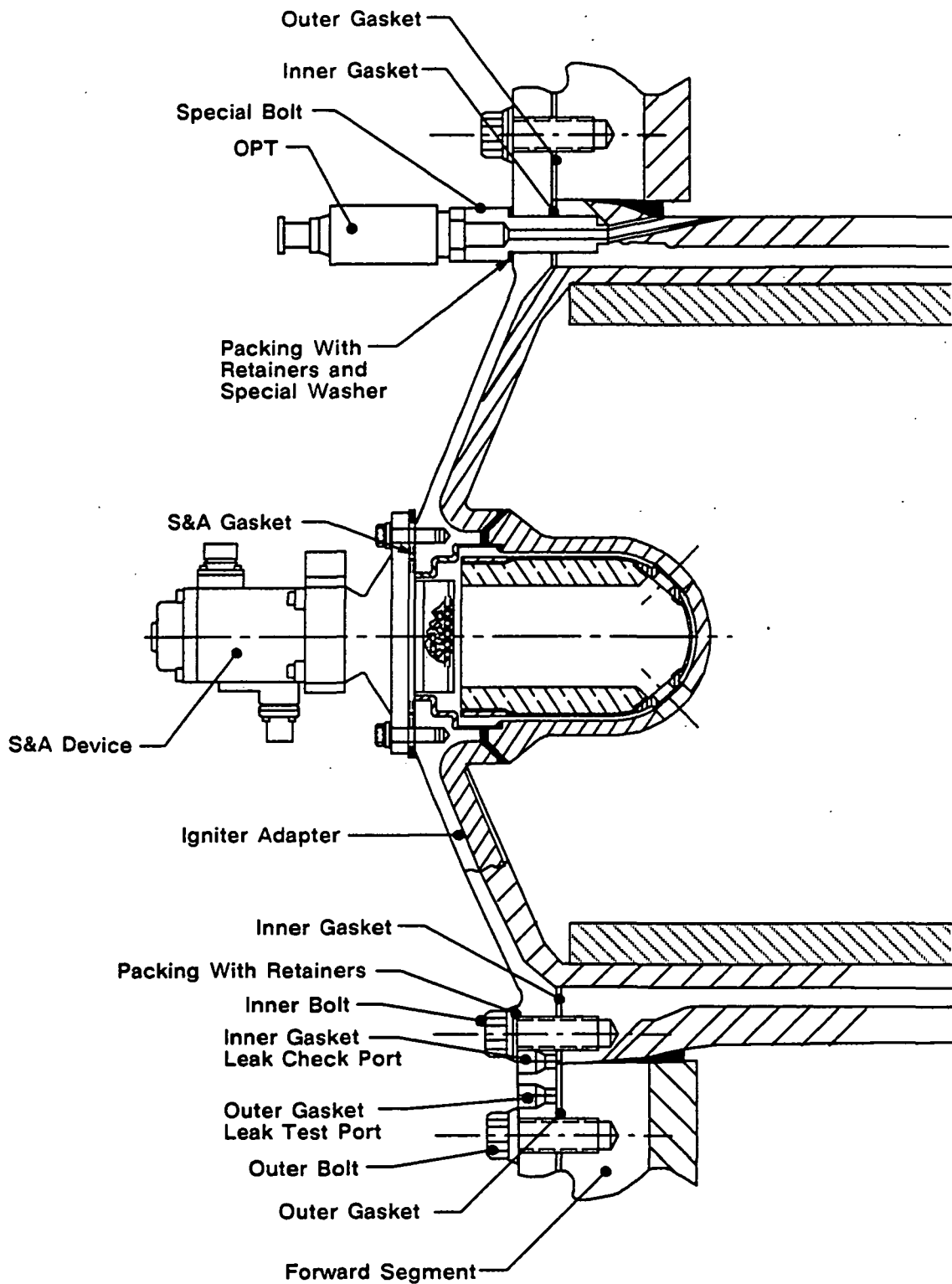
a026375a

Figure 6–42. Ignition System Components and Seals

A022491a

Pressure Transducer/
Special Bolt (four places)

Gasket

S&A Device
(with Krytox grease)

Packing With Retainer
Special Washer (inner bolt)
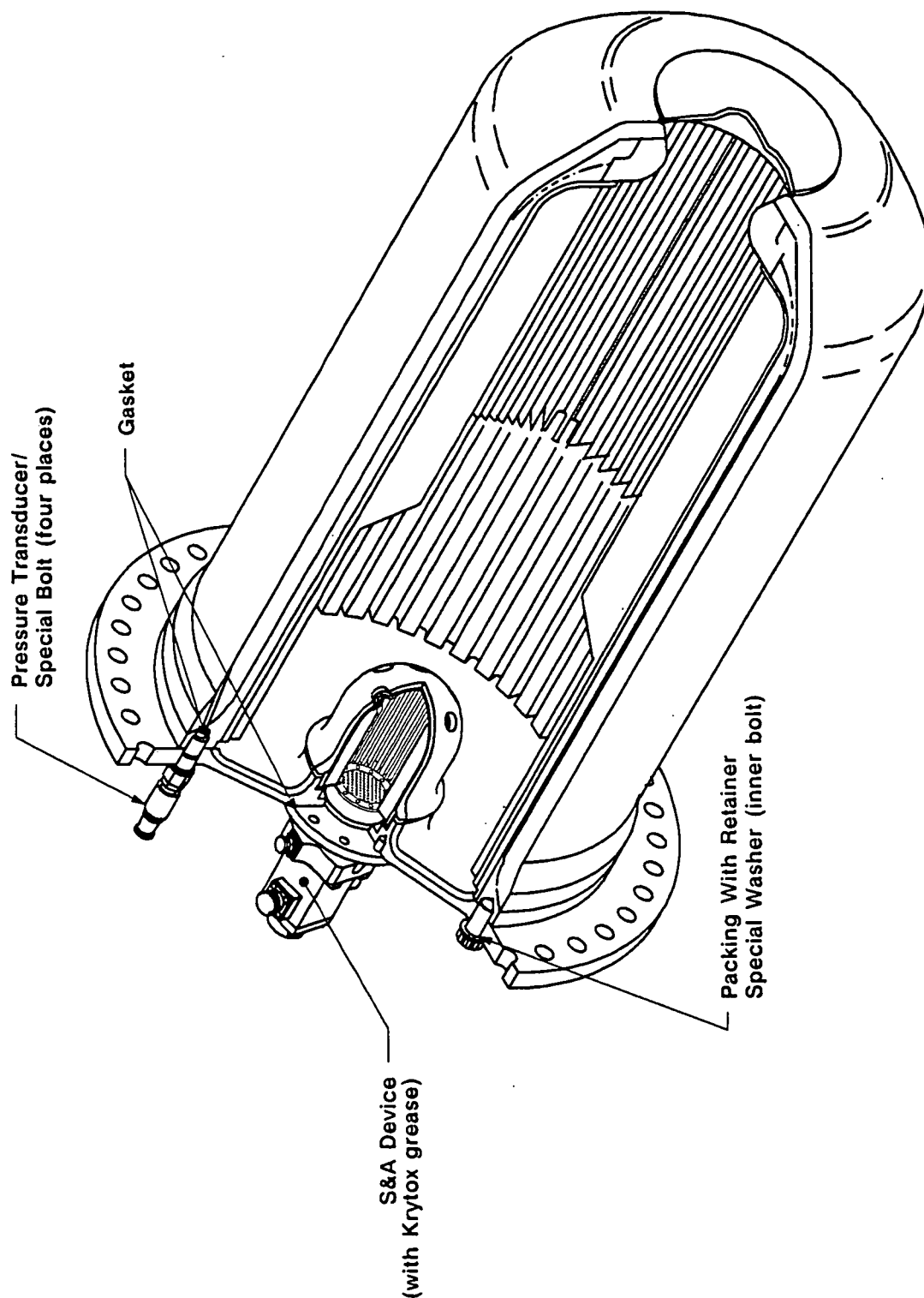
Figure 6-43. Standard HPM Igniter System

The forward-mounted solid-rocket-type igniter (Drawing 1U50776) was modified with a CO_2 quench port. Ultrasonically torqued bolts fastened the igniter adapter to the igniter chamber. A286 bolts in the igniter adapter-to-case joint were replaced with higher strength MP159 bolts which were ultrasonically preloaded to a higher level. This was the first TEM static test motor with ultrasonic bolts in the inner and outer igniter bolt circles.

An S&A device utilizing Krytox grease to lubricate the barrier-booster shaft O-rings was installed on the igniter (Figure 6-44).

Velostat or pink poly plastic sheets were wrapped and tightly sealed around the forward thrust adapter to simulate the thermal protection provided to the igniter and S&A device by flight configuration.

6.7.2 Objectives/Conclusions

There are no objectives from Section 2 concerning the ignition system.

6.7.3 Recommendations

None.

6.7.4 Results/Discussion

6.7.4.1 S&A Device Cycle Times. Performance of the Krytox grease on the barrier-booster shaft was excellent. S&A device cycle times were within the engineering requirements of 2.0 sec or less at 24 Vdc (TWR-17656, Table III).

6.7.4.2 S&A Device Removal. The S&A device was removed on 17 Dec 1990. No anomalous conditions were found during the evaluation of the S&A device sealing surfaces and gasket. Heavy soot was found on the gasket aft face, over the full circumference, up to the primary seal. Cadmium plating was missing inward of the gasket aft face primary seal, 0.020 in. from the seal cushion at 175 deg. No soot was found on the gasket forward face to the primary seal. Heavy soot was found on the

A02671a

Barrier–Booster Housing

Lock Pin

Arming Monitor Switch

Arming Monitor Backfill Port

Visual Indicator Window

Motor Field Windings

Motor Armature

Arming Monitor
Electrical Connector

Gear Reduction (625:1)

Booster Basket

B–KNO$_3$ Pellets

Foam Cushion

B–KNO$_3$ Granules

Perforated Plate

Rotor
(mechanical
barrier)

Barrier–Booster Rotor Shaft Seals
(lubricated with Krytox grease)

Barrier–Booster Position
Indicator Switch

SII

Housing

Figure 6-44. S&A Device Configuration

retainer ID over the full circumference. No damage to the gasket seals or the S&A device sealing surfaces was found.

6.7.4.3 <u>S&A Device Disassembly</u> . The TEM-7 S&A device was disassembled on 20 Dec 1990. One anomalous condition was observed during the disassembly assessment: a small axial scratch was found at 300 deg on the primary seal surface of the barrier-booster housing bore. the scratch was less than 0.1 in. in length and could be felt with a 0.005-in.-thick brass shim. PFAR TEM07-01 was written on the scratch.

Typical soot was seen to have reached the rotor shaft forward primary O-ring. Soot was also observed to reach both SRM ignition initiator (SII) primary O-rings. However, no soot or blowby was observed past any seal. There was no evidence of damage to the rotor shaft or the SII O-rings.

Typical circumferential galling was found on the land between the primary and secondary seal surfaces of both SII ports. This is an acceptable condition per the barrier-booster refurbishment specification.

<u>Special Issue (TWR-61209, Para 3.2.3, Item 1)</u>. An assessment was made at disassembly to determine if any contamination was present in the SII port leak test through holes. (Refer to DR No. 400579.) No contamination was found.

6.7.4.4 <u>Igniter Special Bolts</u> . No damage was found on the primary O-rings and no damage to the bolt threads or sealing surfaces was observed.

6.8 JOINT PROTECTION SYSTEM PERFORMANCE

6.8.1 <u>Introduction</u>

Field joint heater closeout consisted of cork strips retained with Kevlar straps. The external joint temperatures were sensed by two sensor assemblies mounted adjacent to the heater. Improved field joint heaters (Drawing 1U77252), igniter-to-case joint heater (Drawing 1U77253), and nozzle-to-case joint heater (Drawing 7U77118) were installed in accordance with Drawing 7U77328. These heaters consisted of redundant,

chemically etched foil circuits which were superimposed upon one another and laminated in polyamide plastic sheets. The underside Kapton surface of the field joint and nozzle-to-case joint heaters was coated with a pressure-sensitive adhesive. This adhesive provided bonding to the case during assembly. The lead wires extended from the heaters and were terminated in electrical connectors.

RSRM joint protection system power cables (1U76702-01, 1U76702-02, 1U76703-01, 1U76703-02, 1U76704-01, 1U76704-02, 1U76705-01, 1U76705-02, 1U76706-01, and 1U76706-02) were installed to provide 208 vac to the RSRM field joint and igniter-to-case joint heaters.

6.8.2 Objectives/Conclusions

There are no objectives from Section 2 concerning the joint protection systems.

6.8.3 Recommendations

None.

6.8.4 Results/Discussion

The joint protection systems performed within specifications and maintained the joint temperatures within the required temperature range at the time of motor ignition.

A post-test inspection with the field joint protection system still on the motor revealed no evidence of damage.

6.9 BALLISTICS/MASS PROPERTIES PERFORMANCE

6.9.1 Introduction

The SRM propellant, TP-H1148 (STW5-3343), was a composite-type solid propellant formulated of polybutadiene acrylic acid acrylonitrile terpolymer (PBAN) binder, epoxy curing agent, ammonium perchlorate oxidizer, and aluminum powder fuel.

Approximately 0.25 percent by weight (exact amount determined by standardization) of burning rate catalyst (iron oxide) was added to achieve the targeted propellant burn rate of 0.368 in./sec at 625 psia and 60°F (TWR-19121 and TWR-19838).

The propellant grain design consisted of an 11-point star with a smooth bore-to-fin-cavity transition region that tapered into a circular perforated (CP) configuration in the forward segment (Drawing 1U52565). The two center segments (Drawing 1U52566) were double-tapered CP configurations, and the aft segment (Drawing 1U52757) was a triple-taper CP configuration with a cutout for the partially submerged nozzle.

6.9.2 Objectives/Conclusions

The objectives and corresponding conclusions from Section 2 regarding ballistics/mass properties were:

Objective	Conclusion
G. Obtain data on the effect of five-year storage of loaded SRM case segments *upon motor ignition and performance.*	Motor performance was nominal. Five-year storage did not appear to affect *motor ignition and performance.*
J. Obtain additional data on the low-frequency chamber pressure oscillations in the motor forward end and correlate with chamber pressure oscillation measurements in the motor aft end.	There was no useable aft end pressure oscillation data due to the aft end phenolic insulation unbond. However, headend dynamic pressure was obtained.
K. Obtain additional data on chamber pressure drop down the bore by the use of aft end pressure transducers.	One of two Teledyne Taber pressure transducers recorded data until T + 20 sec, then the data became erratic. Software anomaly is believed to have caused both SAPMDs to be inoperable prior to test. The thermocouple data were erratic throughout the firing but did demonstrate the increased temperature into the boot cavity resulting from increased vent hole diameters.

6.9.3 Recommendations

Propellant and grain design in the existing HPM cast segments cannot be altered. The remaining HPM segments should be used on future TEM static tests.

6.9.4 Results/Discussion

TEM-7 ballistic performance was within expected limits. The TEM-7 ballistic performance compared well with previous TEM performance and HPM historical data. The aft end pressure gauges provided very little useful ballistics data due to the aft end anomalous condition. The five-year storage of loaded case segments did not appear to affect motor performance. The measured slag weight in the aft segment was 1,813 lbm.

TEM-7 exhibited chamber pressure oscillations similar to previously tested Space Shuttle HPMs. The first longitudinal (1-L) mode oscillations were typical for an HPM. In general, HPM 1-L mode amplitudes are lower than those for RSRMs. The magnitudes of the TEM-7 oscillations were among the lowest experienced in HPMs. The aft end pressure oscillations could not be analyzed due to lack of data.

A comparison of TEM-7 performance with predicted values and with the nominal HPM performance revealed few differences. The predicted burn rate for TEM-7 was 0.370 in./sec at 625 psia and 60°F, the target burn rate was 0.368 in./sec, and the delivered burn rate was 0.371 in./sec. Predicted and measured performance compared well and was within the current HPM Specifications.

Table 6-7 is a summary of the measured ballistic and nozzle performance data. Figure 6-45 is a comparison of measured and predicted pressure-time histories. The measured and predicted performance compared well for this motor. Thrust was not measured for this static test; only reconstructed thrust based on nominal thrust-to-pressure ratios is available.

Figures 6-46 and 6-47 contain plots of the analytical reconstruction of TEM-7 performance. The analytical model calculated the motor burn rate and surface burn

Table 6-7. Summary of Measured Ballistic and Nozzle Performance Data

A. Ambient conditions		
Time and date at fire pulse	1300 hours, 11 Dec 1990	
Ambient temperature	44.00	°F
Measured mean bulk temperature	65.00	°F
Measured ambient pressure	12.28	psia

B. Weight data		
Total loaded propellant weight	1,109,826.0	lb
Total expended weight	1,114,176.0	lb
Unexpended propellant residue (slag)	2,000.0	lb
Expended inert weight		
1. Forward segment	718.0	lb
2. Forward center segment	598.0	lb
3. Aft center segment	962.0	lb
4. Aft segment (including nozzle from field joint forward)	4,072.0	lb
5. Total expended inerts	6,350.0	lb
Total expended propellant weight	1,107,826.0	lb

C. Nozzle data		
Initial throat area	2,280.3	in.^{2}
Final throat area	2,469.3	in.^{2}
Web time average throat area	2,378.5	in.^{2}
Action time average throat area	2,386.9	in.^{2}
Total time average throat area	2,387.1	in.^{2}
Initial exit area	17,586.5	in.^{2}
Final exit area	17,681.8	in.^{2}
Total time average exit area	17,634.2	in.^{2}
Web time average throat radial erosion rate	0.00972	ips
Action time average throat radial erosion rate	0.00910	ips
Total time average throat radial erosion rate	0.00905	ips
Initial expansion ratio	7.7123	
Web time average expansion ratio	7.4138	
Action time average expansion ratio	7.3878	
Action time average nozzle efficiency	0.97292	
Total time average nozzle efficiency	0.97305	

Table 6-7. Summary of Measured Ballistic and Nozzle Performance Data (cont)

D. Time and ballistic data		
Time at first indication of headend pressure	0.029	sec
Ignition delay time	-0.023	sec
Time at 90 percent maximum igniter pressure	0.052	sec
Ignition interval time	0.235	sec
Ignition rise time	0.206	sec
Time when headend chamber pressure achieves 563.5 psia during ignition	0.235	sec
Time at last indication of headend pressure	120.951	sec
Time at web bisector	109.049	sec
Web time	108.813	sec
Action time	120.203	sec
Total time	120.922	sec
Tailoff thrust decay time	0.512	sec
Maximum change in thrust over 10 ms during ignition	271,759	lb
Maximum igniter pressure	1,840	psia
Maximum measured headend pressure	933.20	psia
Time at maximum headend pressure	0.652	sec
Maximum thrust	3,165,676	lb
Time at maximum thrust	16.504	sec
Maximum thrust corrected to vacuum	3,381,797	lb
Maximum thrust corrected to sea level	3,123,085	lb
Maximum stagnation pressure	863.7	psia
Web time average headend chamber pressure	680.58	psia
Action time average headend chamber pressure	632.04	psia
Web time average nozzle stagnation pressure	663.86	psia
Action time average nozzle stagnation pressure	616.82	psia
Initial thrust	2,942,746	lb
Initial thrust corrected to vacuum	3,158,717	lb
Initial thrust corrected to sea level	2,900,184	lb
Web time average thrust	2,443,689	lb
Web time average thrust corrected to vacuum	2,660,180	lb
Action time average thrust	2,259,953	lb
Action time average thrust corrected to vacuum	2,471,540	lb
Characteristic exhaust velocity	5,079.31	ft/sec

Table 6-7. Summary of Measured Ballistic and Nozzle Performance Data (cont)

E. Impulse data		
Measured total impulse	271.792	Mlb-sec
Total impulse corrected to vacuum	297.302	Mlb-sec
Measured impulse at 20 sec	61.497	Mlb-sec
20-sec impulse corrected to vacuum	65.814	Mlb-sec
Measured impulse at 60 sec	162.382	Mlb-sec
60-sec impulse corrected to vacuum	175.353	Mlb-sec
Web time impulse	265.906	Mlb-sec
Web time impulse corrected to vacuum	289.462	Mlb-sec
Action time impulse	271.653	Mlb-sec
Action time impulse corrected to vacuum	297.087	Mlb-sec
Specific impulse	243.940	sec
Specific impulse corrected to vacuum	266.836	sec
Web time specific impulse	245.379	sec
Web time specific impulse corrected to vacuum	267.117	sec
Action time specific impulse	243.981	sec
Action time specific impulse corrected to vacuum	266.824	sec
Propellant specific impulse	245.338	sec
Propellant specific impulse corrected to vacuum	268.366	sec
F. Pressure integral data		
Total time pressure integral	76,024.1	psia-sec
Web time pressure integral	74,056.6	psia-sec
Action time pressure integral	75,982.6	psia-sec

Table 6-7. Summary of Measured Ballistic and Nozzle Performance Data (cont)

D. Time and ballistic data (corrected to 40 °F)		
Time at first indication of headend pressure	0.031	sec
Time when headend chamber pressure achieves 563.5 psia during ignition	0.247	sec
Time at last indication of headend pressure	124.320	sec
Time at web bisector	112.186	sec
Web time	111.940	sec
Action time	123.572	sec
Maximum measured headend pressure	906.10	psia
Time at maximum headend pressure	0.670	sec
Maximum thrust corrected to vacuum	3,283,433	lb
Maximum nozzle stagnation pressure	838.6	psia
Web time average headend chamber pressure	660.67	psia
Action time average headend chamber pressure	613.84	psia
Web time average nozzle stagnation pressure	644.44	psia
Action time average nozzle stagnation pressure	599.06	psia
Web time average thrust corrected to vacuum	2,582,354	lb
Action time average thrust corrected to vacuum	2,400,403	lb
E. Impulse data (corrected to 40 °F)		
Total impulse corrected to vacuum	296.831	Mlb-sec
20-sec impulse corrected to vacuum	63.837	Mlb-sec
60-sec impulse corrected to vacuum	170.935	Mlb-sec
Web time impulse corrected to vacuum	289.068	Mlb-sec
Action time impulse corrected to vacuum	296.622	Mlb-sec
Specific impulse corrected to vacuum	266.413	sec
Web time specific impulse corrected to vacuum	266.705	sec
Action time specific impulse corrected to vacuum	266.412	sec
Propellant specific impulse corrected to vacuum	267.940	sec

Table 6-7. Summary of Measured Ballistic and Nozzle Performance Data (cont)

D. Time and ballistic data (corrected to 60 °F)		
Time at first indication of headend pressure	0.029	sec
Time when headend chamber pressure achieves 563.5 psia during ignition	0.238	sec
Time at last indication of headend pressure	121.619	sec
Time at web bisector	109.649	sec
Web time	109.411	sec
Action time	120.864	sec
Maximum measured headend pressure	927.72	psia
Time at maximum headend pressure	0.656	sec
Maximum thrust corrected to vacuum	3,361,900	lb
Maximum nozzle stagnation pressure	858.6	psia
Web time average headend chamber pressure	676.60	psia
Action time average headend chamber pressure	628.38	psia
Web time average nozzle stagnation pressure	659.98	psia
Action time average nozzle stagnation pressure	613.25	psia
Web time average thrust corrected to vacuum	2,644,611	lb
Action time average thrust corrected to vacuum	2,457,255	lb
E. Impulse data (corrected to 60 °F)		
Total impulse corrected to vacuum	297.197	Mlb-sec
20-sec impulse corrected to vacuum	65.402	Mlb-sec
60-sec impulse corrected to vacuum	174.446	Mlb-sec
Web time impulse corrected to vacuum	289.350	Mlb-sec
Action time impulse corrected to vacuum	296.993	Mlb-sec
Specific impulse corrected to vacuum	266.741	sec
Web time specific impulse corrected to vacuum	267.033	sec
Action time specific impulse corrected to vacuum	266.740	sec
Propellant specific impulse corrected to vacuum	268.270	sec

Table 6-7. Summary of Measured Ballistic and Nozzle Performance Data (cont)

D. Time and ballistic data (corrected to 90 °F)		
Time at first indication of headend pressure	0.026	sec
Time when headend chamber pressure achieves 563.5 psia during ignition	0.224	sec
Time at last indication of headend pressure	117.670	sec
Time at web bisector	106.040	sec
Web time	105.815	sec
Action time	116.931	sec
Maximum measured headend pressure	961.12	psia
Time at maximum headend pressure	0.634	sec
Maximum thrust corrected to vacuum	3,483,113	lb
Maximum nozzle stagnation pressure	889.5	psia
Web time average headend chamber pressure	700.99	psia
Action time average headend chamber pressure	650.74	psia
Web time average nozzle stagnation pressure	683.77	psia
Action time average nozzle stagnation pressure	635.08	psia
Web time average thrust corrected to vacuum	2,739,954	lb
Action time average thrust corrected to vacuum	2,544,695	lb

| E. Impulse data (corrected to 90 °F)		
Total impulse corrected to vacuum	297.744	Mlbf-sec
20-sec impulse corrected to vacuum	67.820	Mlbf-sec
60-sec impulse corrected to vacuum	179.915	Mlbf-sec
Web time impulse corrected to vacuum	289.929	Mlbf-sec
Action time impulse corrected to vacuum	297.552	Mlbf-sec
Specific impulse corrected to vacuum	267.232	sec
Web time specific impulse corrected to vacuum	267.523	sec
Action time specific impulse corrected to vacuum	267.231	sec
Propellant specific impulse corrected to vacuum	268.764	sec

Thiokol CORPORATION
SPACE OPERATIONS
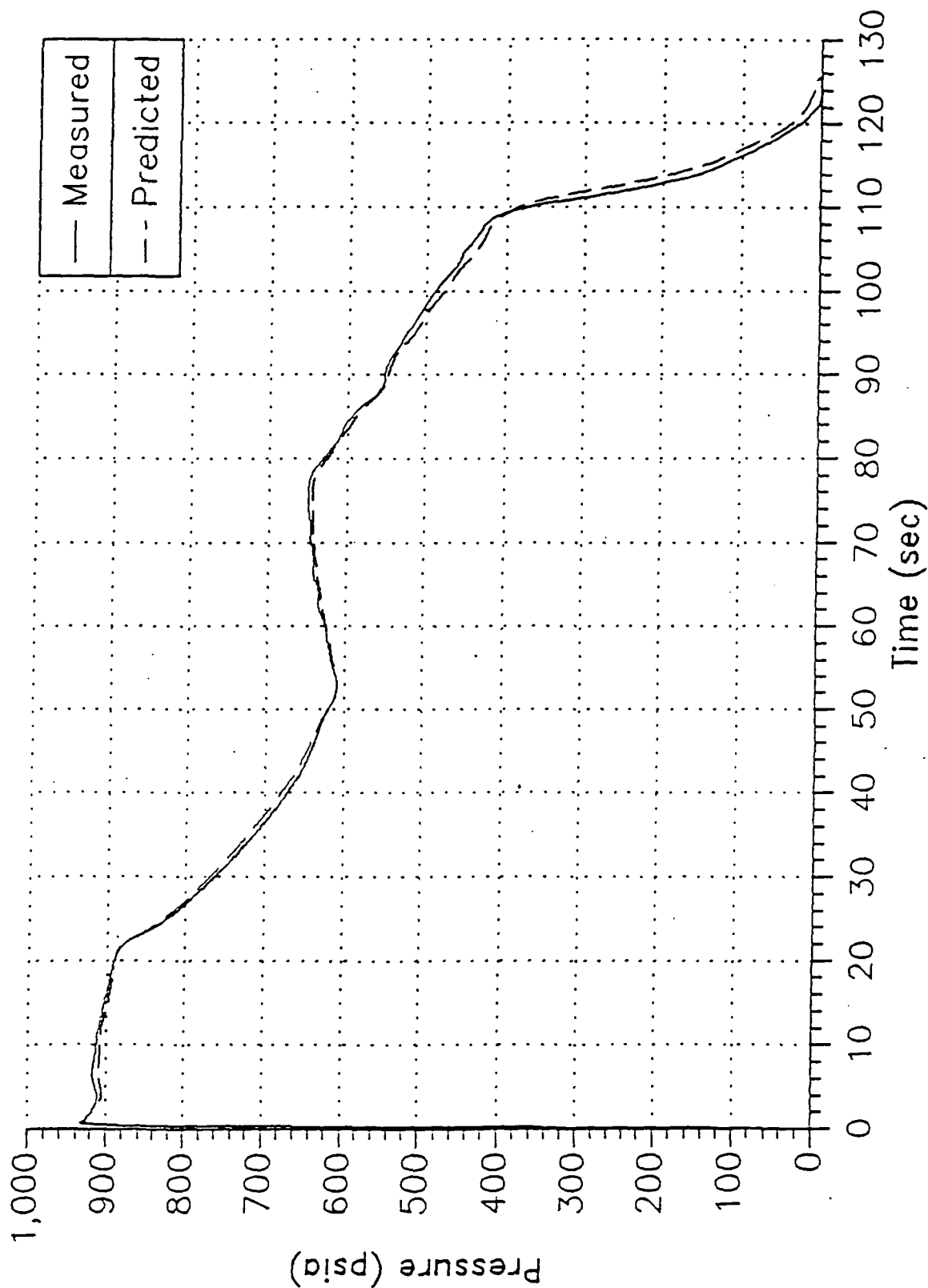
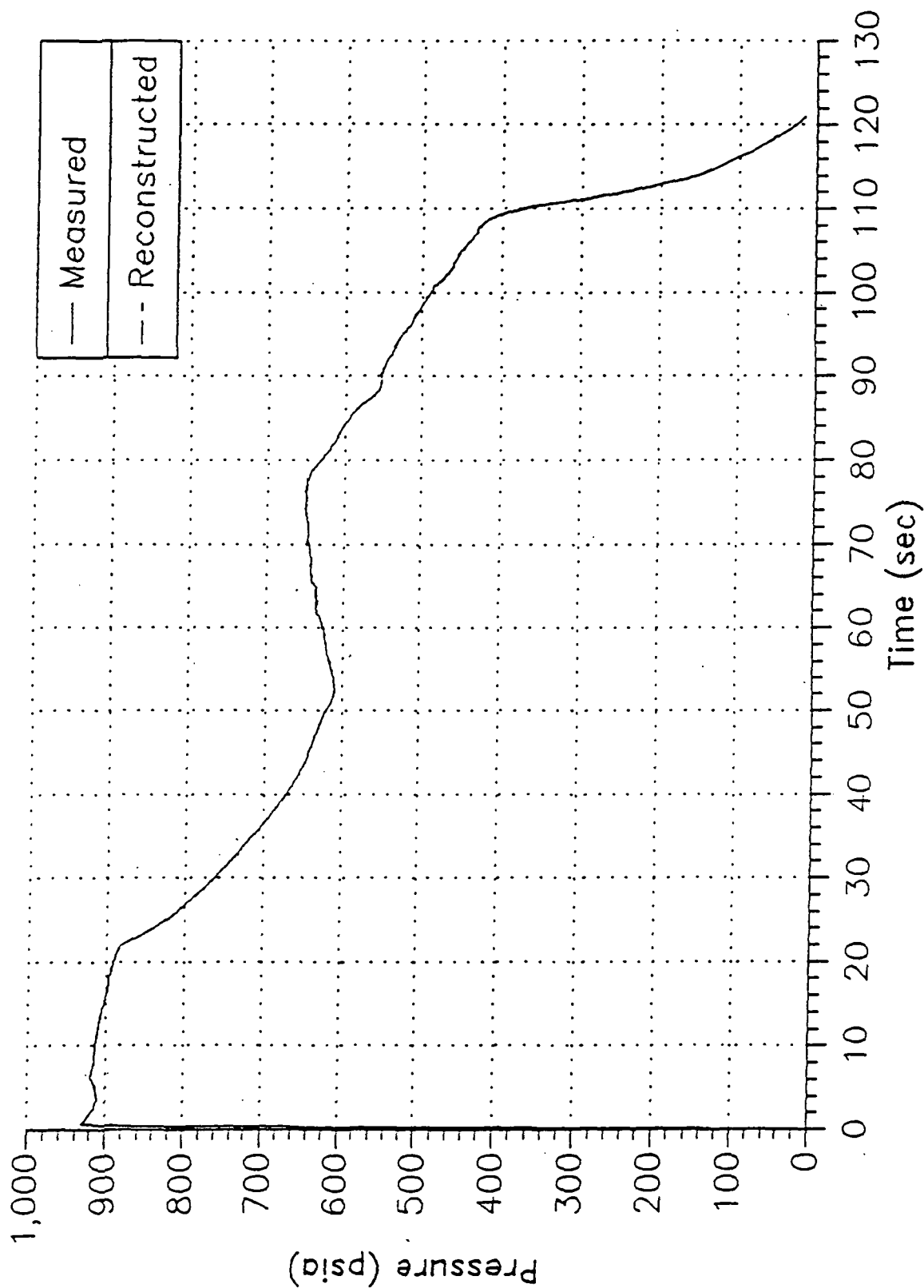**Figure 6-45. Predicted and Measured Pressure at 65°F**

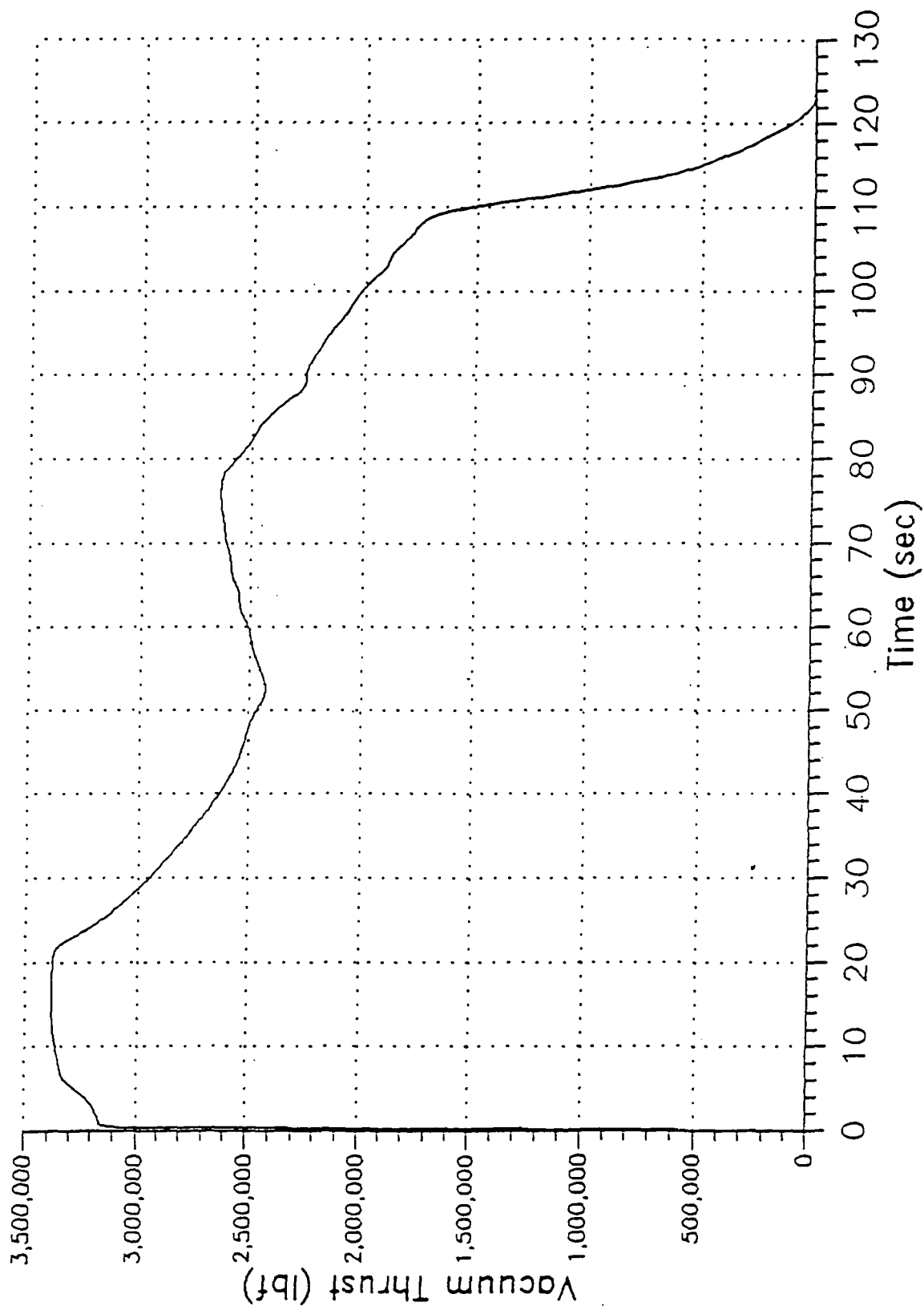Figure 6-46. Reconstructed and Measured Pressure at 65°F

Figure 6-47. Reconstructed Vacuum Thrust at 65°F

rate error (SBRE) factor. The calculated burn rate of 0.3709 in./sec at 625 psia and 60°F was approximately 0.3 percent above the predicted value of 0.3697 in./sec, well within burn rate variation. The calculated SBRE table compared well with the nominal HPM table, as expected, since the propellant grain geometry was the same.

Figure 6-48 shows measured aft end chamber pressure with reconstructed headend pressure and the corresponding aft end pressure data. The reconstruction is forced to match the headend pressure, not aft end pressure. The TEM-6 motor provided good insight to the measured aft end pressure, and the reconstructed aft end data shown in Figure 6-48 are believed to be accurate for TEM-7.

The actual TEM-7 aft end pressure data are scattered. At 2 sec in burn the pressure data rapidly decrease and then recover to a point. After each gauge recovers from the initial pressure drop, all consistently lag headend pressure. Postflight inspection did reveal plugged port holes and heat-affected transducers. As shown in the figure, all aft end pressure readings maintained a higher-than-ambient pressure after the test. Gauge PNNAR006 drops below the other aft end gauges, as was seen on TEM-6.

The ballistics code shows the reconstruction of PSN to be higher than actual measured data, but the reconstruction of pressure at axial location 1577 in. (aft segment factory joint) is very close to measured aft end pressure. The ballistics model is a one-dimensional (1-D) code that does not accurately model the flow field in the aft end of the aft segment. (The 1-D model shows a pressure recovery after location 1,577 inches.) Previous strain gauge data have shown no increase in pressure in this region; thus, the pressure at the factory joint models the aft end pressure very well.

All aft end gauges were acoustically quiet (due to partial plugging), and no oscillation analysis could be made.
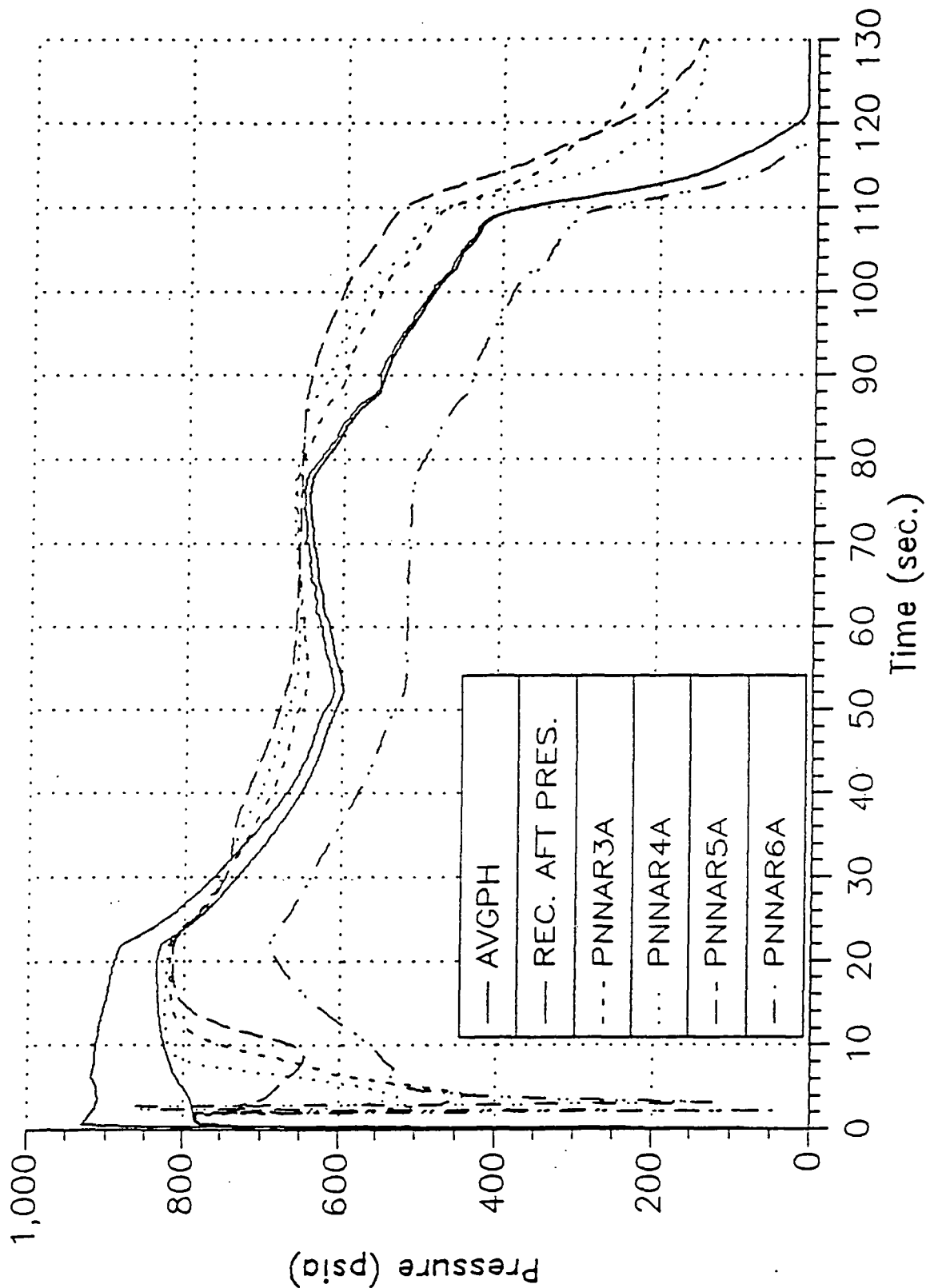
Figure 6-48. Comparison of Reconstructed and Measured Aft End Pressure

The motor average subscale burn rates, full-scale motor burn rates (determined from post-test curve matching), and resulting scale factors for SRM-15 to SRM-24 used to predict the TEM-7 burn rate are listed in Table 6-8. The full-scale motor burn rates were determined form post-test curve matching, in which the analytical model was forced to match the measured motor performance. The mean scale factor was 1.0175 with a sigma 0.00440 and a coefficient of variation of 0.432 percent.

A plot of the measured data comparing the ignition transients of the TEM static tests is shown in Figure 6-49. The TEM-7 transient was very similar to previously measured motor ignition performance. The TEM-7 maximum pressure rise rate was 80.62 psi/10 ms. The historical three-point average pressure rise rate is 90.07 psi/10 ms, with a variation of 6.80 psi/10 ms. TEM-7 had the second lowest measured pressure rise rate but was within two standard deviations of the population average. Table 6-9 is a summary table showing the historical pressure rise rates, thrust rise rates, and ignition intervals. A summary of the TEM-7 ignition events is shown in Table 6-10.

The TEM-7 igniter grain configuration was identical to the HPM flight and static test igniter design. The igniter was cast from propellant batch D760006 using TP-H1178 propellant. The delivered maximum mass flow rate was 330.0 lbm/sec at 65°F for the TEM-7 igniter (65°F is the assumed propellant mean bulk temperature for the igniter). The TEM-7 igniter performance characteristics were within the expected ranges. Comparison of TEM-7 igniter performance at 80°F with the igniter limits at 80°F is shown in Figure 6-50. TEM-7 is within the limits at 80°F.

A comparison of the igniter pressure-versus-motor headend and nozzle stagnation pressure for the first 1.4 sec of motor operation is shown in Figure 6-51. The slight mismatch between igniter and headend chamber pressure values from 0.6 to 1.4 sec is within allowed transducer error. A plot of headend and nozzle stagnation pressure for the full duration of the static test is shown on Figure 6-52. These curves are characteristic of the ratio of the headend-to-nozzle stagnation pressures from previous SRM static test motors.

Table 6-8. Burn Rate Data Comparison--Subscale to Full Scale (625 psia, 60°F)

| Motor | Burn Rate (in./sec) | | | | Scale Factor |
	SRM Target	5-in. CP Standard	SRM Predicted	SRM Delivered	5-in. CP Standard (in./sec)
SRM-15A	0.368	0.366	0.370	0.3701	1.0112
SRM-15B	0.368	0.366	0.370	0.3709	1.0134
SRM-16A	0.368	0.365	0.369	0.3684	1.0093
SRM-16B	0.368	0.365	0.369	0.3688	1.1040
SRM-17A	0.368	0.363	0.367	0.3680	1.0138
SRM-17B	0.368	0.362	0.366	0.3694	1.0204
SRM-18A	0.368	0.362	0.367	0.3693	1.0202
SRM-18B	0.368	0.363	0.368	0.3690	1.0165
SRM-19A	0.368	0.364	0.369	0.3703	1.0173
SRM-19B	0.368	0.364	0.369	0.3704	1.0176
SRM-20A	0.368	0.368	0.373	0.3742	1.0168
SRM-20B	0.368	0.366	0.371	0.3744	1.0230
SRM-21A	0.368	0.367	0.370	0.3737	1.0183
SRM-21B	0.368	0.365	0.368	0.3744	1.0258
SRM-22A	0.368	0.362	0.365	0.3675	1.0152
SRM-22B	0.368	0.362	0.365	0.3697	1.0213
SRM-23A	0.368	0.364	0.367	0.3713	1.0201
SRM-23B	0.368	0.364	0.367	0.3721	1.0223
SRM-24A	0.368	0.360	0.365	0.3678	1.0217
SRM-24B	0.368	0.361	0.366	0.3674	1.0177
Average scale factor = 1.0175, Sigma = 0.00440, % coefficient of variation = 0.432					
ETM-1	0.368	0.365	0.372	0.3681	1.0085
DM-8	0.368	0.360	0.366	0.3677	1.0214
DM-9	0.368	0.362	0.368	0.3691	1.0196
QM-6	0.368	0.360	0.366	0.3665	1.0181
QM-7	0.368	0.358	0.364	0.3657	1.0215
PVM-1	0.368	0.360	0.366	0.3677	1.0214
TEM-1	0.368	0.362	0.368	0.3659	1.0116
TEM-2	0.368	0.362	0.368	0.3664	1.0122
TEM-3	0.368	0.362	0.368	0.3672	1.0155
TEM-4	0.368	0.362	0.369	0.3681	1.0160
TEM-5	0.368	0.362	0.368	0.3654	1.0105
TEM-6	0.368	0.361	0.367	0.3667	1.0166
FSM-1	0.368	0.364	0.370	0.3701	1.0165
TEM-7	0.368	0.363	0.370	0.3709	1.0208
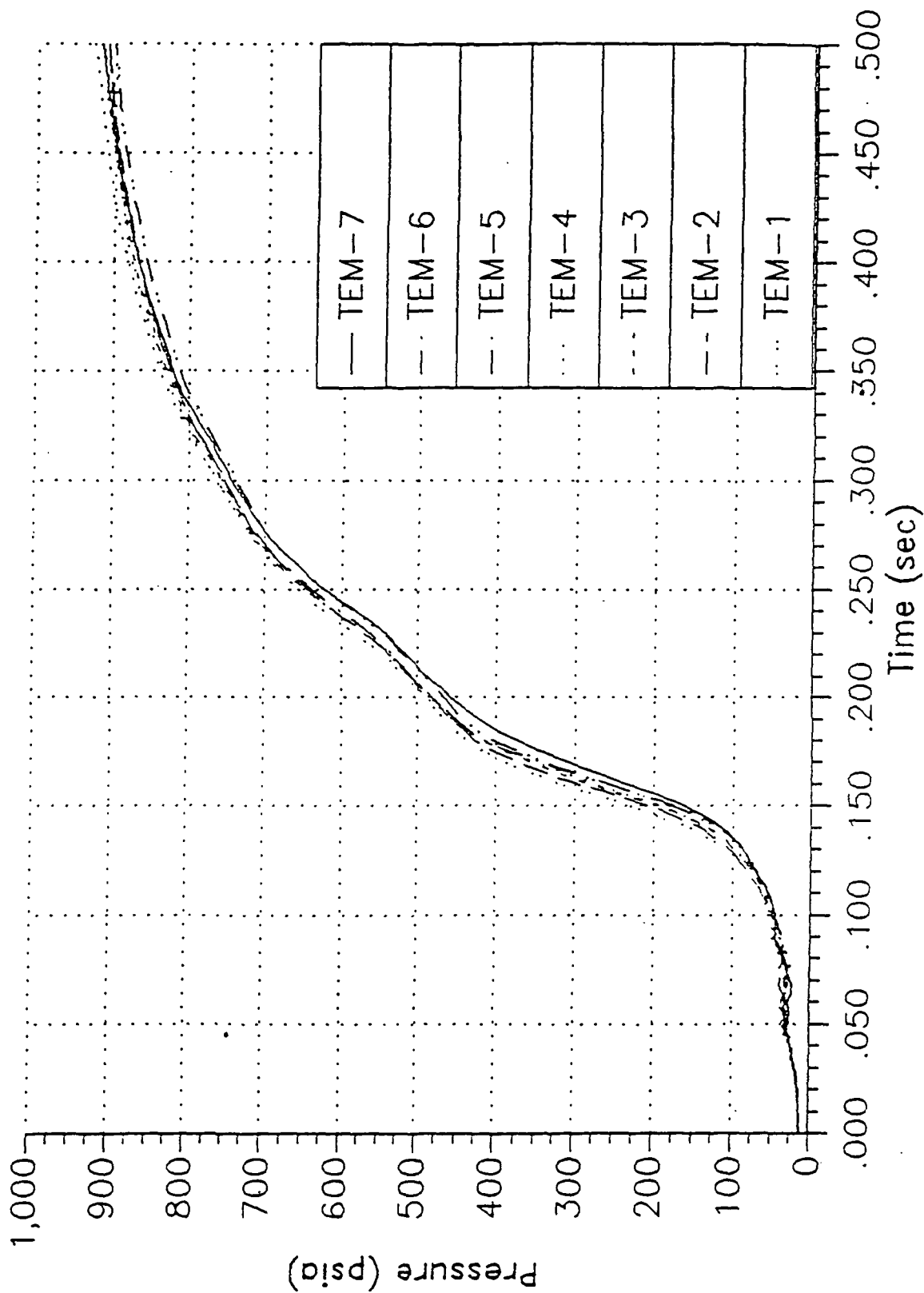
Figure 6-49. Measured Headend Pressure Transients

Table 6-9. Historical Three-Point Average Thrust and Pressure Rise Rate Data

Motor	Occurrence Time	Pressure Rise Rate	Occurrence Time	Thrust Rise Rate	Ignition Interval
Static Test Motors					
DM-2	0.1480	85.30	0.1480	245,380	0.2330
QM-1	0.1560	86.38	0.1560	246,128	0.2362
QM-2	0.1640	93.58	0.1720	234,950	0.2391
QM-3	0.1560	94.45	0.1520	245,615	0.2287
QM-4	0.1505	91.96	0.2225	234,438	0.2192
ETM-1A	0.1520	86.72	0.1560	230,023	0.2279
DM-8	0.1680	77.00	0.1760	257,272	0.2424
DM-9	0.1640	81.00	0.1720	275,525	0.2436
QM-6	0.1480	87.40	0.1520	211,476	0.2321
QM-7	0.1480	99.60	NA	NA	0.2230
PVM-1	0.1520	92.80	0.1520	294,664	0.2338
TEM-1	0.1520	85.13	0.1520	238,583	0.2255
QM-8	0.1720	72.30	NA	NA	0.2517
TEM-2	0.1520	94.40	0.1520	288,772	0.2280
TEM-3	0.1520	88.51	NA	NA	0.2272
TEM-4	0.1480	81.52	0.1520	279,764	0.2283
TEM-5	0.1560	87.12	NA	NA	0.2299
TEM-6	0.1600	84.49	0.1520	273,946	0.2342
FSM-1	0.1520	97.06	0.1440	250,453	0.2278
Flight Motors					
SRM-1A	0.1530	87.58			0.2373
SRM-1B	0.1500	91.57			0.2358
SRM-2A	0.1530	90.74			0.2348
SRM-2B	0.1660	90.27			0.2345
SRM-3A	0.1500	91.05			0.2308
SRM-3B	0.1500	89.68			0.2271
SRM-5A	0.1530	95.10			0.2361
SRM-5B	0.1660	84.43			0.2380
SRM-6A	0.1530	92.72			0.2342
SRM-6B	0.1470	88.22			0.2329
SRM-7A	0.1500	99.90			0.2282
SRM-7B	0.1500	99.32			0.2276
SRM-8A	0.1530	106.29			0.2224
SRM-8B	0.1500	91.06			0.2196
SRM-9A	0.1530	92.31			0.2303
SRM-10A	0.1530	92.89			0.2373
SRM-10B	0.1500	84.56			0.2342
SRM-13B	0.1410	98.85			0.2115
RSRM-1A	0.1501	99.0			0.2296
RSRM-1B	0.1596	80.5			0.2310
RSRM-2A	0.1564	87.3			0.2390
RSRM-2B	0.1501	100.2			0.2342
Number:		43		11	35
Average:		90.07		246,732	0.2321
Standard Deviation:		6.80		22,627	0.0076
% Coefficient of Variation:		7.55		9.17	3.27
TEM-7	0.1600	80.62	NA	NA	0.2359

Table 6-10. Measured SRM Ignition Performance Data at 65°F

Parameter	TEM-7	Specification Requirement
Maximum Igniter Mass Flow Rate (lbm/sec)	330.0	NA
Ignition Transient (sec) (0 to 563.5 psia)	0.2359	0.170-0.340
Maximum Pressure Rise Rate (psi/10 ms)	80.6	109
Pressure Level at Start of Maximum Rise Rate (psia)	231	NA
Time Span of Maximum Pressure Rise (ms)	160-170	NA
Equilibrium Pressure at 0.6 Sec (ignition end) (psia)	931	NA
Time to First Ignition (sec) (begin pressure rise)	0.029	NA

TEM-7 was instrumented with three pressure transducers for headend pressure measurement (PNCAC001 through PNCAC003) and one gage for igniter pressure measurement (PNCAC005). The signal from the headend OPT data channel (PNCAC001) was split to provide both ac coupled data (for chamber pressure oscillation data) and mean pressure. TEM-7 was also instrumented with four aft end pressure gages (PNNAR003 through PNNAR006), and again the aft end OPT data channel (PNNAR006) was split to provide both oscillatory aft end chamber pressure data and mean data. However, aft end data were not useful for dynamic analysis on this test. In addition, the mean pressure data channels are used to calculate dynamic pressure and to verify the accuracy of the ac coupled data.

Data acquired from gage PNCAC001 are displayed in a waterfall plot format in Figure 6-53. The 1-L and second longitudinal (2-L) acoustic modes can be observed at about 15 and 30 Hz, respectively. This waterfall plot is fairly typical of HPM designs. The magnitudes on this static test were among the lowest experienced on HPMs.

Figures 6-54 and 6-55 describe the running, instantaneous, peak-to-peak oscillation amplitudes of the 1-L and 2-L acoustic modes, respectively, for the TEM-7 motor headend pressure. This type of analysis is more representative of instantaneous oscillations than are the time averaged oscillations presented in a waterfall plot.
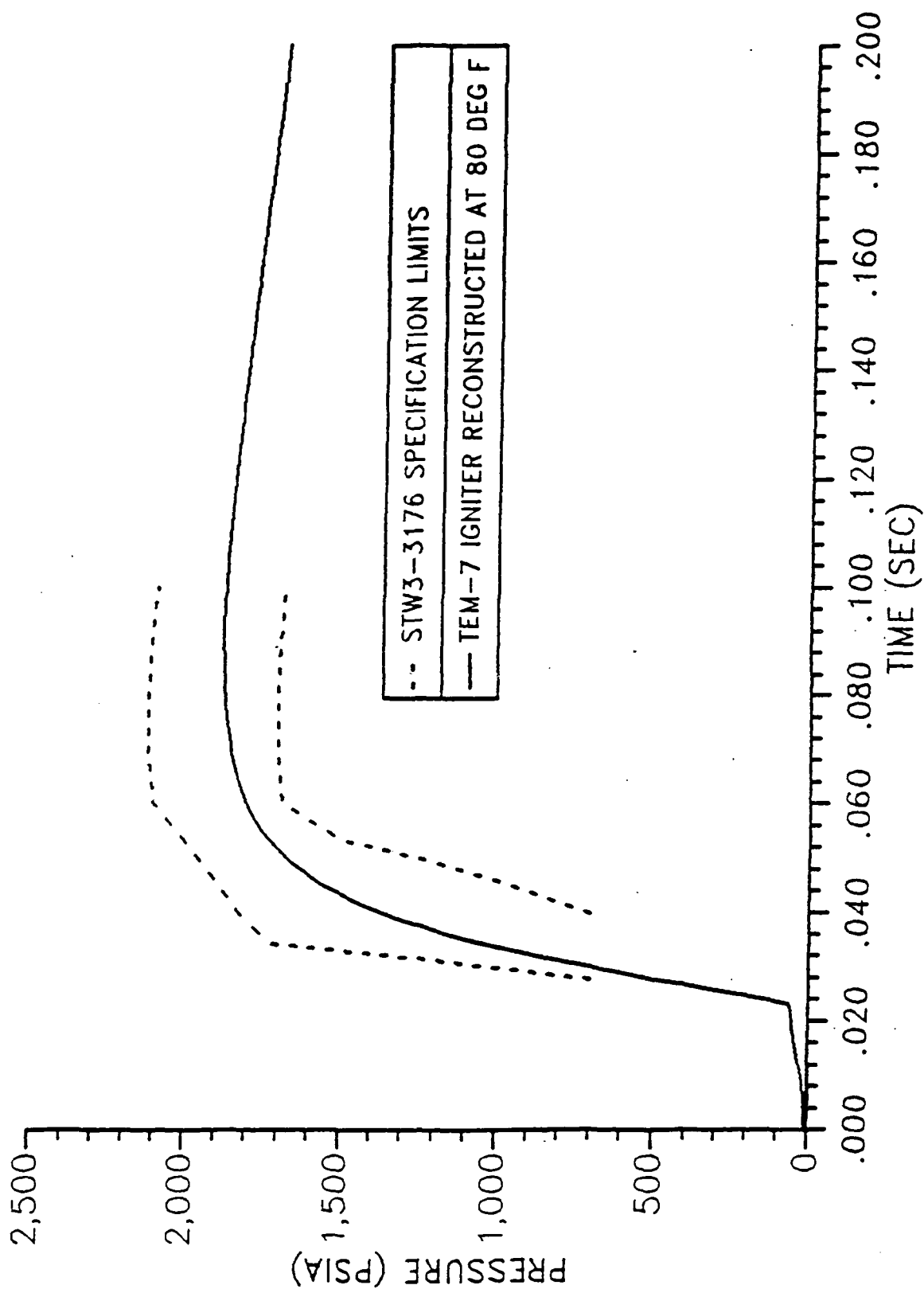
Figure 6-50. Igniter Reconstructed at 80°F in Specification Limits

- - STW3-3176 SPECIFICATION LIMITS

— TEM-7 IGNITER RECONSTRUCTED AT 80 DEG F

TIME (SEC)

PRESSURE (PSIA)
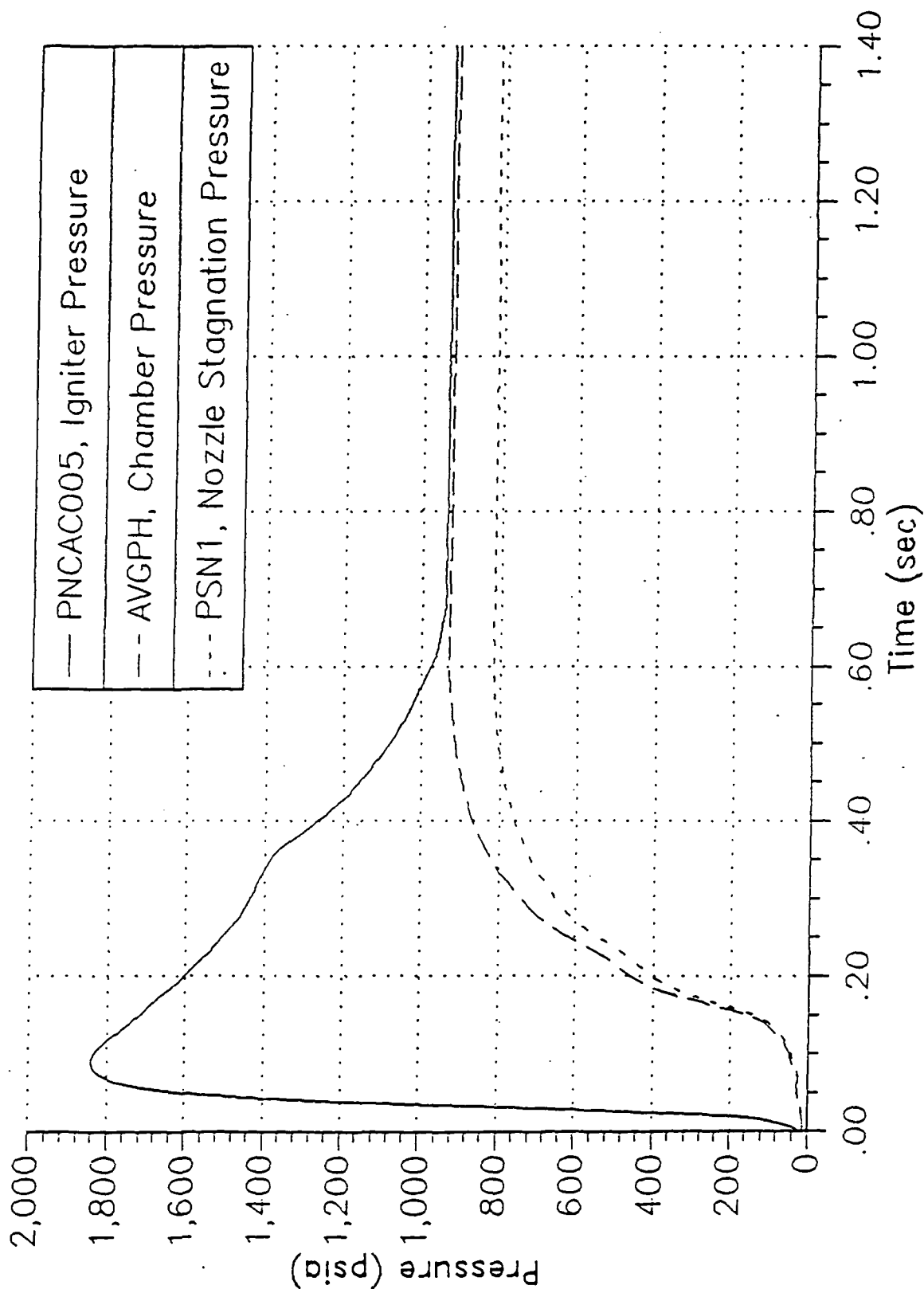
Figure 6-51. Igniter Pressure Versus Headend and Nozzle Stagnation Pressure
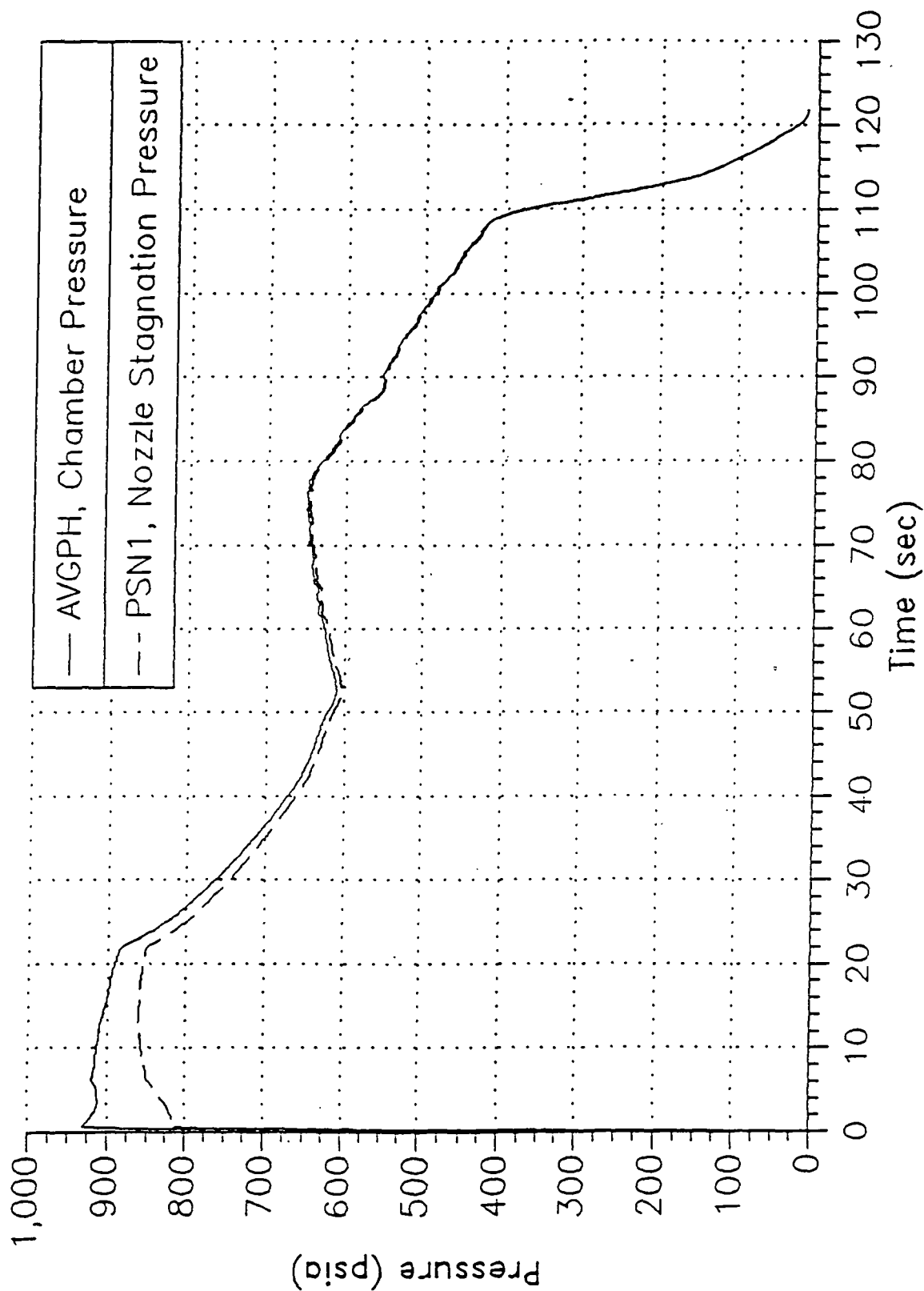
Figure 6-52. Measured Headend and Nozzle Stagnation Pressure Time Histories

Figure 6-53. Waterfall Plot for PNCAC001

SHUTTLE TEM-7 PNCAC001 FM, 750 HZ 1-L, 2-L 2000 S/S

START TIME = 1.00000 SEC
END TIME = 129.000 SEC
TIME SLICE = 2.00000 SEC
SAMPLE RATE 2000. SPS

TIME INCREMENT = 1.00000 SEC
X SKEW VALUE = 0.035000 IN.
Y SKEW VALUE = 0.075000 IN.
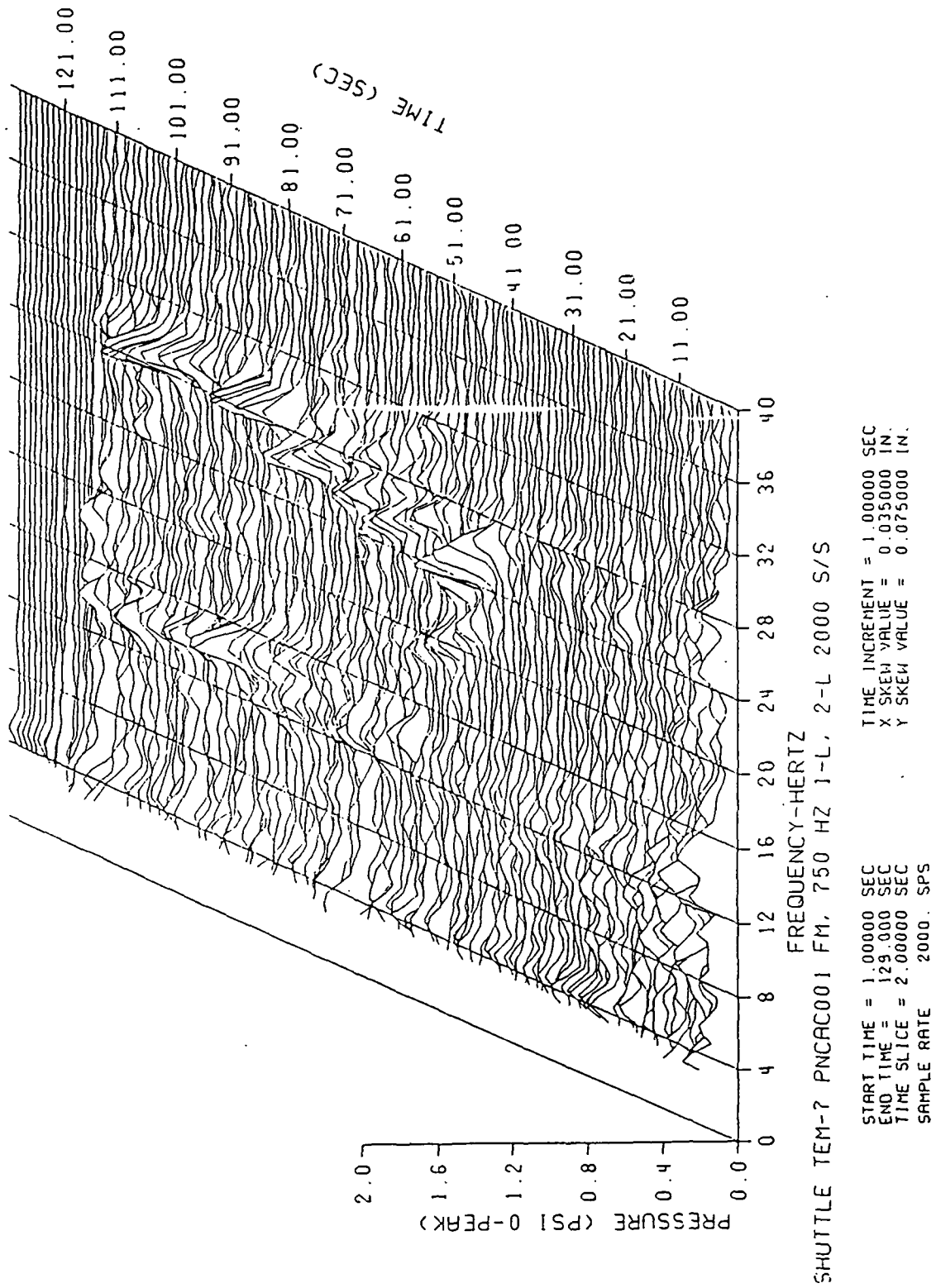
Figure 6-54. Maximum Oscillation Amplitudes for PNCAC001 1-L Acoustic Mode (2,000 sps)

Figure 6-55. Maximum Oscillation Amplitudes for PNCAC001 2-L Acoustic Mode (2,000 sps)

When using waterfall plots to compare static test motor oscillation amplitudes, it is important to remember that this format uses an averaging method of analysis. This presents no difficulty for steady state signals but has an attenuating effect on transient signals. Since most of the data obtained from an SRM are transient, any oscillation magnitudes referre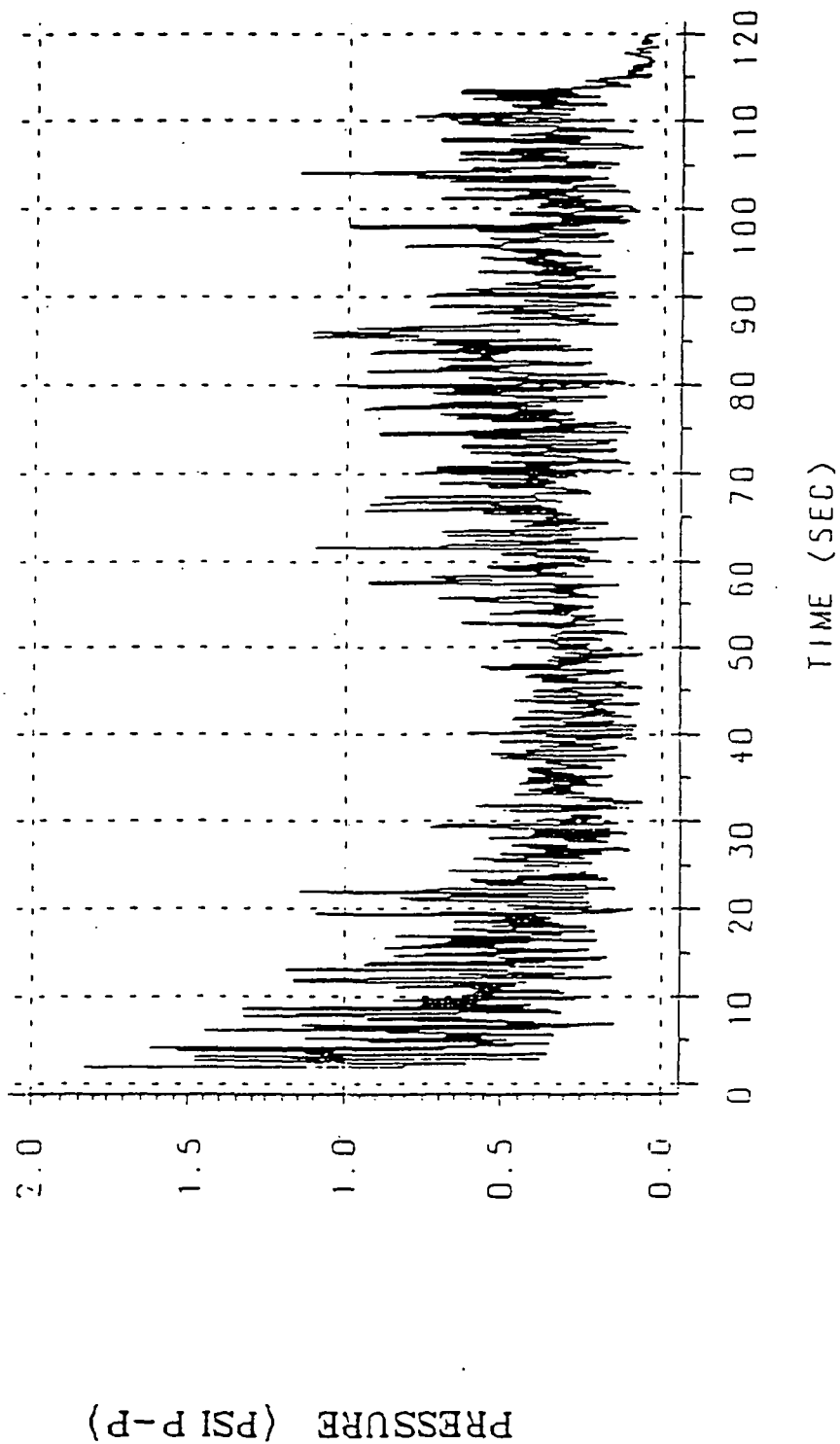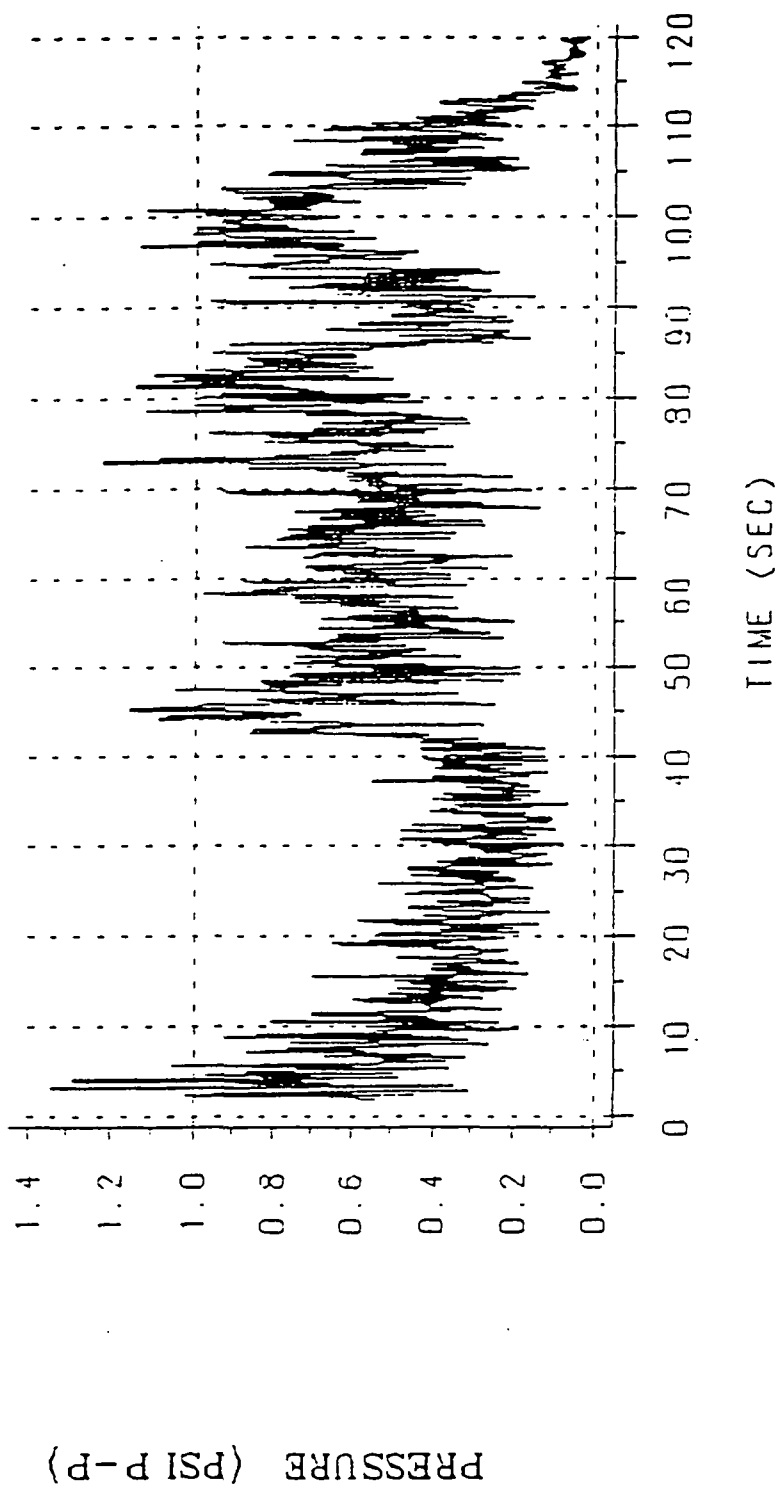d to as maxima are, in fact, not true but averaged values over a given time slice. These numbers are, nonetheless, very useful for comparison. Table 6-11 shows such a comparison for recent static test motors and the flight motors. This table contains the most recent data. DM-6 and DM-7 were filament wound case motors.

A comparison of TEM-7 thrust data at 60°F and a burn rate of 0.368 in./sec, at 625 psia and 60°F, with the CEI Specification CPW1-3300, dated 15 Jan 1986, and thrust-time limits at 0.368 in./sec is shown on Figure 6-56. The TEM-7 performance was within average population limits. Note that the limits are for the average of the historical SRM population, not an individual motor. The historical motor population is well within the limits. None of the individual motor performance tolerances and limit parameters were exceeded. TEM-7 ignition performance satisfied the ignition interval and the maximum pressure rise rate requirements, as shown in Table 6-10.

6.10 STATIC TEST SUPPORT EQUIPMENT

6.10.1 Introduction

The deluge system and related instrumentation were similar to previous TEMs. Deluge system nozzle arrangement is shown in Figure 6-57.

This was the first TEM static test motor with nozzle vectoring. As a result, the TEM-7 test arrangement included the MAEHS normally used for static tests with vectored nozzles. A nozzle-to-case joint heater (Section 6.8.1), normally used for TEM static tests, was also installed. TEM-7 was the first use of both the MAEHS and a nozzle-to-case joint heater.

Table 6-11. Maximum Pressure Oscillation Amplitude Comparison

Motor	Source of Measurement	Mode	Time of Measurement (sec)	Frequency (Hz)	Maximum Pressure (psi, 0 to peak)
TEM-7	Waterfall PNCAC002	1-L 2-L	85 100	15.5 29.5	0.45 0.53
FSM-1*	Waterfall PNCAC001	1-L 2-L	100 79	14.0 29.5	0.64 0.74
TEM-6	Waterfall PNCAC001	1-L 2-L	92 98/99	15.0 29.5	0.41 0.67
TEM-6 (Aft)	Waterfall PNNAR005	1-L 2-L	92 98/99	15.0 29.5	0.31 0.44
TEM-5	Waterfall PNCAC005	1-L 2-L	81 100	16.0 29.5	0.46 0.57
TEM-4	Waterfall	1-L 2-L	115 87	14.5 29.5	0.37 0.96
TEM-3	Waterfall	1-L 2-L	106 102	15.0 30.0	0.36 0.58
STS-29 (left)	Waterfall ac OPT	1-L 2-L	86 89	15.5 28.0	0.31 0.44
STS-29 (right)	Waterfall ac OPT	1-L 2-L	85 83	15.5 29.5	0.38 0.54
TEM-2	Waterfall	1-L 2-L	78 100	16.0 29.5	0.43 0.68
QM-8*	Waterfall (P000002)	1-L 2-L	104 55	14.5 27.5	1.32 0.47
TEM-1	Waterfall	1-L 2-L	79 95	15.5 29.5	0.37 0.78
STS-27 (left)	Waterfall ac OPT	1-L 2-L	82 82	15.5 29.5	0.37 0.60
STS-27 (right)	Waterfall ac OPT	1-L 2-L	82 83	15.5 29.5	0.57 0.72
* RSRM static test motors					

Table 6-11. Maximum Pressure Oscillation Amplitude Comparison (cont)

Motor	Source of Measurement	Mode	Time of Measurement (sec)	Frequency (Hz)	Maximum Pressure (psi, 0 to peak)
STS-26 (left)	Waterfall ac OPT	1-L 2-L	79 95	16.0 29.5	0.70 0.87
STS-26 (right)	Waterfall ac OPT	1-L 2-L	83 94	15.0 30.0	0.54 0.47
PVM-1*	Waterfall	1-L 2-L	99 79	14.5 29.5	1.23 0.77
QM-7*	Waterfall P000001	1-L 2-L	93 79	14.5 29.5	1.40 0.95
QM-6*	Waterfall	1-L 2-L	107 85	14.5 29.5	1.05 0.53
DM-9*	Waterfall	1-L 2-L	107 96	14.5 30.0	0.81 0.64
DM-8*	Waterfall	1-L 2-L	78 97	16.0 29.5	0.58 0.62
ETM-1A	Waterfall	1-L 2-L	84 101	15.5 29.5	0.45 0.61
DM-7**	Waterfall	1-L 2-L	77 96	15.5 29.0	0.90 0.62
DM-6**	Waterfall	1-L 2-L	76 86	15.5 29.0	0.51 0.78
QM-4	Waterfall	1-L 2-L	81 80	15.5 29.5	0.31 0.30

*   RSRM static test motors
**   Filament wound case HPM motors

911520.10-2
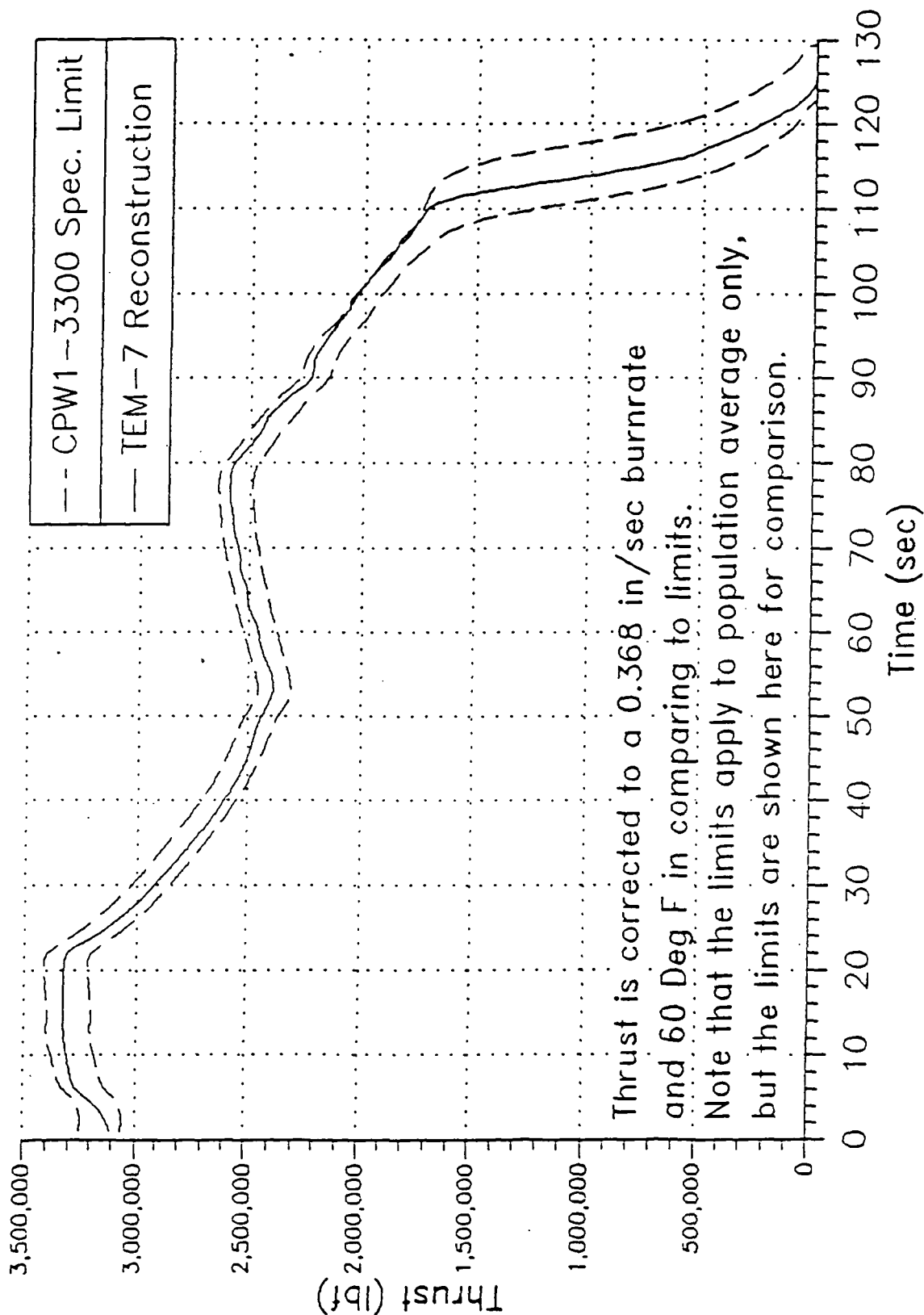
Figure 6-56. Reconstructed Thrust Compared to CEI Specification Limits

Thrust is corrected to a 0.368 in/sec burnrate and 60 Deg F in comparing to limits. Note that the limits apply to population average only, but the limits are shown here for comparison.

- - CPW1-3300 Spec. Limit
— TEM-7 Reconstruction

0.75-in. Nozzles (9 each)

0.75-in. Nozzles (6 each)

0.75-in. Nozzles (6 each)

0.75-in. Nozzles (9 each)

ET Attach Ring Area

Tray

ET/Stiffener Factory Joint
(forward factory joint of
aft segment)

Nozzles (27 each)

0.75-in. Nozzles (12 each)

A027440a

Figure 6-57. Plan View of Deluge System Nozzle Arrangement

6.10.2 Objectives/Conclusions

There are no objectives from Section 2 concerning static test support equipment.

6.10.3 Recommendations

A nozzle-to-case joint heater, used only on TEM static tests, should continue to be used on future TEM motors. TEM motors with nozzle vectoring should use the MAEHS in addition to a nozzle-to-case joint heater.

Case data sampling is recommended from one month prior to the test through ignition. Nozzle region sensor data sampling is recommended to be extended through a four-hr period following motor firing.
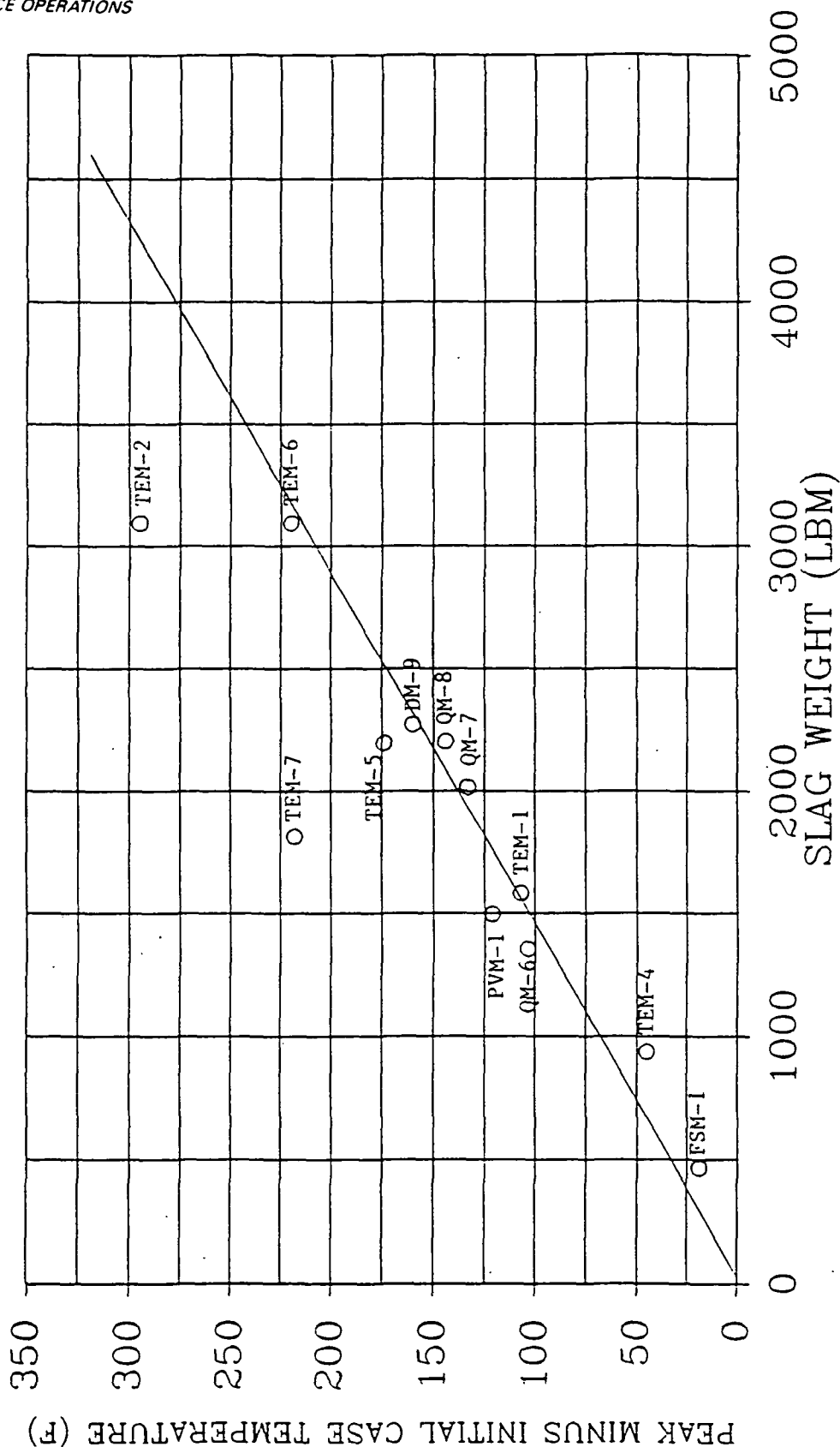
6.10.4 Results/Discussion

The nozzle-to-case joint heater and MAEHS performed as designed.

The deluge system operated as expected with no measured or observed indications of hot spots on the case. No anomalous temperature data were recorded by the deluge system instrumentation prior to, during, or following its operation. The recorded initial and peak TEM-7 case temperatures were 50° and 265°F, respectively.

The weight of slag accumulation was measured to be 1,813 lbm. The expected peak case temperature corresponding to this slag weight was approximately 174°F. Figure 6-58 shows peak minus initial case temperature versus slag weight for static motor firings. (Only test motors fired since the redesign of the deluge system are included.) TEM-7 represents a normal slag accumulation of the 12 test firings (data points) presented.

Nozzle region temperature plots show no unexpected or unusual temperature rise. Table 6-12 shows these temperatures at motor ignition and at the end of motor burn. As can be seen in Table 6-12 and in Figure 6-59, a circumferential gradient existed prior to and at motor firing. The operation of the aft skirt purge did not appear to significantly alter the natural existing gradient present in the T-97 Test Bay. At the time of motor firing the sensors controlling the operation of the

Figure 6-58. Maximum Static Test Motor Case Temperatures Versus Amount of Slag (peak case temperature minus initial case temperature at the same location)

*NOTE: PREDICTED WORST CASE SLAG WEIGHT IS 4600 LBM

nozzle-to-case joint heater, located on the aft dome, registered temperatures of 76°
and 77°F. At the same time the six nozzle-to-case joint sensors, located at 60-deg
intervals on the fixed housing, recorded temperatures between 79° and 88°F. The
upper temperature of 88°F did not violate the 85°F maximum as no temperature
requirement existed at this location. One reason why these six sensors registered
higher temperatures than the controlling sensors on the aft dome due is the fact that
the strip heater is attached to the fixed housing, and a temperature drop would be
expected across the nozzle-to-case joint.

There was a concern, prior to motor firing, that TVC system temperatures
would drop below the 50°F minimum temperature before the TVC could be serviced
three to four hr following motor firing. This test showed that the nozzle region of
the motor returned to the ignition temperatures six hr following motor firing.

Figure 6-59 shows temperature as a function of time at a nozzle-to-case joint
heater control sensor. This plot indicates the long term temperature environment
existing in the nozzle region following motor firing. This was a concern because of
the fixed housing debond issue.

The final predicted PMBT at the time of motor firing, using hygrothermograph
data, was 65°F (Figure 6-59). A reconstructed propellant mean bulk temperature,
using the available case temperature sensor data between November 29 and
December 7, resulted in a final propellant mean bulk temperature of 68°F
(Figure 6-60). Figures 6-61 and 6-62 graphically show these two analyses. The
difference between these two predictions demonstrates the need to use the most
accurate method, which is case temperature sensor data.

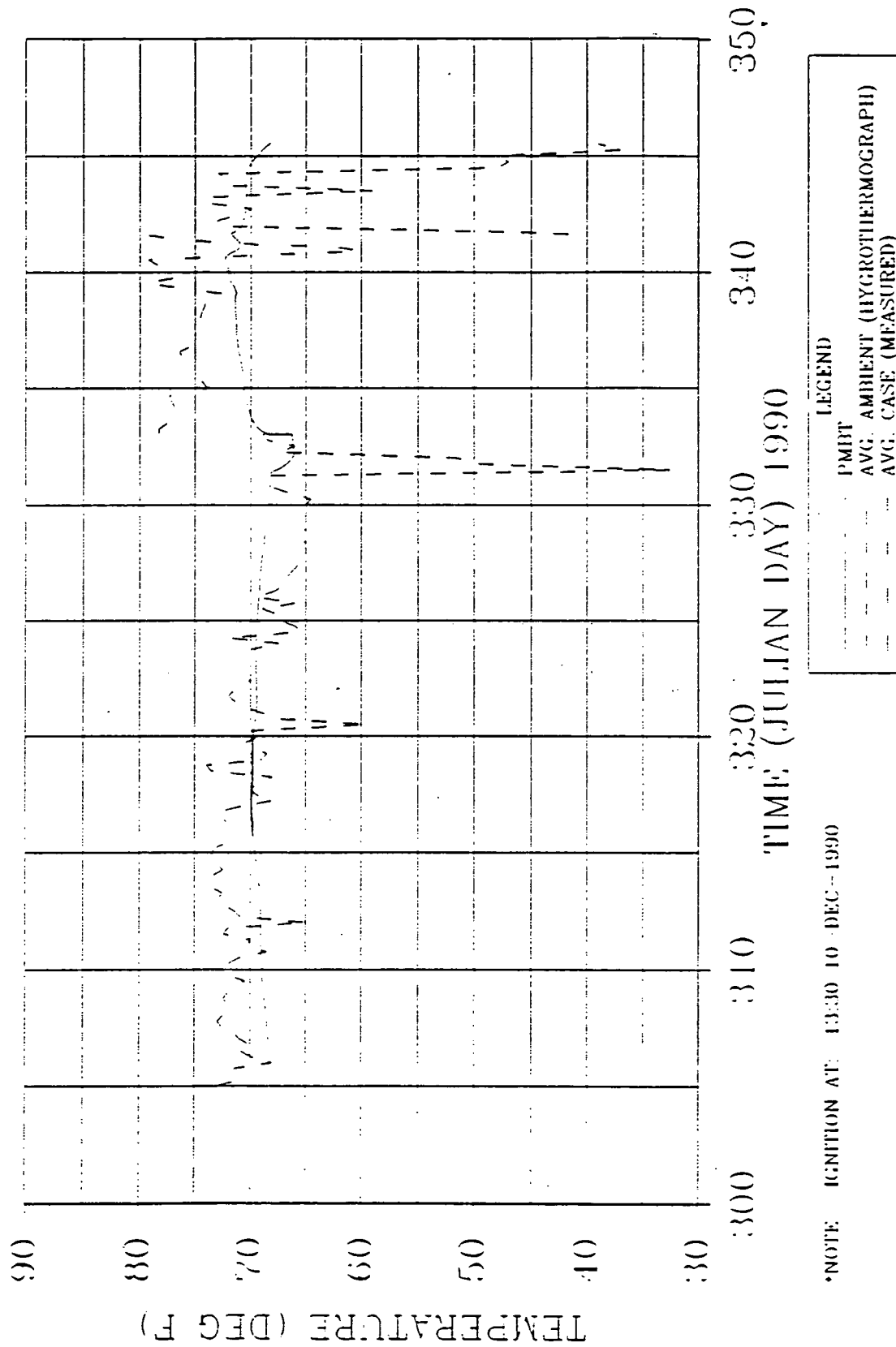Figure 6-60. Propellant Mean Bulk Temperature--68°F Using SINDA 2-D Heat Transfer Model
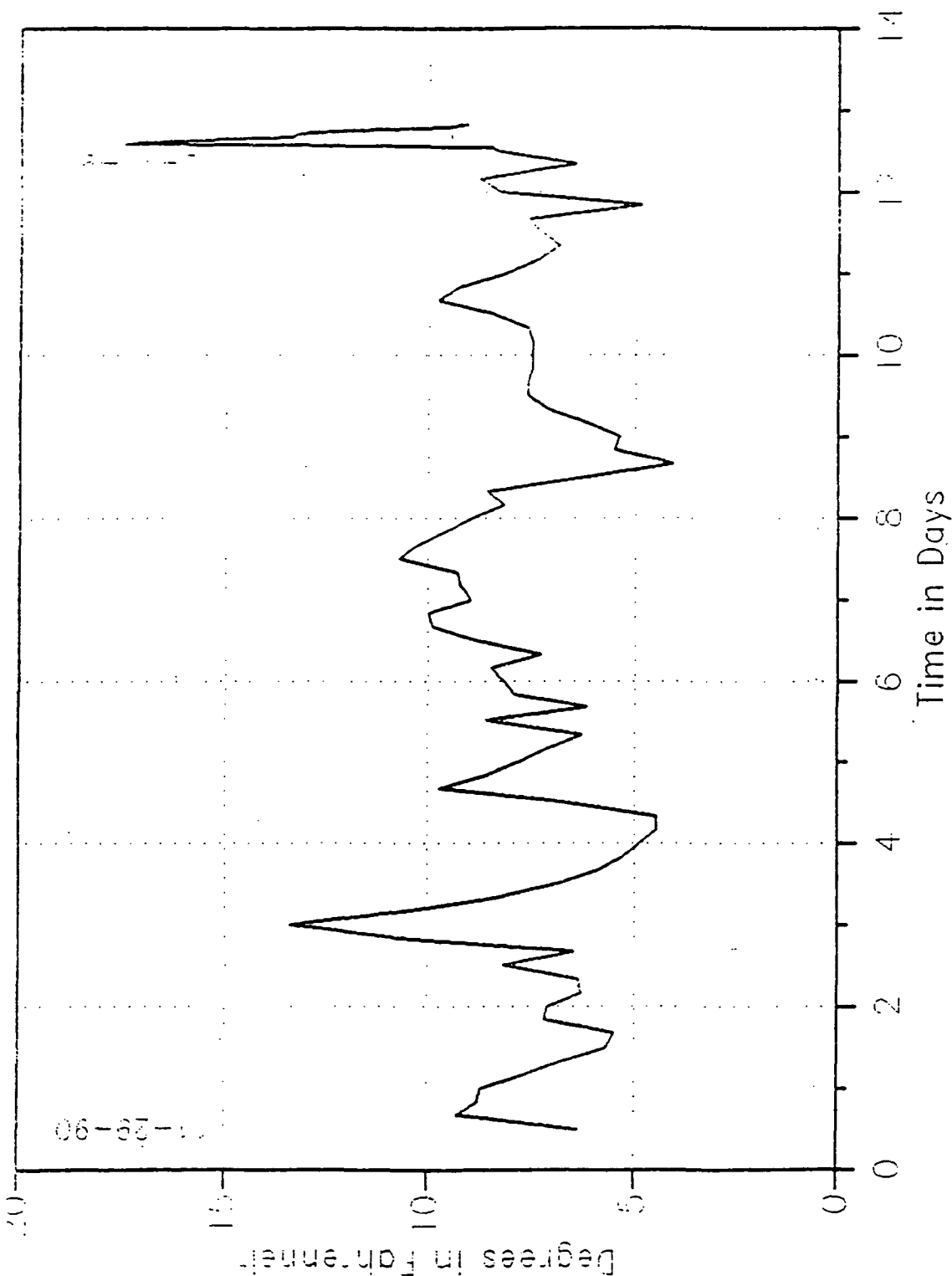
Thiokol CORPORATION
SPACE OPERATIONS

Figure 6-61. Nozzle-to-Case Joint Maximum Temperature Differential as a Function of Time
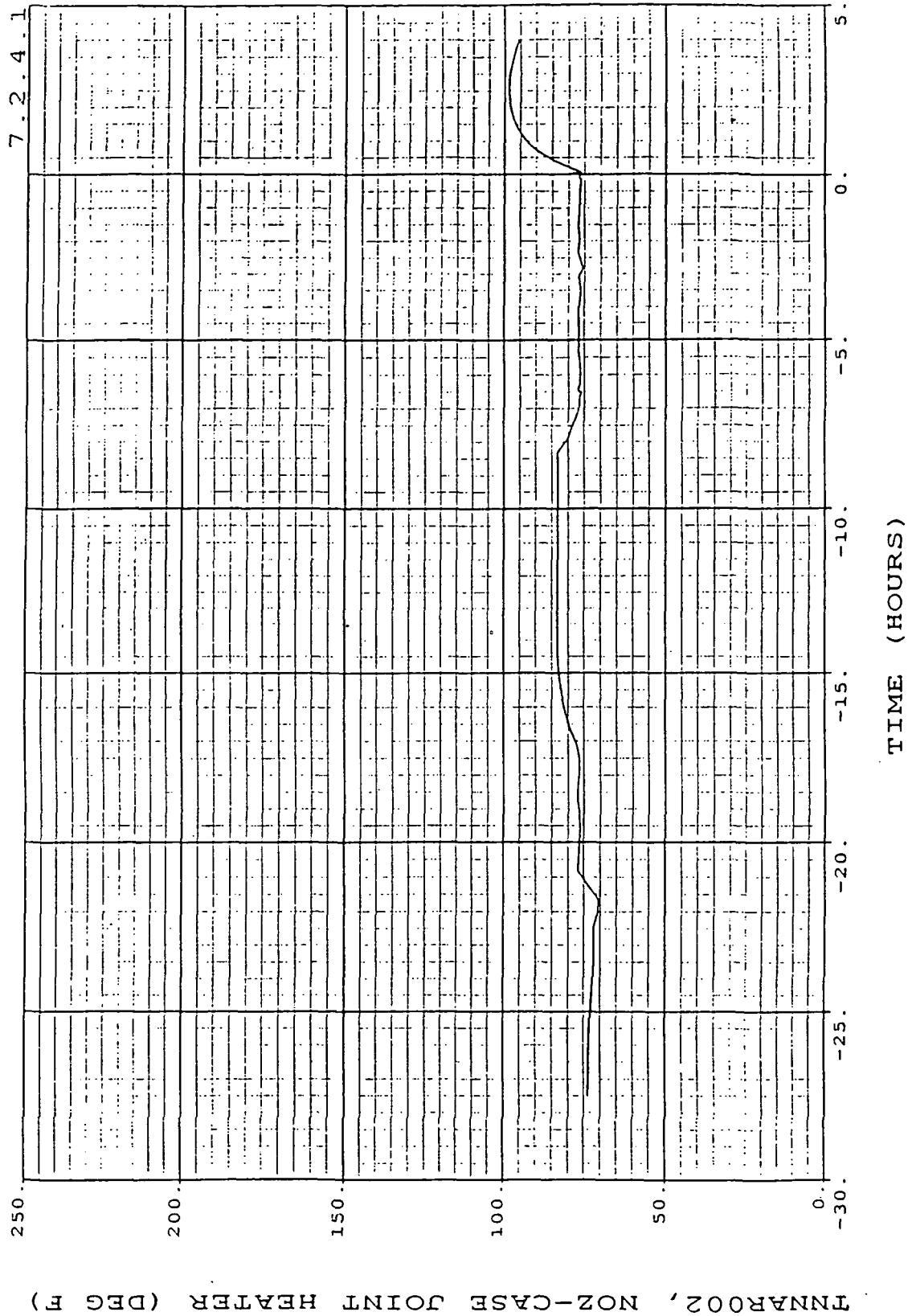
Figure 6-62. TNNAR002, Nozzle-to-Case Joint Heater

Drawing	Title
1U76705	Cable Assembly, Power, Electrical, Branched-Heater, Aft Ctr Segment
1U76706	Cable Assembly, Power, Electrical-Heater, Aft Segment
1U77252	Heater--Field Joint
1U77253	Heater--Igniter to Case Joint
1U82840	Band Pin Assembly Retainer
1U100269	Plug, Machine Thread
2U65686	Transducer Leak Test Fixture
2U65848	Leak Test Assy--Barrier Booster Assy, S/A Device
2U65040	Assembly Fixture--Nozzle
2U129361	CO_2 Quench System T-97
2U129363	Water Deluge System
2U129714	Assembly, RSRM Joint Leak Check System
2U129760	Static Test Arrangement
2U129764	Aft Test Stand Ass'y Sequence T-97
2U129765	Forward Test Stand Sequence
4U69505	Shield, Deluge System
7U76321	Transducer, Pressure
7U76608	Boot Assy, Flexible Bearing, Nozzle
7U76609	Cowl, Flexible Boot, Nozzle
7U76736	Exit Cone Assy, Fwd Section
7U76738	Nozzle Assembly, Final
7U76827	Boot Cavity Pressure Transducer Assy

Drawing	Title
7U76864	Bearing Protector, Flexible
7U76865	Housing Assembly, Modified--Nozzle, Fixed
7U76879	Test Assembly, TEM
7U76881	Motor Assy, Test, TEM
7U76882	Nozzle Assembly Segment, TEM
7U76899	Igniter/Fwd Segment Assy, TEM
7U76902	Transducer Assy, Pressure
7U76983	Insulated SAPMD
7U77011	Instrumentation Assembly, TEM-07
7U77118	Heater--Field Joint, Nozzle and Igniter, Refurbished
7U77266	Nose Inlet Assembly
7U77267	Exit Cone Assy, Aft--Modified
7U77310	Throat--Inlet Assy, Nozzle
7U77328	Joint Protection Systems, Technical Evaluation Motor
8U75902	Leak Check System, Installation
8U76500	Leak Check System, Safe & Arm Device, Installation

Specification

CPW1-3600A	Prime Equipment Contract End Item Detail Specification (CEI)
STW4-2621	Insulation, Acrylonitrile Butadiene Rubber (NBR), Asbestos and Silicon Dioxide-Filled
STW4-2868	Thermal Insulation, Ethylene Propylene Diene Monomer (EPDM)--Neoprene Rubber, Carbon Fiber-Filled
STW4-3266	Putty and Caulking or Glazing Compounds, Other

Specification	Title
STW4-3339	Rubber, Fluorocarbon, Elastomer; High Temperature and Compression Set Resistant
STW5-2833	TP-H1178 Propellant, Solid Rocket Motor, Igniter Space Shuttle Project
STW5-2931	Adhesive Liquid Epoxy Resin, Silicon Dioxide Filled
STW5-3223	Inhibitor, UF-3267, Solid Rocket Motor, Space Shuttle Projects
STW5-3224	Liner, Solid Rocket Motor, Space Shuttle Project.
STW5-3292	Adhesives, Epoxy
STW5-3343	Propellant, Solid Rocket Motor, TP-H1148
STW7-2831 No Change	Inspection and Process Finalization Criteria, Insulated Components, Space Shuttle Solid Propellant Rocket Motor
STW7-2853	Leak Test, Pressure Transducer Assemblies, Space Shuttle Project SRM
STW7-2913	Procedure, Leak Test of Barrier-Booster Redundant Seals
STW7-3475	Leak Testing, Forward-to-Aft-Exit-Cone Joint, Space Shuttle Redesigned Solid Rocket Motor
STW7-3476	Leak Testing, Forward-End-Ring-to-Nose-Inlet Housing Joint, Space Shuttle Redesigned Solid Rocket Motor
STW7-3477	Leak Testing, Nose-Inlet-to-Throat Support Housing Joint, Space Shuttle Redesigned Solid Rocket Motor
STW7-3478	Leak Testing, Throat-Support-Housing-to-Forward-Exit-Cone Joint, Space Shuttle Redesigned Solid Rocket Motor
STW7-3632	Leak Test, Inner and Outer Igniter Joints, Space Shuttle Project Solid Rocket Motor
STW7-3633	Leak Test, S&A

Thiokol CORPORATION
SPACE OPERATIONS

Specification	Title
STW7-3682	Leak Testing, Field and Case to Nozzle Joints
STW7-3688	Grease Application and O-Ring Installation, Field and Case to Nozzle Joints
STW7-3745	Putty, Aft Segment and Nozzle Assembly Joint, Application of
STW7-3746	Putty, Vacuum Seal, Field Joint Assembly, Application of

Document	
TWR-17656	TEM-07 Flash Report
TWR-18011	RSRM Structural Material Properties Data Book
TWR-18965	Program Plan for Development and Qualification of a Second Source Rayon Supplier (1650 Denier)
TWR-19121	Predicted Ballistic Performance Characteristics for TEM-7
TWR-19524B	Program Plan for Low Cost Nozzle Improvements
TWR-19838	Technical Evaluation Motor 7 (TEM-07) Performance Information Summary
TWR-60273	TEM Postfire Engineering Evaluation Plan
TWR-60857	Cowl Vent Hole Diameter Study and TEM-2 Nozzle Boot Cavity Pressurization
TWR-61209	Postfire Hardware Special Issues TEM-7
TWR-61490	TEM-7 Nozzle Quick-Look Report
TWR-61585	TEM-07 Fixed Housing Unbond Investigation
CTP-0107	Space Shuttle Technical Evaluation Motor #7 (TEM-07) Static Fire Test Plan

DISTRIBUTION

Recipient	No. of Copies	Mail Stop
G. Abawi	1	L61C
R. Ash	1	L61C
N. Black	1	L71
D. Bright	1	L63
D. Bullard	1	L62A
R. Buttars	1	L63
N. Carpenter	1	L72
J. Curry	1	L52
A. Drendel	1	L63
J. Dykstra	1	L72
M. Fairbourn	1	L63
L. Frary	1	L72A
D. Garceau	1	L62B
R. George	1	L62A
W. Gerhart	1	L62B
P. Hughes	1	L71
R. Lange	1	L62A
S. Manz	1	L62B
E. Mathias	1	L63
A. Neilson	1	L72
L. Nelsen	1	L61C
R. Papasian	40	E62A
J. Passman	1	L62B
C. Propkop	1	L62B
D. Pulleyn	1	L72
K. Rees	1	L62
D. Ruddell	1	L63
J. Seiler	1	L72
D. South	1	L62
K. Speas	1	L63
T. Swauger	1	L61
S. Vigil	1	E62C
F. Weiler	1	L62A
Data Management	1	L72B
Print Crib	5	Q51B1